AD-A136 912 A WIND TUNNEL INVESTIGATION TO DETERMINE DOMINANT FOREBODY STRAKE DESIGN.. (U) AIR FORCE INST OF TECH WRIGHT-PATTERSON AFB OH SCHOOL OF ENGI.. T A DUNCAN 1/2

UNCLASSIFIED DEC 83 AFIT/GAE/AA/83D-7 F/G 20/4 NL

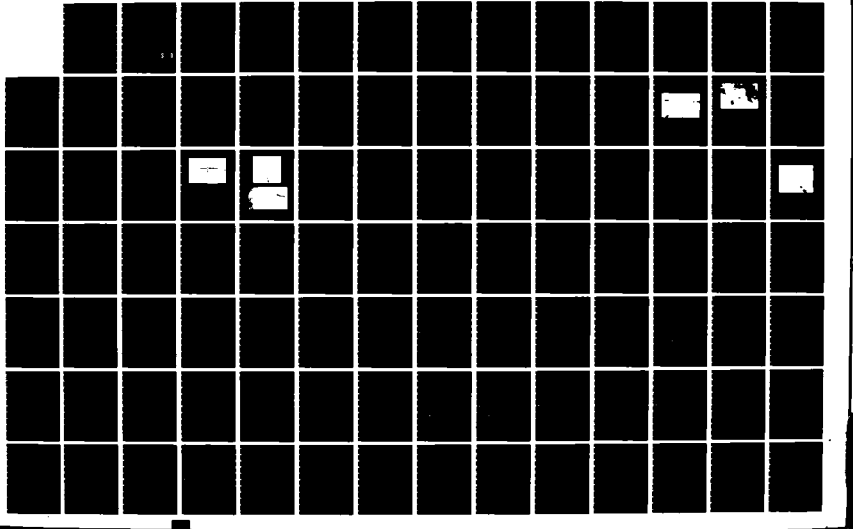

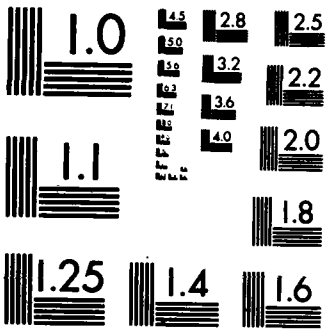

A WIND TUNNEL INVESTIGATION TO DETERMINE DOMINANT FOREBODY STRAKE DESIGN CHARACTERISTICS FOR AN F-15 EQUIPPED WITH CONFORMAL FUEL TANKS

THESIS

AFIT/GAE/AA/83D-7 Terry A. Duncan
Captain USAF

DEPARTMENT OF THE AIR FORCE
AIR UNIVERSITY
AIR FORCE INSTITUTE OF TECHNOLOGY

Wright-Patterson Air Force Base, Ohio

AFIT/GAE/AA/83D-7

A WIND TUNNEL INVESTIGATION TO DETERMINE DOMINANT FOREBODY STRAKE DESIGN CHARACTERISTICS FOR AN F-15 EQUIPPED WITH CONFORMAL FUEL TANKS

THESIS

AFIT/GAE/AA/83D-7 Terry A. Duncan
Captain USAF

Approved for public release; distribution unlimited.

AFIT/GAE/AA/83D-7

A WIND TUNNEL INVESTIGATION TO DETERMINE DOMINANT FOREBODY STRAKE DESIGN CHARACTERISTICS FOR AN F-15 EQUIPPED WITH CONFORMAL FUEL TANKS

THESIS

Presented to the Faculty of the School of Engineering
of the Air Force Institute of Technology
Air University
in Partial Fulfillment of the
Requirements for the Degree of
Master of Science

by
Terry A. Duncan, B.S.E.M.
Captain USAF
Graduate Aeronautical Engineering
December 1983

Preface

In this thesis I examined the effects of a parametric family of strakes on the longitudinal and lateral stability of an F-15C aircraft equipped with CFT's. The test was performed in the AFIT 5 foot wind tunnel using a specially constructed 1/32nd scale injection molded, plastic aircraft model.

This thesis continued a test program begun at Wright-Patterson AFB by the F-15 Systems Project Office. The previous work showed the specially constructed, plastic model produced stability data which compared favorably with data from a much more costly model tested in the Ames 12 foot pressurized wind tunnel.

It should not, however, be construed that plastic models may be indiscriminately used and still produce reliable results. Great credit must go to the AFIT Model Shop where Mr. Jack Tiffany, model maker, converted the hobby kit into an accurate, wind tunnel test article. I would also like to express my appreciation to Mr. Russel Murry, machinist, for his advice and the construction of the many test strakes. Credit must also be given to Mr. Nick Yardich and Mr. Andy Rimenschneider, AFIT wind tunnel technicians, whose cumulative knowledge, experience, and concerned effort made possible the quantity and quality of data collected in this experiment. The skill, dedication,

and cooperative spirit of AFIT's technical staff are one of its greatest assets.

Invaluable technical and material support were provided by the program's sponser, Flight Dynamics Laboratory, Aerodynamics and Airframe Branch. Appreciation is also extended to my advisor, Capt. Wesley R. Cox, for his advice and guidance, and to Professor Harold C. Larsen whose technical skill, fatherly guidance, and friendly encouragement has helped so many of us begin our engineering careers.

Table of Contents

List of Figures

Appendices

Longitudinal Stability Data

Low Angle of Attack

High Angle of Attack

Lateral Stability Data

$C_{N_{\beta\ DYN}}$ vs β

C_N vs β

List of Symbols

α	Angle of Attack (degrees)
β	Sideslip Angle (degrees)
ε	Total Blocking Correction Factor
ε_{sb}	Solid Blocking Correction Factor
ε_{wb}	Wake Blocking Correction Factor
ρ	Atmospheric Density
a_f	Lift Curve Slope of the Vertical Fin
AFIT	Air Force Institute of Technology
b	Model Wing Span
C	Wind Tunnel Test Section Area
C_D	Drag Coefficient (D/ qS)
C_{D_o}	Zero Lift Drag Coefficient from C_L vs C_D plot
C_L	Lift Coefficient (L/ qS)
C_{L_α}	Lift Curve Slope
C_{L_t}	Lift Coefficient for the Horizontal Tail
C_{L_f}	Lift Coefficient for the Vertical Tail
$C_{L\ MAX}$	Maximum Lift Coefficient
C_ℓ	Rolling Moment Coefficient (ℓ/ qSb)
C_{ℓ_β}	$\partial\ell/\partial\beta$ (per degree)
C_M	Pitching Moment Coefficient (M/qSc)
$C_{M_{ac}}$	Pitching Moment Coefficient About the Aerodynamic Center
$C_{M_{acwb}}$	Pitching Moment Coefficient About the Aerodynamic Center for the Wing-Body Only

C_{M_α}	$\partial C_M / \partial \alpha$ (per degree)
C_N	Yawing Moment Coefficient (N/qSb)
C_{N_β}	$\partial C_N / \partial \beta$ (per degree)
$C_{N_{\beta\ DYN}}$	Parameter for Predicting Lateral-Directional Stability (See Section III)
c	Model Chord Length
CFT	Conformal Fuel Tank
ΔD_b	Horizontal Bouyancy Correction to Drag
D	Drag
D_u	Drag Uncorrected for Wind Tunnel Errors
$dp/d\ell$	Longitudinal Variation in Static Pressure
D.C.	Direct Current
F/B	Forebody
fps	Feet per Second
I_X	Moment of Inertia about the X axis
I_Z	Moment of Inertia about the Z axis
h	Location of Center of Mass
h_N	Neutral Point
h_{Nwb}	Neutral Point for Wing-Body Only
K_N	Static Margin (h_N-h)
L	Lift
L_u	Lift Uncorrected for Wind Tunnel Errors
ℓ	Rolling Moment
ℓ_u	Rolling Moment Uncorrected for Wind Tunnel Errors
M	Pitching Moment
M_u	Pitching Moment Uncorrected for Wind Tunnel Errors

MAC	Mean Aerodynamic Chord
N	Yawing Moment
N_u	Yawing Moment Uncorrected for Wind Tunnel Errors
q	Dynamic Force ($\rho V/2$)
q_b	Dynamic Force Corrected for Blockage
q_u	Dynamic Force Uncorrected for Wind Tunnel Errors
S	Model Wing Area
V	Free Stream Velocity
V	Volume of the Test Model
V_v	Vertical Tail Volume
$\bar{V}_H$	Horizontal Tail Volume

Abstract

A parametric study of forebody strakes was made on an F-15C model equipped with conformal fuel tanks in the AFIT 5 foot wind tunnel. Parameters of interest were the strake planform area and the strake angle of incidence. Twenty configurations were evaluated for longitudinal and lateral stability at angles of attack from -4 to 46 degrees.

Lift coefficient (C_L), drag coefficient (C_D), and pitching moment coefficient (C_M) were plotted versus angle of attack (α). Data indicated that an excessive positive increase in $\partial C_M / \partial \alpha$ can be expected at angles of attack of 20 degrees or less. Above 20 degrees, C_M may be tailored by varying the strake area and incidence angle. For each strake examined, an angle of incidence of either -3 or -6 degrees (depending on planform area) produced a more nearly linear C_M versus α curve than 0 degrees; therefore, incidence angle should be considered in strake design optimization.

Lateral stability data were taken on 12 configurations from 16 to 44 degrees angle of attack. To determine spin susceptibility, $C_{N_\beta\ DYN}$ (see Section III) was plotted for the most promising configurations. Very little constructive change in lateral stability was noted for the configurations tested.

I. Introduction

Background

Beginning with the "C" model, the F-15 was modified to carry conformal fuel tanks, frequently called CFT's or FAST packs. These tanks (see Fig 1) fit outboard of the engine inlet and beneath the wing allowing the aircraft to carry additional fuel and electronics (5). While these tanks were originally intended for ferry missions, the flexibility they add to the combat role makes it likely they will see combat.

Early flight testing of an F-15 equipped with the production version of the CFT's indicated that there might be a slight reduction in both longitudinal and lateral stability at high angles of attack (13). Wind tunnel testing followed at the Ames 12 foot pressurized wind tunnel. Several armament configurations of an F-15 both with and without the CFT's were tested. Data confirmed that there was a small reduction in static longitudinal and lateral stability at angles of attack greater than 30 degrees (6). While the reduction in stability is small, it may present an undesirable difference in handling qualities between configurations.

It is well recognized that strakes may be used to influence the longitudinal and lateral stability of swept

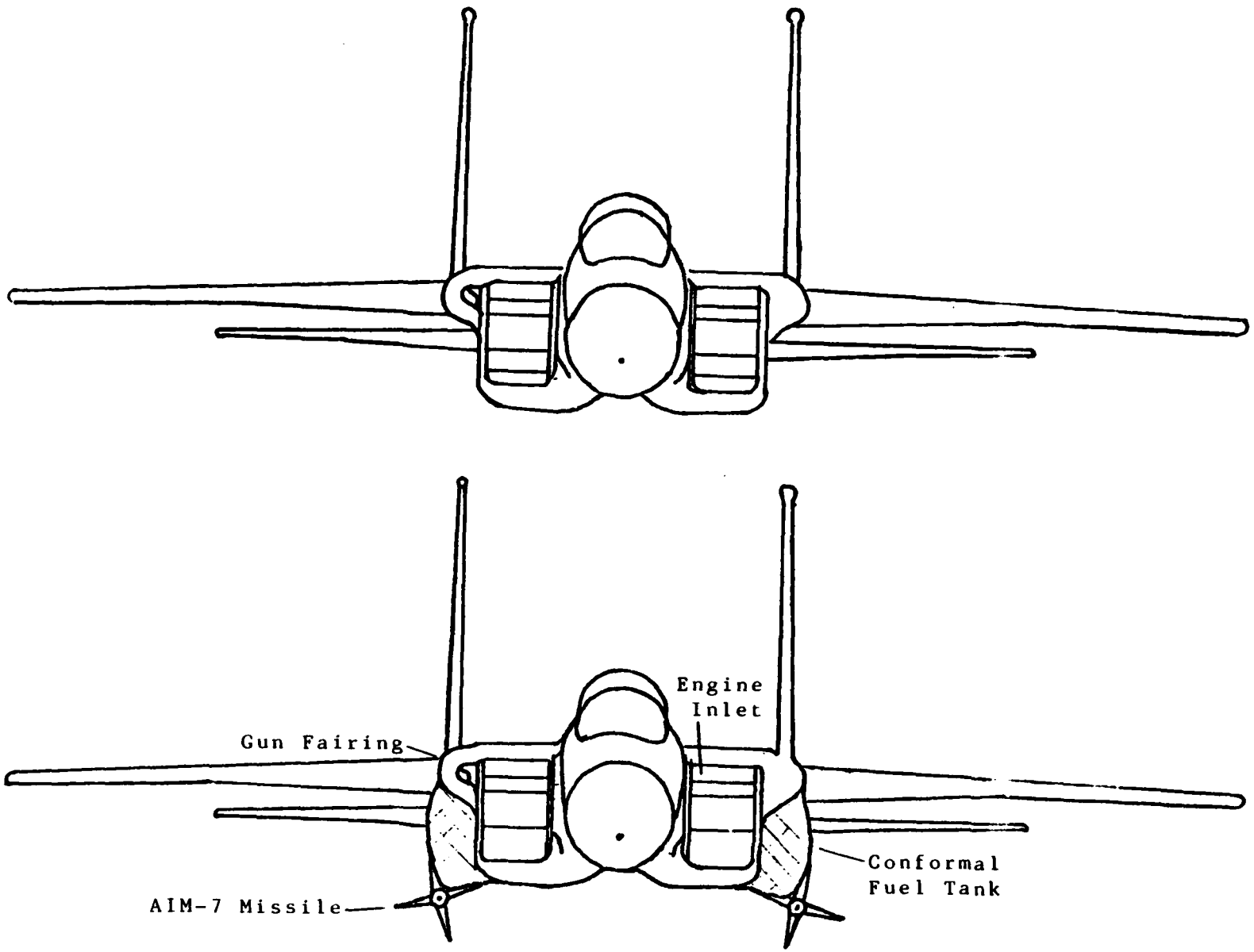

Fig 1. Change in cross-section with addition of conformal fuel tanks

wing aircraft at high angles of attack (10). A combination of nose and forebody strakes, if properly optimized, may be used to improve the longitudinal and lateral stability, and also increase the aircraft's lift while decreasing its drag (10).

With this in mind, the F-15 Systems Project Office conducted a series of tests in early 1983. The tests evaluated the static longitudinal and lateral stability of a 1/32nd scale F-15C in the AFIT 5 foot wind tunnel. Both the clean aircraft and the CFT equipped model were evaluated with several armament configurations and forebody strakes, nose strakes, and ventral fins. Results of these tests indicated that forebody strakes were the best candidate to improve the overall performance of the F-15 (14).

Problem

The purpose of this test was to define the strake effects on the overall performance of a CFT equipped F-15. Primary importance was attached to stable longitudinal dynamics at high angle of attack, an increase in lateral stability at high angle of attack, and minimal degradation of the low angle of attack longitudinal stability.

Strake Effects

Strake characteristics which will produce the desired performance are difficult to predict. A configuration which

works well on one aircraft may not work on another (11). Additionally a forebody strake produces a forward shift in the aircraft's center of pressure and may cause low angle of attack instabilities (15). For the present, wind tunnel testing is the best means to evaluate the total configuration (10).

Strake performance is dependent upon many parameters such as: shape, area, fineness ratio, and leading edge radius (references 2,3,and 15). Installation effects such as strake dihedral and inlet mass flow can also play a part in the overall performance (8) (9). The installed angle of incidence of the strake should produce an effect that will allow the test engineer to change the angle of attack at which maximum strake vorticity occurs. This will change both the magnitude of $C_{L\ MAX}$ and its position on a C_L versus α curve. The ability to vary strake angle of incidence should allow improved tailoring of the high angle of attack stability and overall performance.

Procedure

A parametric family of 20 strakes (see Appendix A) was designed to evaluate the static, aerodynamic performance of a CFT equipped F-15 at angles of attack of -4 to 46 degrees and sideslip angles of -6 to 6 degrees. The installed angle of incidence and planform area of the strake were varied to

form the family. The angle of incidence varied from 0 to -9 degrees, while the strake area was increased by changing the span and holding the chord constant (see Fig 2).

Testing was performed with the original 1/32nd scale model in the AFIT 5 foot wind tunnel. Aerodynamic data were taken using a Task, Mk1, 6 component strain gauge balance and a Hewlett-Packard, Model 3497A, data acquisition system. Data were reduced on a Hewlett-Packard 85 computer.

Coefficients of lift, drag, and pitching moment were plotted versus angle of attack (see Appendix B). Coefficients of yaw and roll were calculated, and $C_{N_{\beta\ DYN}}$ was synthesized and plotted versus sideslip angle (see Appendix C).

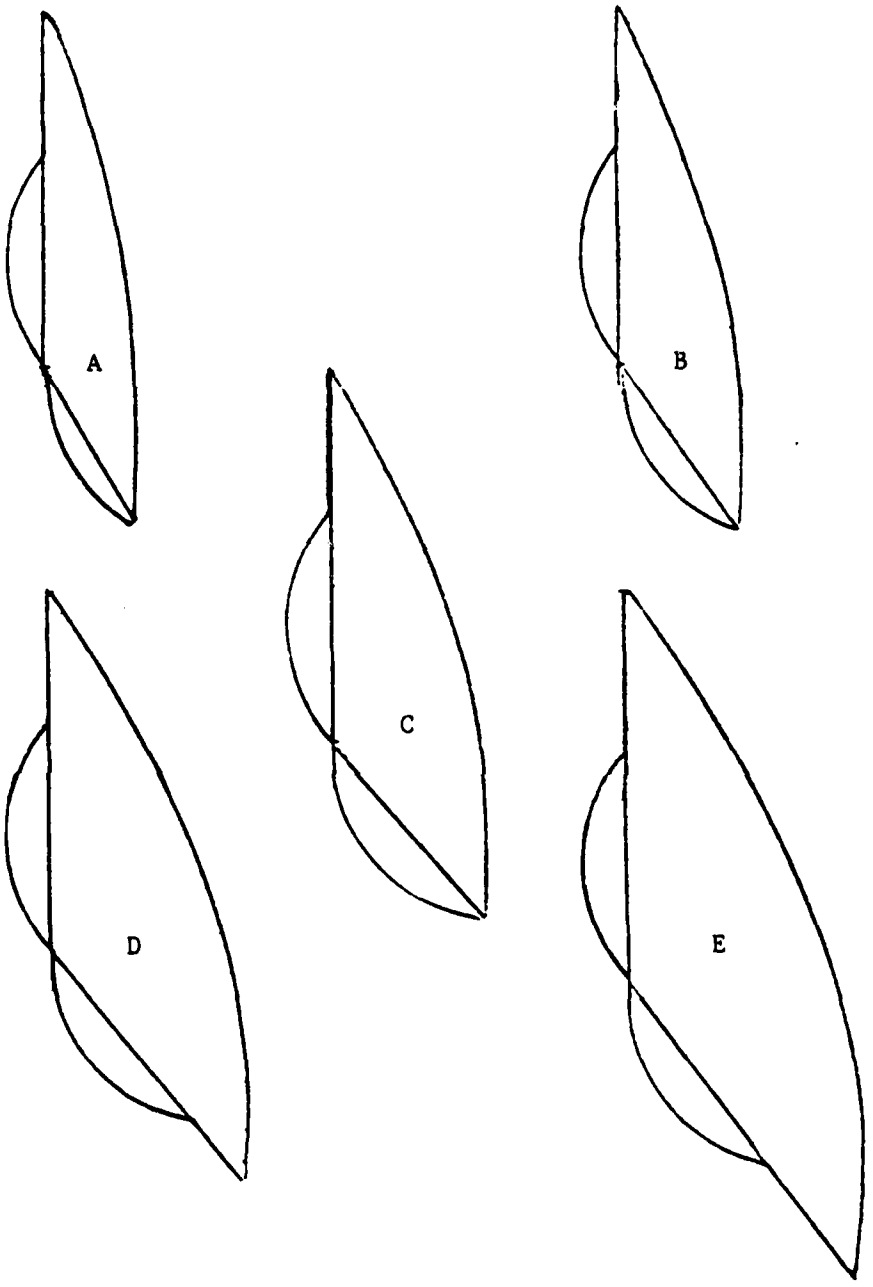

Fig 2. Strake families A through E shown actual size. Installation tabs shown.

II. Test Equipment

Wind Tunnel

The AFIT 5 foot wind tunnel was built in 1919 at McCook Field, Dayton, Ohio, and moved to its present location in 1921. It is an open circuit, continuous flow type. The tunnel has a closed test section, five feet in diameter and 18 feet in length, with a contraction ratio of 3.7 to 1. The wooden tunnel, including the intake and diffuser, is contained within a large building which provides a double return passage for the air. Tunnel airflow is induced by two 12 foot counterrotating fans, driven by four 400 horsepower, direct current motors, and is capable of providing test section speeds up to 293 feet per second (fps), which corresponds to a Reynolds Number (Re) of 1.876 x 10^6 per foot under standard conditions. Total pressure is atmospheric. Static pressure is measured by a manifold containing eight static pressure ports 30 inches from the tunnel entrance and 2.5 feet forward of the test section. Dynamic pressure is measured by a micromanometer connected to static and atmospheric pressure (12).

Instrumentation

This test used a Task, Mk1, six component, .75 inch outside diameter internal strain gauge balance and bridge conditioners to acquire data. Each channel was sampled 10

times and the readings were averaged by a Hewlett-Packard 3497A data acquisition system. The averaged data were reduced to aerodynamic forces and moments by a Hewlett-Packard 85 computer and then stored on cassette for further reduction and plotting.

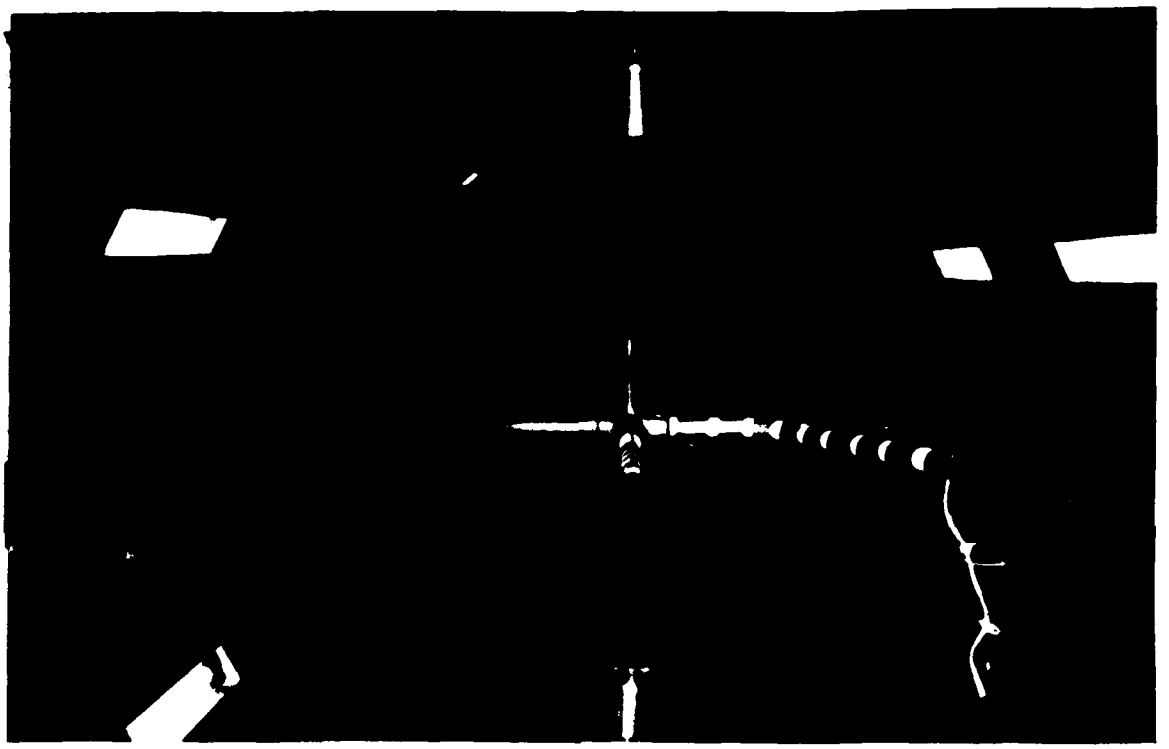

Fig 3. Model, sting, and yoke mounted in the test section. The circular arc tracks (for sideslip control) and angle of attack control cable are also visible.

The balance was fitted to a steel sting and "Y" yoke support structure (see Fig 3). The two forward attachment points of the yoke are supported on each side of the tunnel by a roller in a circular arc track. This permits -6 to +6 degrees of sideslip. The sideslip angle is controlled from

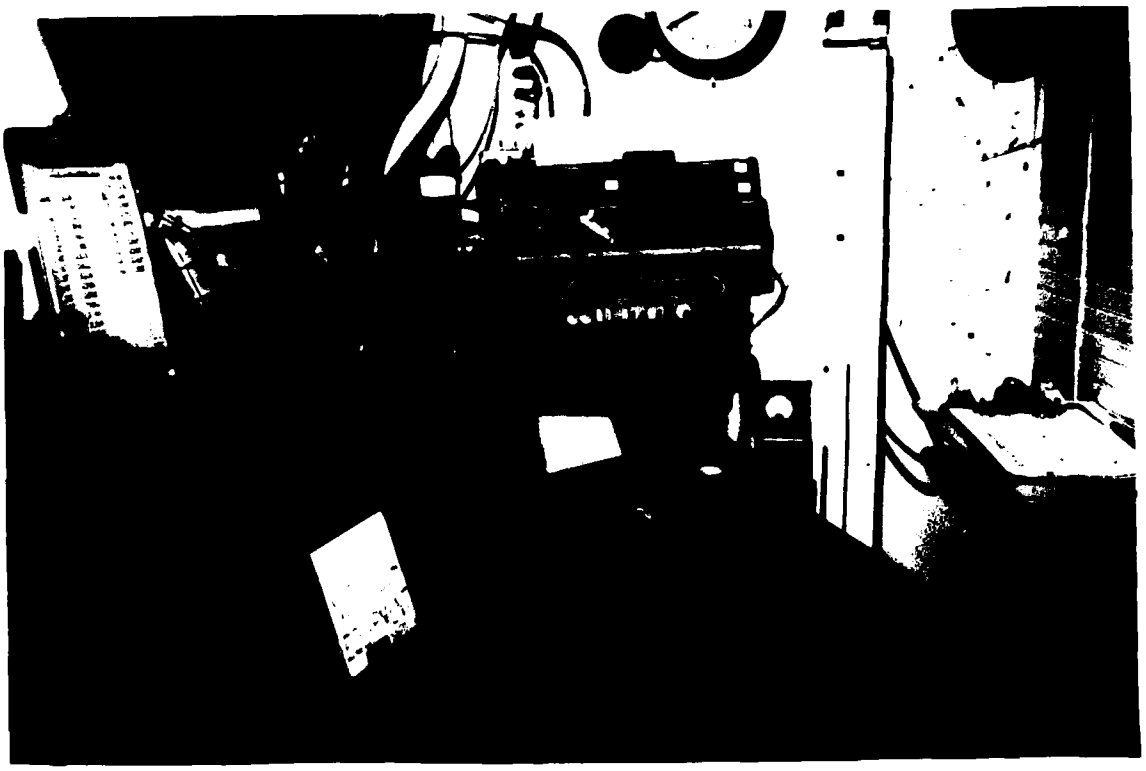

Fig 4. Tunnel operator's station, AFIT 5 foot wind tunnel.

the tunnel operator's station (see Fig 4) through direct control of a D.C. cable drive motor. A potentiometer attached to the closed loop, cable drive provided direct readout of the sting sideslip angle. (see Fig 5). Pitch was controlled by adjusting the vertical height of the leg of the yoke. This was accomplished from the tunnel operator's position by direct control of a D.C. cable drive motor (see Fig 6). An open loop cable drive was used for pitch control with lead weights providing the necessary vertical tension. A potentiometer attached to the pitch, cable drive provided direct readout of the sting angle of attack.

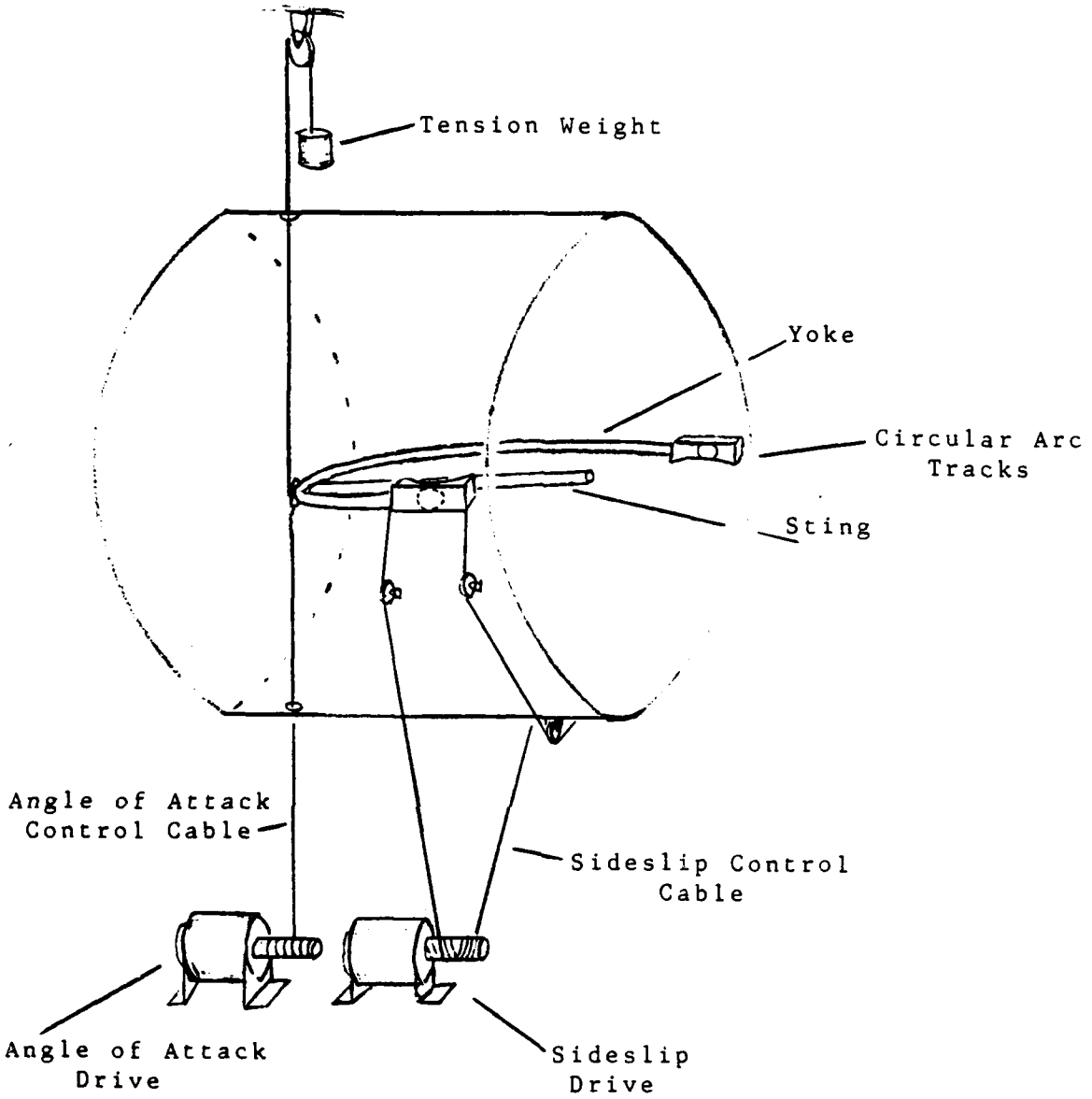

Fig 5. Angle of attack and sideslip drives, side view of test section.

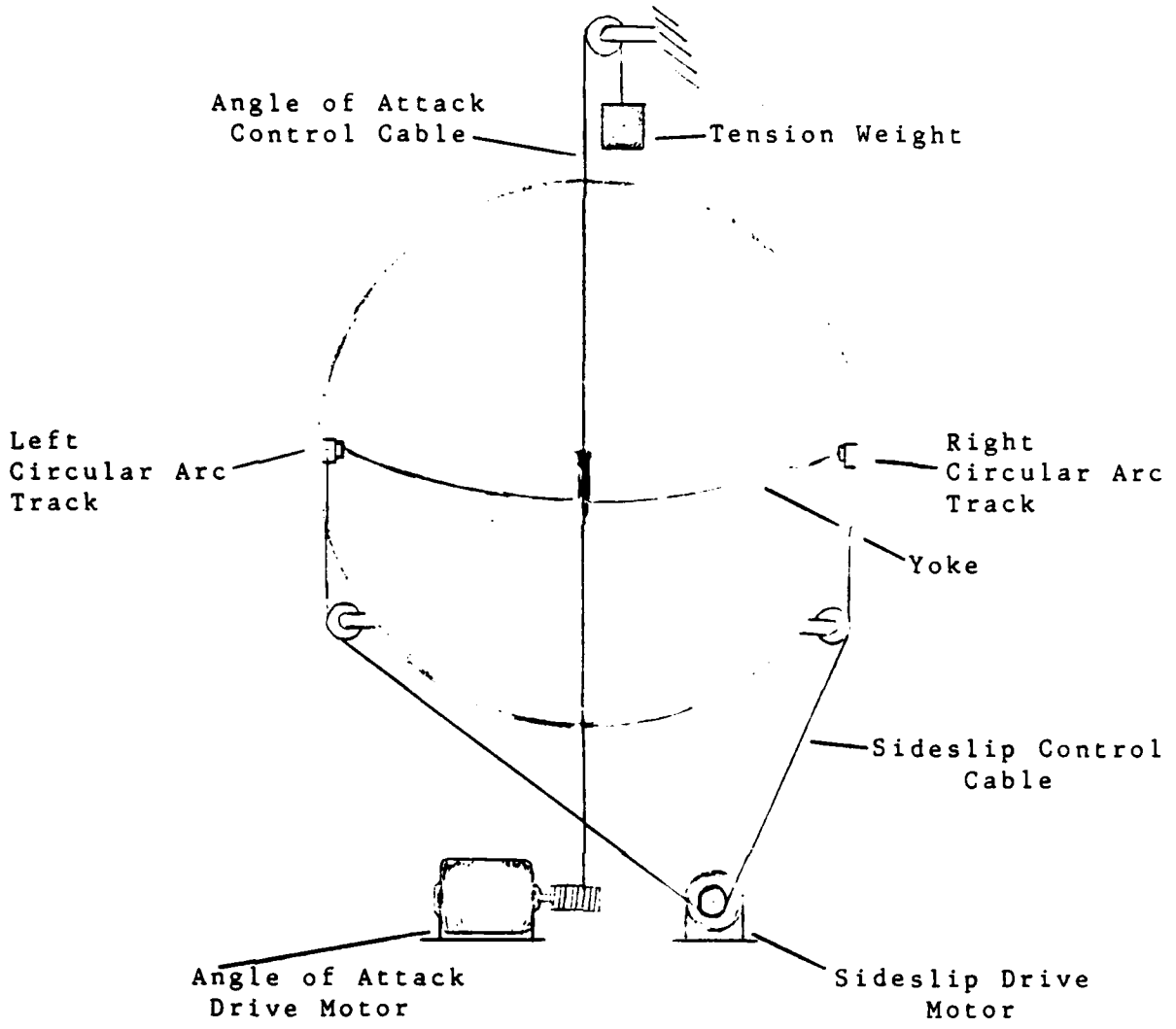

Fig 6. Angle of attack and sideslip drives, aft view of test section.

Potentiometer output was recorded by the Hewlett-Packard data acquisition system. Corrections for sting deflection and balance deflection were later applied by the H/P 85 computer software to compute the actual angles of attack and sideslip. A drawback to this system was that the actual control variables differ from those requested by the tunnel engineer by a few minutes of arc.

Calibration

Calibration of the strain gauge balance was done by manually test loading each of the six components separately and recording the output. Interactions among components was unavoidable in balances of this type. For accurate results, computer software subtracted the component interactions. A matrix of first order interactions was formed by reading the output of the five "unloaded" components after each component was test loaded. The interaction matrix was applied to all test data to compute the actual loadings.

Sideslip angle was calibrated using a "ray" board and a plumb. The ray board was installed in the tunnel with its apex directly under the center of curvature of the sting with the rays extending forward. The plumb was suspended from the center of the sting and allowed to come to rest over the calibrated ray board. Sideslip calibration was performed by rotating the sting with the sideslip drive to

reach a desired sideslip angle (referenced to the ray board) and recording the sideslip potentiometer output versus sting sideslip angle.

Angle of attack was calibrated using a special model leveling block and an inclinometer. The leveling block is an epoxy block which was cast to fit flush on the back of the test model. The top of the block was aligned parallel with the model X-Y plane and ground flat. Alignment pins in the block and holes drilled in the model insure accurate position. An inclinometer resting on the block was used to determine accurately zero roll angle and all calibration angles of attack. Pitch calibration was performed by rotating the sting with the pitch drive to reach a desired model angle of attack (referenced to the inclinometer) and recording the pitch potentiometer output versus the model angle of attack.

Model

The test model (see Figs 7-9) was constructed from a 1/32nd scale F-15 injection molded, plastic, hobby kit. The original kit came with only the two place canopy; this required the AFIT Model Shop to manufacture and fit the one place canopy which was used in this test. Metal stiffeners were added to the wings and stabilizers prior to final assembly. Flow-through inlets were added with an inlet to

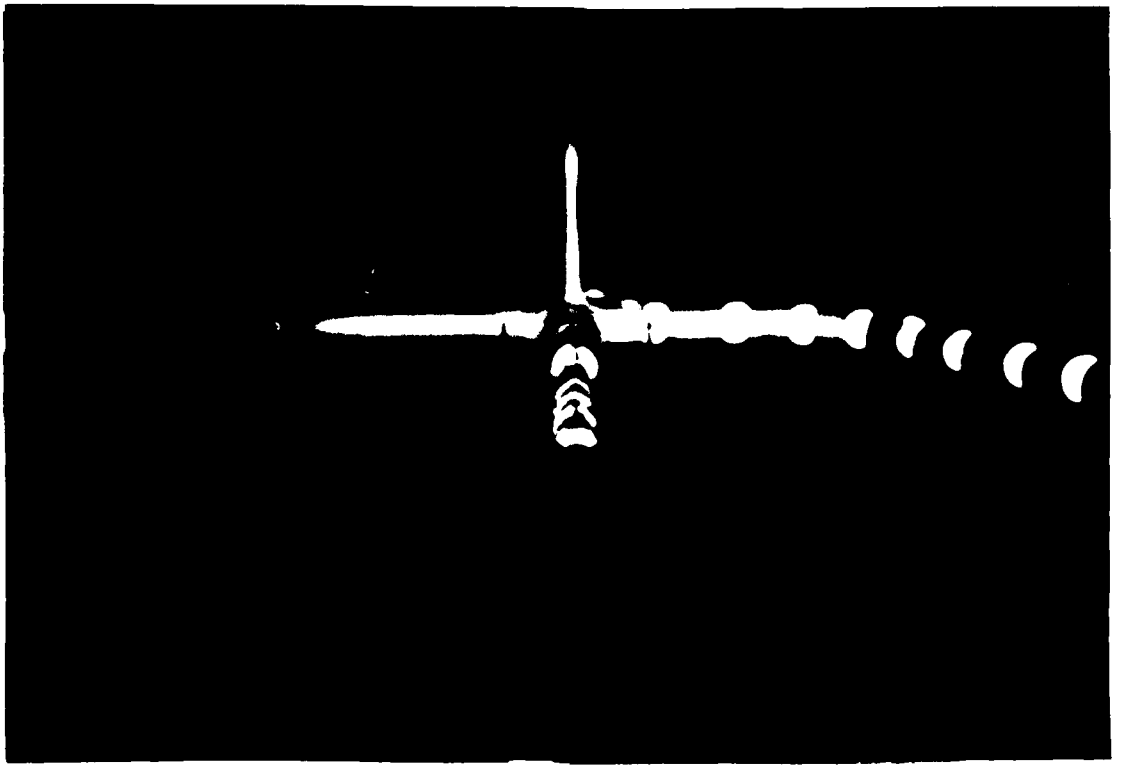

Fig 7. Test model without CFT's and strakes.

exhaust area ratio equivalent to military power. A stainless steel sleeve was permanently fitted into the fuselage to allow easy installation and removal of the balance. The sleeve was positioned so that the balance would be secured at the aircraft's normal center of gravity (25% MAC) (13). A high temperature epoxy casting resin was used to fill all internal voids to further stiffen the model. The engine inlet ramps were set to full down (-11 degrees) to simulate operations at high angle of attack.

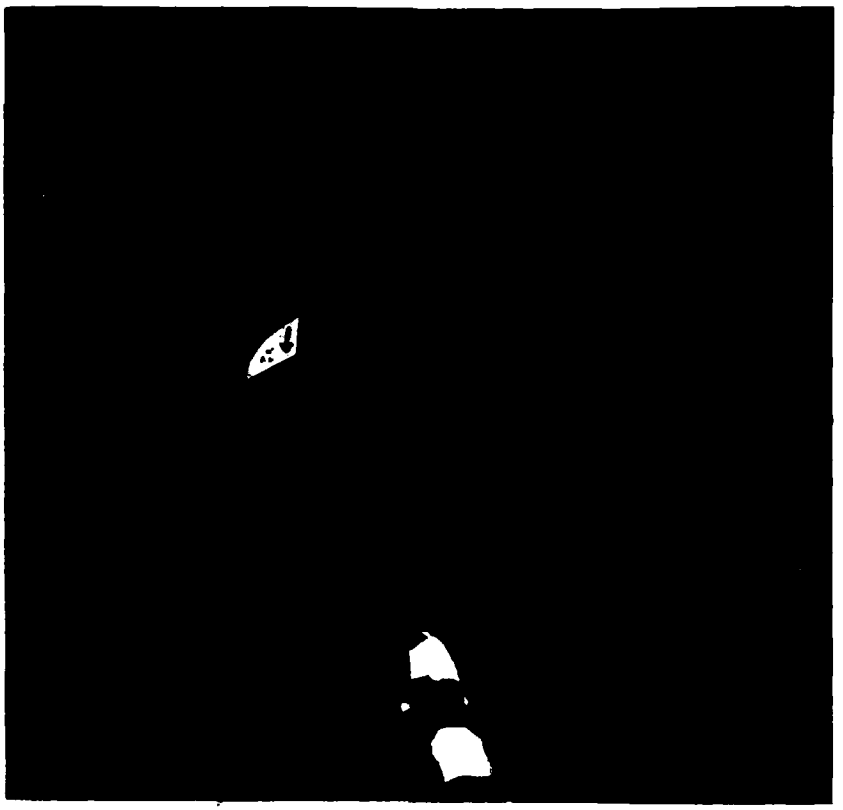

Fig 8. Model configured for high angle of attack. Note the forebody strakes and horizontal stabilizer set at -27 degrees.

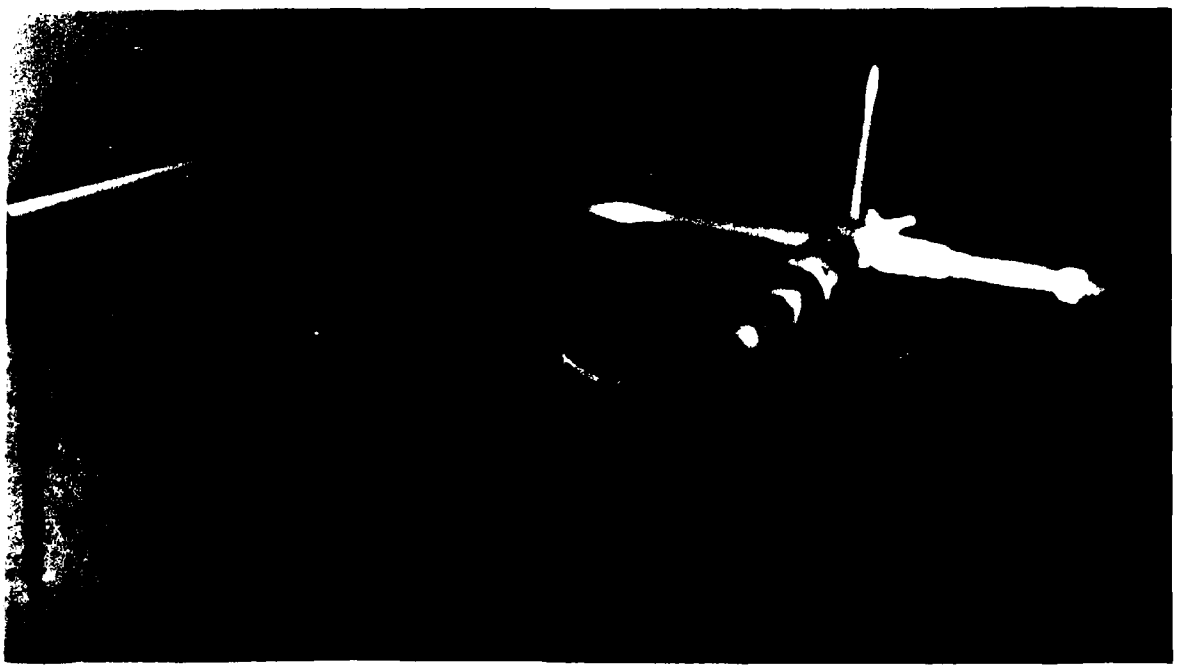

Fig 9. CFT only configuration. Model installed for high angle of attack testing.

The horizontal stabilizers could be set to neutral (0 degrees) or full leading edge down (27 degrees) to simulate a full aft stick configuration. Strakes, made of .020 inch aluminum, were manufactured with tabs for easy installation and removal (see Fig 2). Slots for the strakes' tabs were machined into the wing leading edges and the gun fairings at 0 degrees angle of incidence. All installation gaps and screw holes were smoothed with modeling clay before each run. (All angles are referenced to the aircraft's waterline.)

Once the model was assembled, it served only as a reasonably accurate blank from which a test article could be manufactured. Aesthetic details such as rivets and plate margins which improve the appearance of a hobby kit, destroy the performance of a wind tunnel model and must be removed. Many hours of additional measuring, sanding, and shaping went into the final, fully scaled test article.

III. Stability Theory

Longitudinal Static Stability Theory

For an aircraft to have positive static longitudinal stability, pitching moment coefficient (C_M) must decrease as the angle of attack (α) increases (with nose up pitching moment defined positive). Thus for positive static stability $\partial C_M/\partial\alpha$ (C_{M_α}) must be negative. In general the wing-body combination produces a destabilizing (positive) C_{M_α}. It is the addition of the tail and its stabilizing contribution that results in an overall longitudinally stable combination. Generally the effects of three areas on pitching moment are considered: wing, body, and tail. Neglecting propulsion effects and assuming the existence of a true aerodynamic center.

$$C_{M_\alpha} = C_{L_\alpha}(h - h_{n_{wb}}) - \bar{V}_H \frac{\partial C_{L_t}}{\partial \alpha} \tag{1}$$

where the effects of the wing-body and tail are separated. Following a development in Chapter Six, Reference 4, this can be simplified to:

$$C_{M_\alpha} = C_{L_\alpha}(h-h_n) \tag{2}$$

where,

$$h_n = h_{n_{wb}} - \frac{1}{C_{L_\alpha}} \frac{\partial C_{M_{ac_{wb}}}}{\partial \alpha} - \bar{V}_H \frac{\partial C_{L_t}}{\partial \alpha} \tag{3}$$

$$K_N = (h_n - h) \tag{4}$$

K_N is the static margin which clearly must be positive in sign for positive longitudinal stability. While the pitching moment effects of the wing, body, and tail are combined in Eqn (2), it must be emphasized that simple superposition of the aerodynamic forces which act upon them separately does not give the correct result (4:204-209).

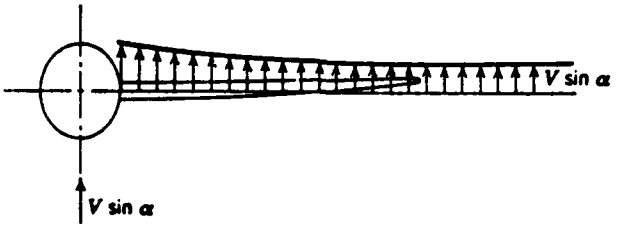

Fig 10. Upwash pattern induced along wing by the cross-flow past the body.

With the addition of the CFT's to the F-15, the complex relationship between the wing-body flow fields was changed. When the body axis is at angle α to the free stream, there is a cross-flow component V Sin α. The body distorts this flow locally, leading to cross-flow components that can be of the order 2V Sin α at the wing-body intersection. This results in a change in the wing lift distribution (see Fig 10) (4:204-205). The original F-15 minimized this cross-flow by judicious placement and shape of the gun fairings (see Fig 11). Installation of the CFT's allows the

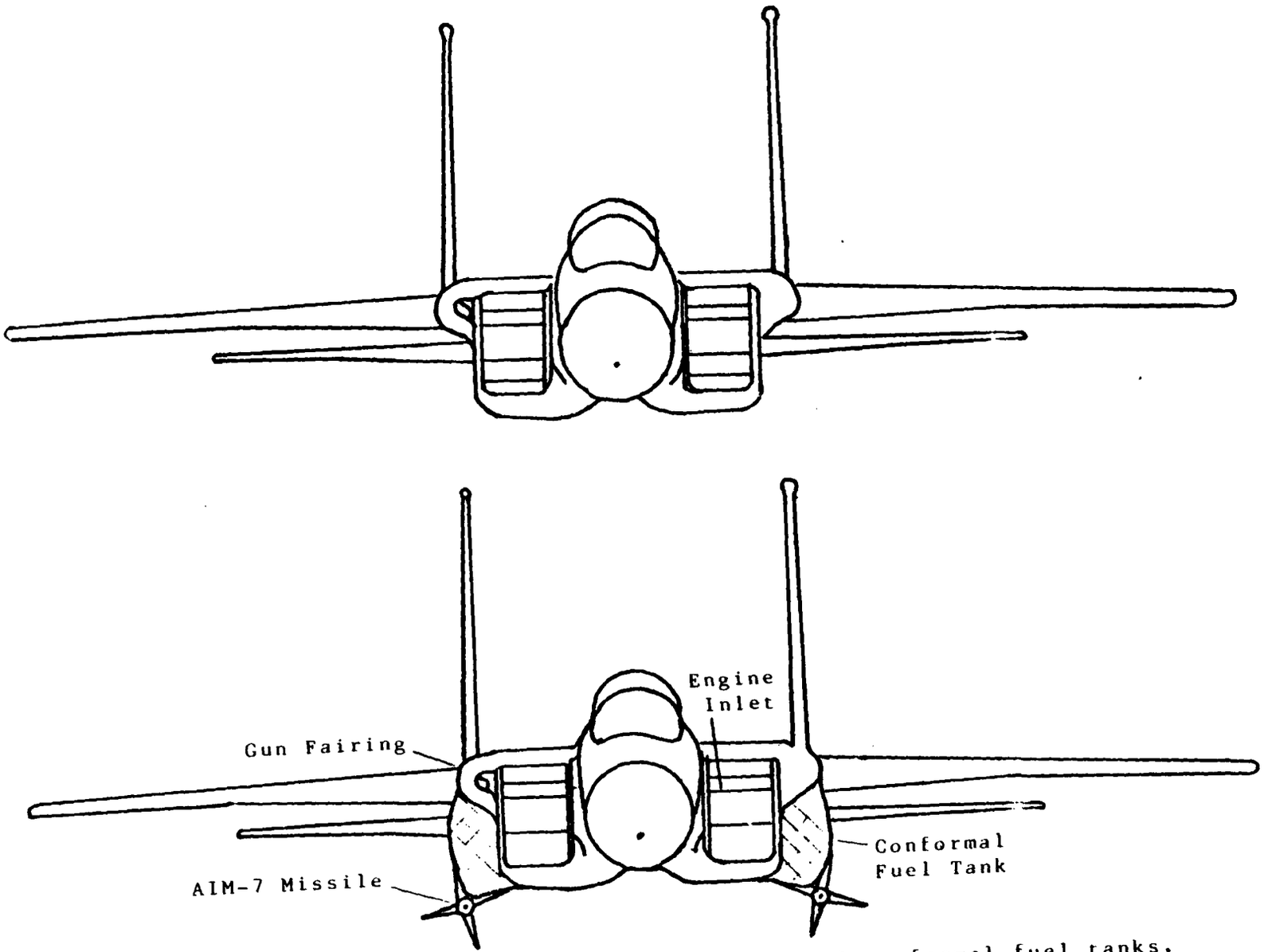

Fig 11. Change in cross-section with addition of conformal fuel tanks.

cross-flow to wrap smoothly around the fuselage increasing the effect of the body on the wing. The result of adding a body to a wing may usually be interpreted as a destabilizing shift (forward) of the mean aerodynamic center, an increase in the lift-curve slope, and a negative increment in $C_{M_{ac}}$ (4:205).

The addition of forebody strakes to a CFT equipped F-15 will diminish the strength of the cross-flow and restore the wing-body relationship nearer to that of the original aircraft. Use of strakes is not, however, without problems. The strake is a small, thin, highly swept wing installed forward of the main wing. Its own aerodynamic center when added to the wing's will cause the mean aerodynamic center to shift forward. At high angles of attack, however, the vorticity of the strake will energize the flow over the wing and delay the forward center of pressure shift which occurs with separation. Several researchers have tried to predict the high angle of attack performance of strakes using calculations of leading edge suction (7); however, wind tunnel testing remains the best means to evaluate the total configuration (10).

Lateral Static Stability Theory

For positive directional stability, a perturbation in sideslip (β) must produce a restoring moment (C_N). The direction of C_N must be such that the velocity of the

vehicle tends to remain in the plane of symmetry. This requires that a plot of C_N vs β have positive slope ($\partial C_N/\partial\beta = C_{N_\beta}$) for positive stability. The term "weathercock stability" is aptly derived from this definition. C_{N_β} is found from wind-tunnel measurements of the yawing moment, or it can be estimated by synthesising the contributions of the various components of the vehicle (4).

The addition of CFT's to the F-15 causes a reduction in the directional stability. A development from Reference 4 leads to

$$C_{N_\beta\ fin} = \frac{\partial C_{N_f}}{\partial\beta} = V_v \frac{\partial C_{L_f}}{\partial\beta} = V_v\, a_f \left(1 - \frac{\partial\sigma}{\partial\beta}\right) \qquad (5)$$

where $\partial\sigma/\partial\beta$ is defined as the sidewash factor. The CFT's cause a reduction in the gun fairing's ability to disrupt crossflow (see Fig 11). This leads to an increasing sidewash factor and a corresponding decrease in directional stability.

Dihedral effect (C_{ℓ_β}) is defined as $\partial C_\ell/\partial\beta$. Its effect on lateral stability is paramount. While the primary contribution to C_{ℓ_β} comes from the wing, the fuselage, horizontal tail and vertical fin also play an important part. Consider a fuselage yawed with respect to the main stream flow. The resulting crossflow induces vertical velocities as it moves around the fuselage (see Fig 12). When the induced vertical velocities are combined with the

mainstream velocity, alterations of the local wing angle of attack occur (4). The addition of CFT's to the fuselage results in change in the crossflow. While an increase in the local angle of attack causes an improvement in lateral stability ($C_{\ell_\beta} < 0$), the effect of the CFT's on the cross-flow is difficult to predict. The vertical location of the wing has a significant influence on the dihedral effect.

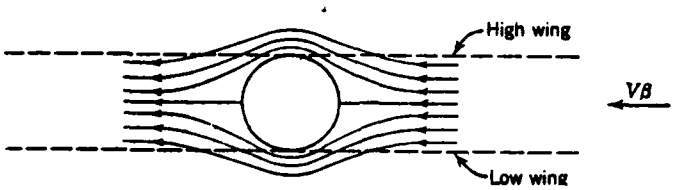

Fig 12. Influence of the body on dihedral effect.

The effect of strakes on lateral stability is also difficult to predict. Several experimenters have found that nose strakes can produce large increases in directional stability (10). There is, however, little experimental evidence that forebody strakes have this useful effect. If one considers an aircraft at high angle of attack, yawed flight, it would be reasonable to expect a delay in the separation of the flow over the wing to improve the flow over the fin. Historically this has been difficult to achieve. The improvement of directional stability with F/B strakes, if possible, requires thorough wind tunnel investigation.

$C_{N_{\beta\ DYN}}$ is a useful parameter for predicting spin entry conditions. It is defined as

$$C_{N_{\beta\ DYN}} = C_{N_\beta} \cos\alpha - (I_Z/I_X)C_{\ell_\beta} \sin\alpha \qquad (6)$$

for principal axes, and it must be positive for directional stability. Various authors have used the parameter for predicting lateral-directional instability and found it to yield a reasonable correlation with test data (1). It also provides a single parameter which combines effects of C_{N_β} and C_{ℓ_β} for evaluation of the overall lateral stability of test configurations.

IV. General Test and Data Analysis Procedures

General Test Procedure

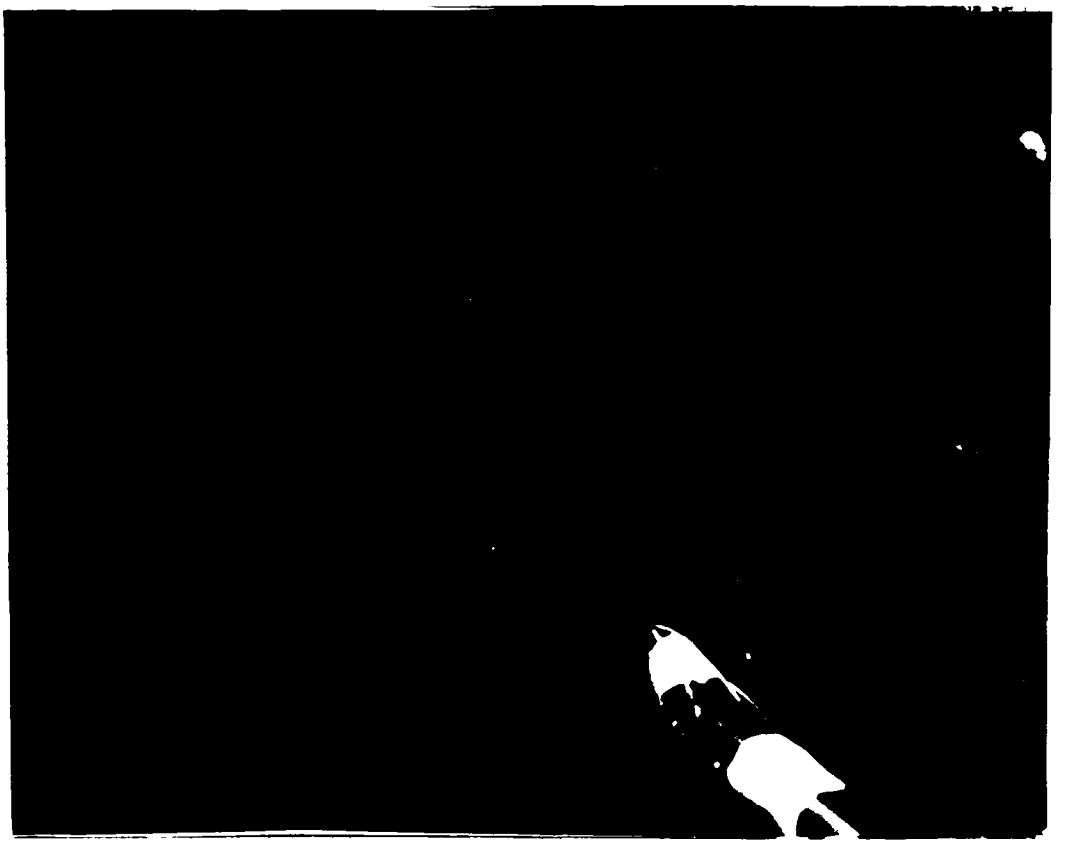

Fig 13. Model installed on hinged sting with a 20 degree prebend.

The test was performed in three segments. Low angle of attack longitudinal stability was evaluated first. This was followed by high angle of attack longitudinal stability tests and high angle of attack lateral stability tests. The experiments were accomplished at a dynamic pressure of approximately 37 psf, and a Reynold's number of 1.14×10^6

per ft to 1.16 x 10^6 per ft. For all low angle of attack sweeps, the horizontal tail was set at 0 degrees, while a setting of -27 degrees was used for high angle of attack sweeps. The use of grit on the leading edges to simulate increased Reynold's number was evaluated by comparing sweeps made with "gritted" and "ungritted" configurations. With the exception of drag, no significant differences were noted, and "gritting" was discontinued.

The low angle of attack longitudinal stability tests were performed with a hinged sting (see Fig 13) set at 0 degrees. This allowed an α range of -4 to 26 degrees (the pitch drive's normal limits). Alpha sweeps were performed with β set at 0. All test points were approached from negative to positive α to avoid hysteresis. Data were recorded every 2 degrees.

High angle of attack longitudinal stability tests were performed with the hinged sting set at 20 degrees. This allowed an α range of 16 to 46 degrees. Alpha sweeps were performed with β set at 0, and test points were approached from negative to positive. In some cases, where response was linear, data were recorded at 4 rather than 2 degree increments.

Because the configurations were expected to be laterally stable at low angles of attack, lateral stability tests were required only at high angles of attack. Beta sweeps from +6 to -6 degrees were performed while holding α

constant. Data were recorded every 2 degrees during the sweeps. The hinged sting was used to allow high angles of attack. The α range was 16 to 44 degrees with increments of 4 degrees. All test points were approached from the same direction to minimize hysteresis.

Data Analysis

The conditions under which a model is tested in a wind tunnel are not the same as those in free air. There is no difference traceable to having the model still and the air moving instead of vice versa, but the longitudinal static pressure gradient and the jet boundaries usually present in the test section will produce extraneous forces that must be subtracted out. A long list of corrections which may be required can be found in any text on wind tunnel testing. Fortunately few tests require most of these corrections (7).

Aerodynamic data presented in this paper were corrected for solid blockage, wake blockage, horizontal buoyancy, and flow angularity. The dynamic pressure, q, used in non-dimensionalization was also corrected for total blockage.

Data from the strain gauge balance were corrected for first order balance interactions (see Section II). The 6 component data were then combined to arrive at the conventional body axis lift (L), pitching moment (M), drag (D), yawing moment (N), and rolling moment (ℓ) (see Fig 14).

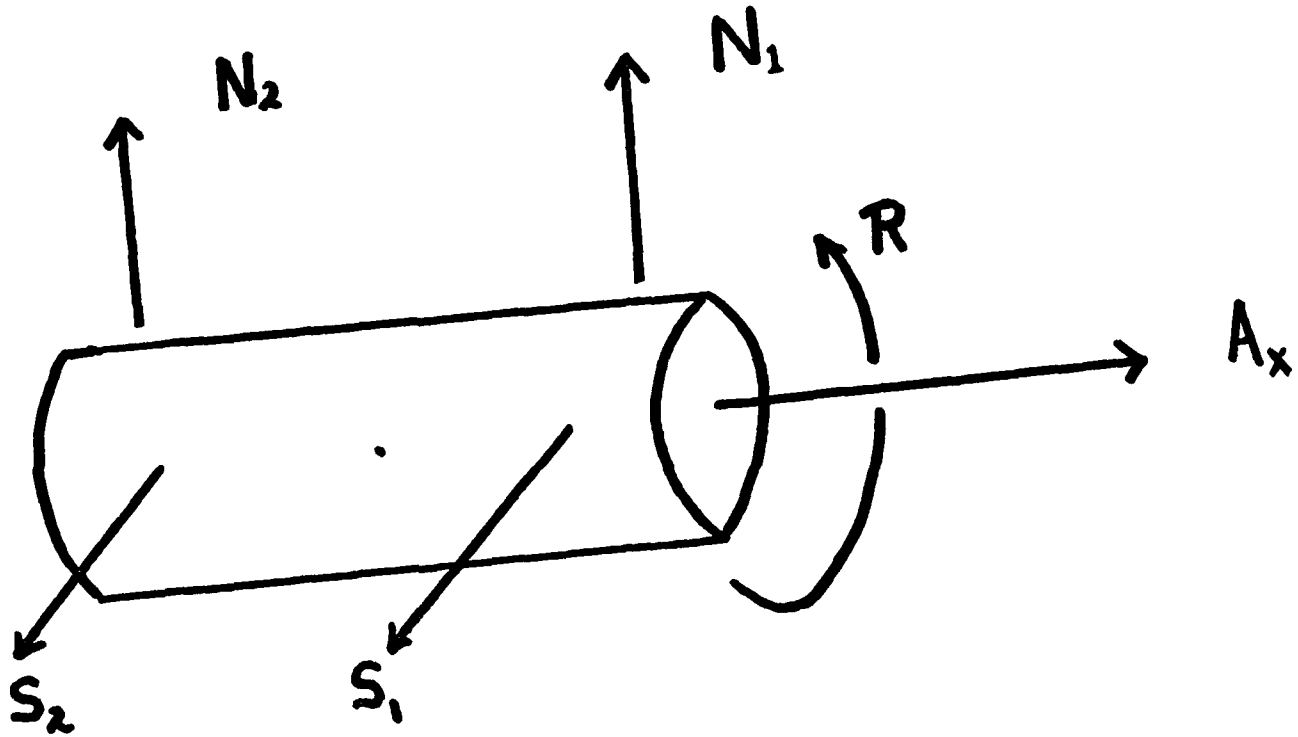

Fig 14. Task strain gauge balance typical positive axis system.

Care must be taken to differentiate between the symbols L (lift) and ℓ (roll). The H/P 85 computer performed the following calculations to arrive at the nondimensional data which were tabulated and plotted. Following the convention established in ref 7, data which has not yet been corrected for wind tunnel errors is subscripted "u" (uncorrected).

A blockage correction factor (ε) which combines the effects of solid and wake blockage must be arrived at first. Following the development of ref 7, it can be shown that

$$\varepsilon = \varepsilon_{wb} + \varepsilon_{sb} \tag{7}$$

where $\varepsilon_{wb} = (S/4C)C_{D_u}$ and $\varepsilon_{sb} = KV/C^{3/2}$.

The parameter S is the model wing area, C is the tunnel test section area, K is a constant for the test shape, and V is the model volume (7).

Since the tunnel velocity varies with blockage, a corrected "q"

$$q_b = q_u (1 + 2\varepsilon) \tag{8}$$

must be used in nondimensionalization.

Flow angularity was corrected for by adding the lift curves for an erect and an inverted model. The curves should sum to zero. Any deviation is due to flow angularity and can be treated as a constant to be subtracted from the measured α.

Horizontal buoyancy is a correction to drag for the longitudinal variation in tunnel static pressure caused by a thickening boundary layer. The change in drag can be calculated from

$$\Delta D_b = (-dp/d\ell)V \tag{9}$$

where $-dp/d\ell$ is a constant for the tunnel, and V is the model volume.

Aerodynamic forces and moments can now be corrected and nondimensionalized following conventional rules (see references 4 and 7).

LIFT: $$C_L = L_u/q_bS \tag{10}$$

DRAG: $$C_D = \{(D_u - \Delta D_b)/(q_bS)\} + (.125)C_L{}^2S/C \tag{11}$$

PITCHING MOMENT $$C_M = M_u/(q_uSc) \tag{12}$$

YAWING MOMENT: $$C_N = N_u/(q_uSb) \tag{13}$$

ROLLING MOMENT: $$C_\ell = \ell_u/(q_bSb) \tag{14}$$

Longitudinal data were evaluated by plotting C_L vs α, C_M vs α, and C_L vs C_D (Appendix B). Lateral data were evaluated first by plotting C_N vs β and C_ℓ vs β (Appendix C).

$C_{N_{\beta\ DYN}}$ was calculated using the Aeronautical Systems Division's Cyber computer. Because accurate slopes, C_{N_β} and C_{ℓ_β}, were needed, the lateral data were approximated using the method of cubic splines provided by IMSL. The derivates of the "splined" data were then taken at the original data points. These derivatives, C_{N_β} and C_{ℓ_β}, were then used to calculate $C_{N_{\beta\ DYN}}$ (see Section III). $C_{N_{\beta\ DYN}}$ was plotted vs β to help evaluate spin susceptibility (Appendix C).

V. Results

A parametric family of twenty forebody strakes were evaluated for an CFT equipped F-15 in the AFIT 5 foot Wind Tunnel. The objective was to define further strake design and installation characteristics relevant to stability and performance optimization. Parameters of interest were strake installation angle of incidence and strake area (see Fig 2). Aerodynamic data collected include C_M, C_L, C_D, C_N, and C_ℓ (roll). The spin susceptibility parameter, $C_{N_{\beta\ DYN}}$, was synthesized following the method described in Sections III and IV. Data were plotted for evaluation of configuration performance (see Appendices B and C).

Longitudinal Data

Previous research had indicated that strakes would increase pitch stability at high angles of attack. In addition, lift could be increased while decreasing drag. All three would be valuable improvements for the CFT equipped F-15.

All moments were resolved about the 25% MAC (Mean Aerodynamic Chord). Since both the magnitude and direction of moments are directly related to the position of the center of mass, care must be taken in making absolute statements about stability. An unstable configuration at

25% MAC may be stable at 20% MAC. A standard, however, must be defined and maintained for engineering evaluation to be meaningful. All statements about pitch stability should be considered with respect to the selected center of mass.

Significant improvements in pitch stability were recorded at angles of attack from 38 to 44 degrees. The parameter C_{M_α} improved from -.005/degree to less than -.008/degree with the addition of forebody strakes. As documented by several previous researchers, the strake area is the dominant characteristic in achieving large changes in pitch stability.

While strake area controlled the magnitude of the change, the strake angle of incidence controlled the quality of the change. Strakes with 0 degrees angle of incidence generally showed undesirably strong nonlinearities at angles of attack of 16 to 24 and 40 to 44 degrees (see Fig 15). In these cases, C_{M_α} was frequently positive (unstable) between 16 and 24 degrees angle of attack. For each strake family (see Appendix A) one of the angles of incidence always produced a C_M vs α curve which was very linear. While this configuration did not completely cure the droop in pitch stability between 16 and 24 degrees, it did minimize the loss (see Fig 16). In several cases it caused positive pitch stability throughout the high angle of attack range.

Low angle of attack pitch stability was evaluated for each configuration. Strake areas were limited to .65% to

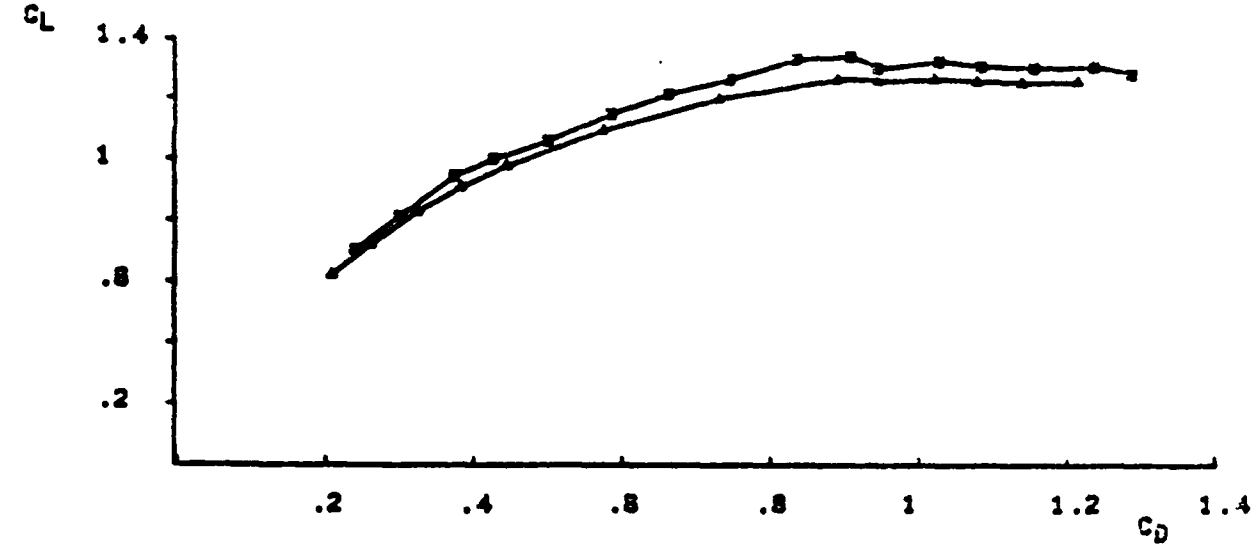

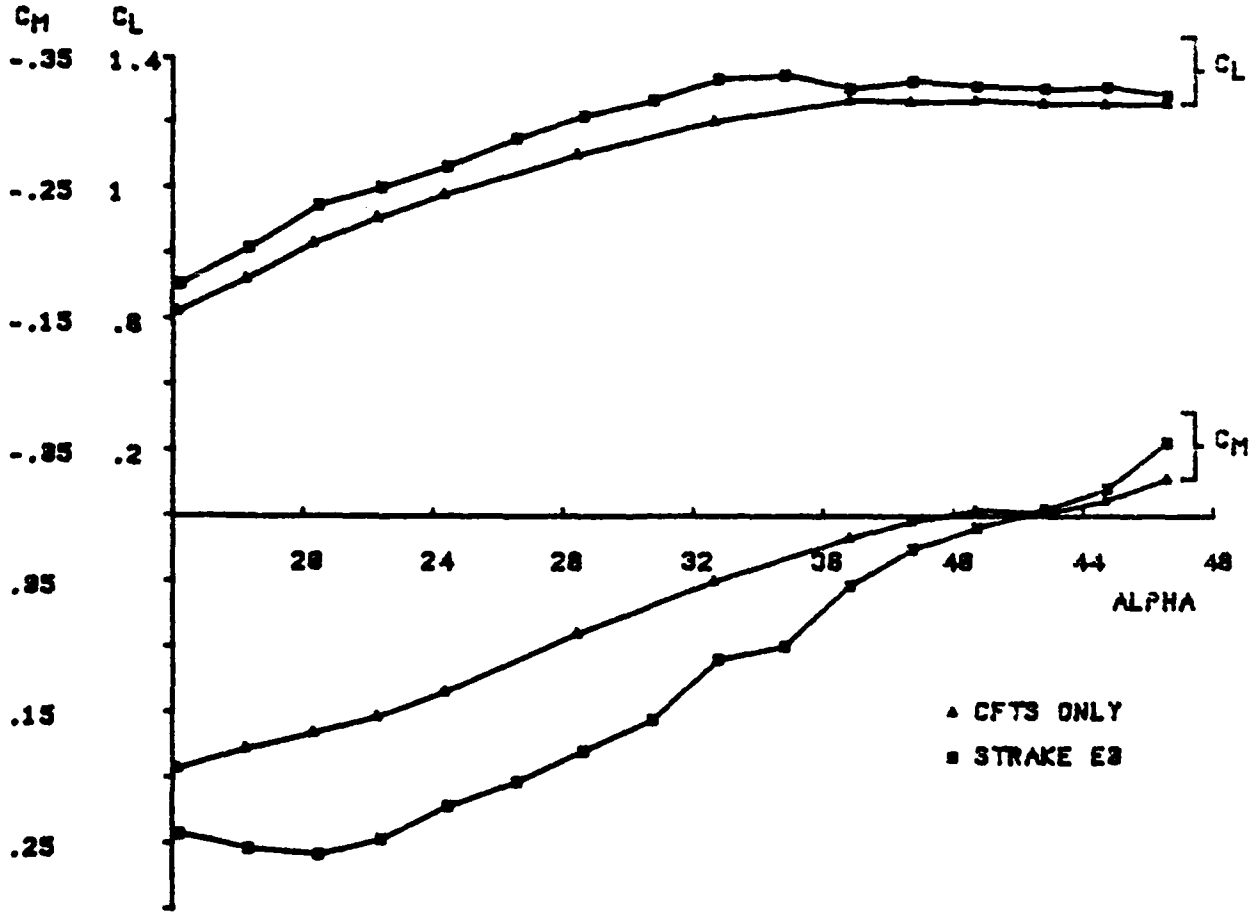

FIG 15. LONGITUDINAL STABILITY DATA FOR AN F-15 WITH ONLY CFTS AND AN F-15 WITH CFTS AND F/B STRAKES.

2.2% of wing area, and only small changes in low angle of attack stability were expected due to the forward shift in the neutral point. All configurations, however, demonstrated large losses in pitch stability from -4 to 24 degrees angle of attack. The larger strake areas, which produced the significant gains in high angle of attack stability, exhibited the greatest losses in low angle of attack stability. For all but the smallest strake areas, pitch stability was either neutral or unstable in this region.

Pitch stability at low angles of attack does vary with strake incidence angle; however, the effects are less obvious. Close examination of figures B-17 through B-20 shows that from -4 to +2 degrees angle of attack, C_{M_α} becomes more positive (less pitch stable) with increasing angle of incidence. The effect reverses, however, from 2 to 14 degrees angle of attack; in this region stability becomes more positive with increasing angle of incidence. The same effects occur with all of the configurations tested; however, they are more easily seen when the strake area is large.

Significant increases in C_L and C_L/C_D were realized. Once again strake area controlled the magnitude of the change, while the incidence angle controlled its quality. Plots of C_L vs α indicate an increase in C_L from 1.27 for the CFT only to about 1.38 for strakes of 2.2% wing area.

Plots of C_L vs C_D at high angle of attack show about a 9% increase in C_L/C_D with the largest strakes. Strake incidence angles of 0 degrees produced nonlinearities in C_L which were visible in both plots. The same incidence angle which produced the most linear C_M vs α graph also produced the smoothest C_L plots.

At low angles of attack the addition of strakes made very small changes in plots of C_L vs α and C_L VS C_D. Most significant was an almost undetectible increase in C_{D_o} (drag at zero lift) for all of the strake configurations. Even the -9 degree incidence angle on the largest strakes did not increase C_{D_o} noticeably.

Lateral Data

Previous researchers have indicated that forebody strakes may produce small improvements in lateral stability if properly tuned to the configuration (10). Twelve strakes were evaluated on the CFT equipped F-15 to determine if the aircraft was sensitive to the parameters of interest. The spin susceptibility parameter $C_{N_{\beta\ DYN}}$ was plotted versus β to evaluate each configuration (see Appendix C).

Several configurations do show improvements at angles of attack greater than 30 degrees (see Fig 16). The same configurations, however, exhibit decreases in stability between 16 and 24 degrees. The C_N vs β and C_ℓ vs β data show the reason for this. The strakes produced either no

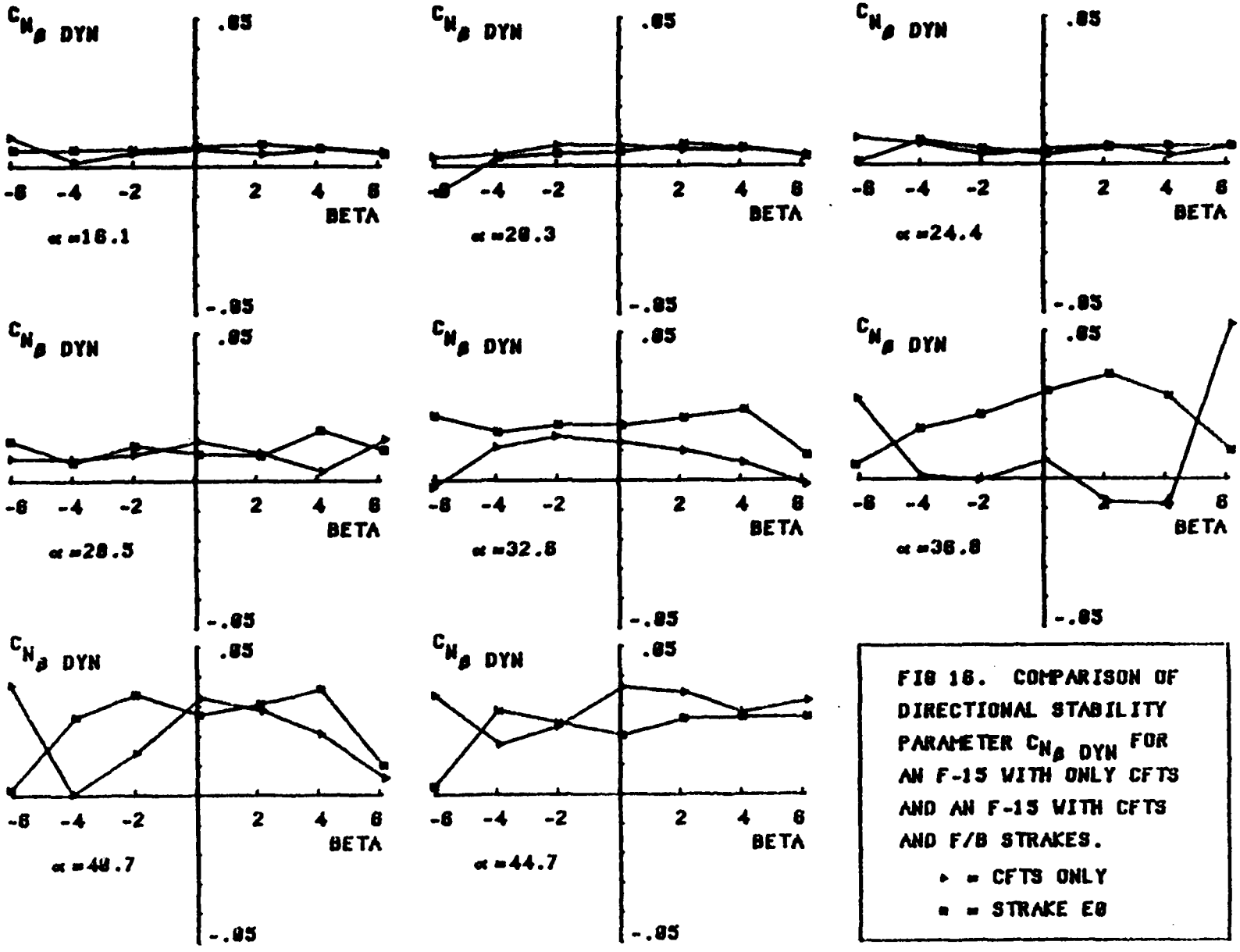

FIG 16. COMPARISON OF DIRECTIONAL STABILITY PARAMETER $C_{N_\beta\ DYN}$ FOR AN F-15 WITH ONLY CFTS AND AN F-15 WITH CFTS AND F/B STRAKES.

▸ = CFTS ONLY

▪ = STRAKE E8

changes or small losses to C_N throughout the β range; however C_ℓ improved (decreased) dramatically above 30 degrees angle of attack. Examination of

$$C_{N_{\beta\ DYN}} = C_{N_\beta} \cos\alpha - (I_Z/I_X)C_{\ell_\beta} \sin\alpha$$

shows that with C_{ℓ_β} normally negative, and C_{N_β} normally positive and small, as angle of attack increases C_{ℓ_β} becomes the dominant term. To generalize, at lower angles of attack the sign of $C_{N_{\beta\ DYN}}$ will be determined by the sign of the C_{N_β} of the aircraft without strakes, and at higher angles of attack the strakes will force a positive $C_{N_{\beta\ DYN}}$ by dramatically decreasing C_{ℓ_β}.

The lateral data also appears to vary when strake incidence angle is changed. Close examination of figures C-5 through C-9 shows large changes in lateral stability at high angles of attack. More experimentation is required, however, before it can be concluded that strake incidence angle is the dominant cause of these stability changes.

VI. Conclusions

The results of the wind tunnel evaluation of forebody strakes on a CFT equipped F-15 are presented in Section V and Appendices B and C. These data show mixed blessings resulting from the addition of strakes to the model in most areas.

While the high angle of attack longitudinal stability was improved, the low angle of attack stability decreased an alarming amount when the small size of the strakes was considered. Similarly the parameter $C_{N_{\beta\ DYN}}$ showed increases in high angle of attack lateral stability with the addition of strakes; however, the strakes were unable to improve the stability between 16 and 24 degrees angle of attack and sometimes worsened it.

When the lift to drag ratio was considered, strakes had no drawbacks. A 9% increase in C_L/C_D was recorded at high angle of attack, while the drag at zero lift (C_{D_o}) showed virtually no increase in low angle of attack drag. The lack of change in C_{D_o} is particularly significant when the high negative incidence of some of the strakes is considered.

As anticipated the strake area controlled the magnitude of the changes in the high angle of attack stability and lift. Surprising importance, however, can be attached to the new parameter "strake incidence angle."

It was originally thought that perhaps strake incidence

might be of some use in delaying the point at which maximum vorticity occurs. This would allow the designer to move the α at which $C_{L_{MAX}}$ occurs, and permit minor reshaping to C_L vs α and C_M vs α curves. While this does occur, the strake incidence angle's effect on the entire curve was unexpected.

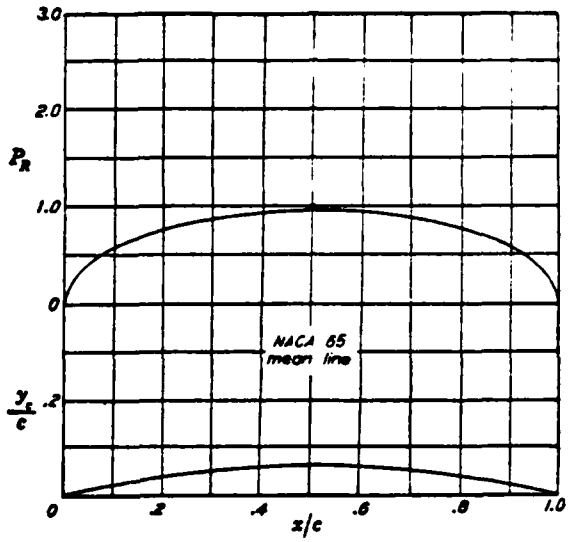

Fig 17. Mean camber line of a NACA 65 airfoil.

In every case tested, strakes installed at the same incidence angle as the wing resulted in data with large deviations from a smooth curve (for longitudinal data). Decreasing the strake incidence angle to -3 or -6 degrees (depending on strake size) did not change the height of the curves significantly; however, it did smooth the curve noticeably. This probably indicates a stronger more stable vortex is being generated by the strake-wing combination.

The reason for the strake incidence angle's effect on the entire flow can be explained if one considers the mean

camber line of a fighter wing in use today (see Fig 15). The slope of the mean camber line becomes very steep as one approaches the leading edge. An uncambered strake installed parallel to the wing's cord line would produce a flow discontinuity at the strake-wing juncture. This discontinuity would likely result in a less stable vortex and early vortex bursting. The optimum flow pattern would likely result from a strake whose contour smoothly matched that of the wing. Decreasing the incidence angle of the strake approximates the optimum contour and clearly results in smoother, more predictable performance.

An unreserved endorsement of the use of forebody strakes to improve the performance of the CFT equipped F-15 is not possible; however the strake characteristics which effect performance are now better understood. Strake area remains the most important single variable, but the size and shape of the strake must be properly oriented to achieve stable vortex generation. As previous research has shown, an improperly optimized strake can do more harm than good (10).

Finally, the knowledge that strakes are an asset at high angle of attack, and a hindrance at low angle of attack is not new. Dr. Rao (see Ref 8) investigated the use of hinged strakes in 1980. In his approach strakes are carried flush with the fuselage at low angles of attack. When pressure sensors detect advancing separation on the

wing, actuators actively deploy the strakes into the flow just the right amount to optimize performance. In this method, however, the trailing edge of the strake may not even meet the wing. This causes a large discontinuity in the flow, and if these conclusions are correct, should lead to ragged performance curves. A system which employed actuated strakes which were contoured to the wing camber would not likely suffer the low angle of attack problems documented in this report.

VII. Recommendations

This thesis leaves two questions unanswered. Both the high angle of attack data and low angle of attack data showed a large unexpected drop in C_{M_α} between 16 and 20 degrees angle of attack whenever strakes were installed. Several attempts were made in the wind tunnel to determine the cause of this loss of stability. It is possible that the strake vorticity is interacting with the horizontal stabilizer changing its local angle of attack; however, no conclusive answers were produced.

Any attempt to add strakes to the F-15 will likely show this same frustrating loss of stability. A water tunnel investigation of the CFT equipped F-15 would probably show the cause of this stability loss and hopefully lead to its cure.

As mentioned in the previous section, an actuated strake which was contoured to match the wing camber would have all of a strake's advantages with none of its drawbacks. An investigation into this area should be made to confirm or deny the importance of strake angle of incidence, and add greatly to our body of knowledge on this subject.

Bibliography

1. Calico, Robert A. "A New Look at $C_{N_{\beta\ DYN}}$." AIAA J. of Aircraft. Vol 16, No. 12, 1979, pp. 895-896.

2. Campbell, James F. "Vortex Flow Aerodynamics-An Emerging Design Capability." Astronautics & Aeronautics. May 1981.

3. Carr, Peter C. and William P. Gilbert. Effects of Fuselage Geometry on Low-Speed Lateral-Directional Characteristics of Twin Tail Fighter Model at High Angles of Attack. NASA Technical Paper 1592, December 1979.

4. Etkin, Bernard. Dynamics of Atmospheric Flight. New York: John Wiley and Sons, Inc. 1972.

5. Jane's All The World's Aircraft 1982-83. Jane's Publishing Co. Limited, London, England.

6. Kingman, Bruce B. F-15 With Conformal Fuel Tanks (CFT) High Angle of Attack (AOA) Wind Tunnel Test. A Published Report. Wright-Patterson AFB, OH: HQ AFSC/ENFTC, 4 February 1983.

7. Pope, Alan and J. J. Harper. Low Speed Wind Tunnel Testing. New York: John Wiley and Sons, Inc. 1966.

8. Rao, Dhanvada M. "Hinged Strakes for Enhanced Maneuverability at High Angle of Attack." Journal of Aircraft. Vol. 19, 1981.

9. Skow, A. M. "Modern Fighter Design for High Angle of Attack." AGARG-LS-121, March 1981.

10. Smith, C. W. and C. A. Anderson. "Design Guidelines for the Application of Forebody and Nose Strakes to a Fighter Aircraft Based on F-16 Wind Tunnel Experience." AGARD-CP-247, October 1978.

11. Smith, C. W., J. N. Ralston, and H. W. Mann. "Aerodynamic Characteristics of Forebody and Nose Strakes Based on F-16 Wind Tunnel Experience." NASA Contractor Report 3053, July 1979.

12. Sprinkel, David M. Wind Tunnel Test of a C-18 Aircraft Modified with the Advanced Range Instrumentation Aircraft Radome. Unpublished Thesis. Wright-Patterson AFB, OH: Air Force Institute of Technology, December 1982.

13. Thor, Wayne. Personal Interviews with the Author. April-September 1983.

14. Thor, Wayne. Summary Report of ASD Wind Tunnel Investigation of the High Angle of Attack Characteristics of CFT Equipped F-15 Configurations. An Unpublished Report. Wright-Patterson AFB, OH: ASD/TAEF, June 1983.

15. Vigevano, L. Strake-Wing-Body Combinations. AGARD-LS-121, March 1982.

Vita

Terry A. Duncan was born on March 19, 1950 in Dayton, Ohio. He received a Bachelor of Science Degree in engineering mechanics and his commission from the U.S. Air Force Academy on 4 June 1975. He attended pilot training at Columbus Air Force Base, Mississippi and was then assigned to the C-141 at McGuire Air Force Base, New Jersey. He was assigned to AFIT in May 1982.

Appendix A

Configurations

Previous research had indicated that gothic shaped strakes were the most likely to produce the desired changes in lateral and longitudinal stability. The chord length of the strake (L) was limited by the distance between the wing root and the gun port on the right gun fairing. With L at its maximum length, the strake planform areas were still smaller than desired for optimization. The chord length could not, however, have been made longer and still practically investigated the effects of incidence angle. This left the strake span (S) as the variable to control area changes. Professor Larsen suggested the function

$$y = (Kx / 12)(2L-x)$$

where $K = (12S) / L$. This function produces the desired gothic shape and results in a slope parallel to the flow at the strake-wing juncture.

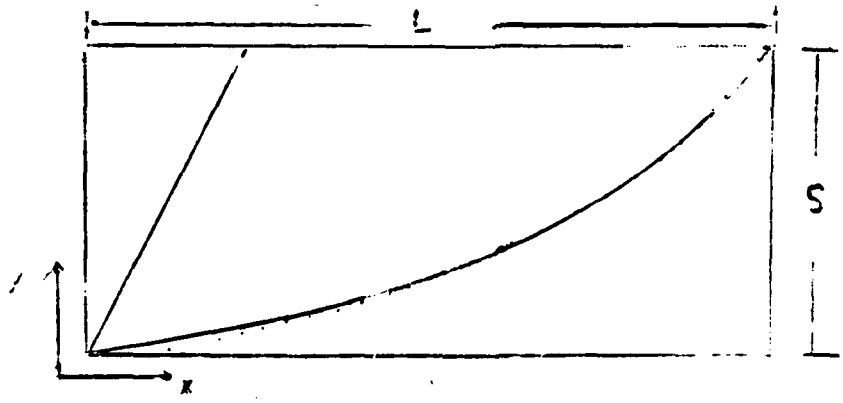

Fig A-1. Coordinate system for strake layout.

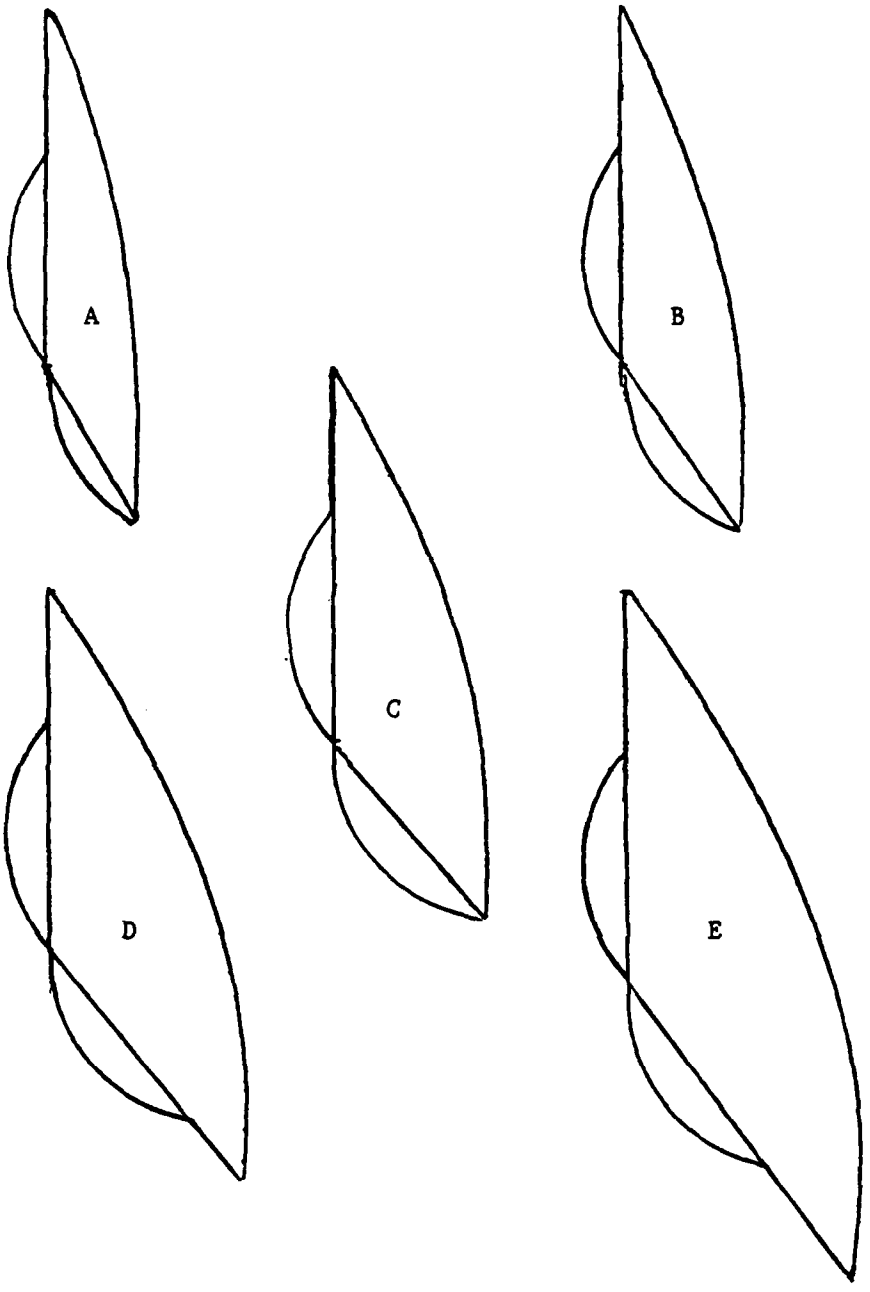

Fig A-2. Strake families A through E shown actual size. Installation tabs shown.

Five strake families (A through E) were developed by varying the strake span as a percentage of total span. Each family consisted of the same strake size at four different angles of incidence (0,-3,-6, and -9 degrees). The normal model configuration included CFT's, the one-man canopy, and 4 AIM-7 missiles. CFT only refers to the model with a 4 AIM-7 missiles but without strakes. All low angle of attack (-4 to 26 degrees) tests were made with the horizontal stabilizer at 0 degrees. All high angle of attack tests (16 to 46 degrees) were made with the stabilizer set at -27 degrees.

The following grid can be used to identify model configurations with strakes. Areas are in percent of wing area, spans in percent of wind span, and strake incidence angle in degrees.

CONF.	AREA	SPAN	ANGLE
A0	.65%	2.5%	0
A3	.65%	2.5%	-3
A6	.65%	2.5%	-6
A9	.65%	2.5%	-9
B0	1.0 %	3.7%	0
B3	1.0 %	3.7%	-3
B6	1.0 %	3.7%	-6
B9	1.0 %	3.7%	-9
C0	1.4 %	5.0%	0
C3	1.4 %	5.0%	-3
C6	1.4 %	5.0%	-6
C9	1.4 %	5.0%	-9
D0	1.8 %	6.2%	0
D3	1.8 %	6.2%	-3
D6	1.8 %	6.2%	-6
D9	1.8 %	6.2%	-9
E0	2.2 %	7.5%	0
E3	2.2 %	7.5%	-3
E6	2.2 %	7.5%	-6
E9	2.2 %	7.5%	-9

Appendix B

Longitudinal Data

This section contains both low angle of attack (-4 to 26 degrees) and high angle of attack (16 to 46 degrees) longitudinal data. All plots show the CFT Only data for reference. Pitching moment versus angle of attack and lift versus angle of attack are presented on the same axis system for convenience. Negative pitching moment is plotted to avoid data intersection.

The following grid can be used to identify model configurations with strakes. Areas are in percent of wing area, spans in percent of wind span, and strake incidence angle in degrees.

CONF.	AREA	SPAN	ANGLE
A0	.65%	2.5%	0
A3	.65%	2.5%	-3
A6	.65%	2.5%	-6
A9	.65%	2.5%	-9
B0	1.0 %	3.7%	0
B3	1.0 %	3.7%	-3
B6	1.0 %	3.7%	-6
B9	1.0 %	3.7%	-9
C0	1.4 %	5.0%	0
C3	1.4 %	5.0%	-3
C6	1.4 %	5.0%	-6
C9	1.4 %	5.0%	-9
D0	1.8 %	6.2%	0
D3	1.8 %	6.2%	-3
D6	1.8 %	6.2%	-6
D9	1.8 %	6.2%	-9
E0	2.2 %	7.5%	0
E3	2.2 %	7.5%	-3
E6	2.2 %	7.5%	-6
E9	2.2 %	7.5%	-9

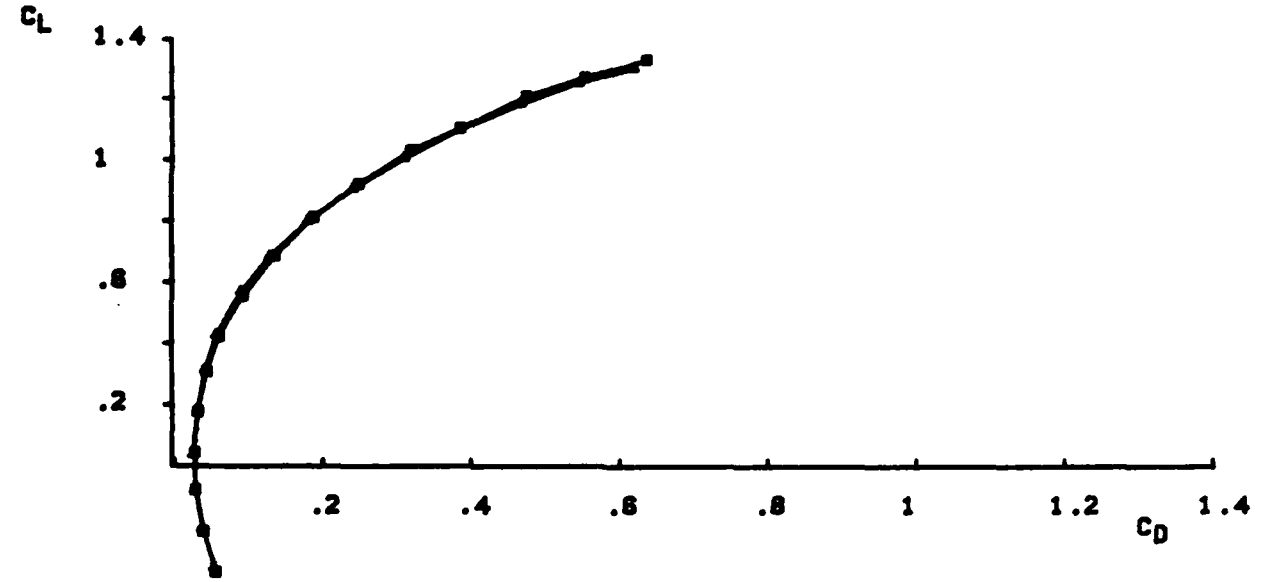

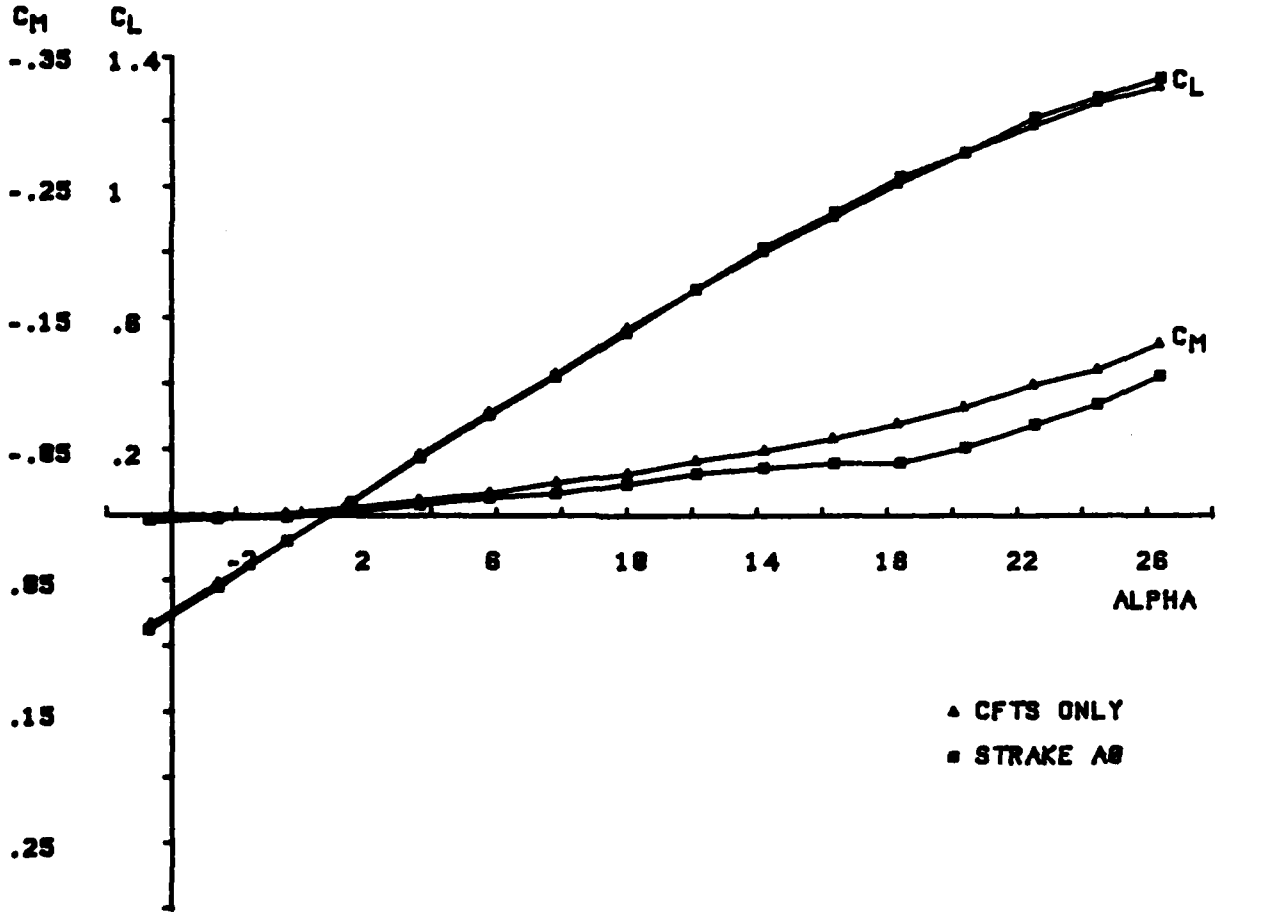

FIG B-1. LONGITUDINAL STABILITY DATA FOR AN F-15 WITH ONLY CFTS AND AN F-15 WITH CFTS AND F/B STRAKES.

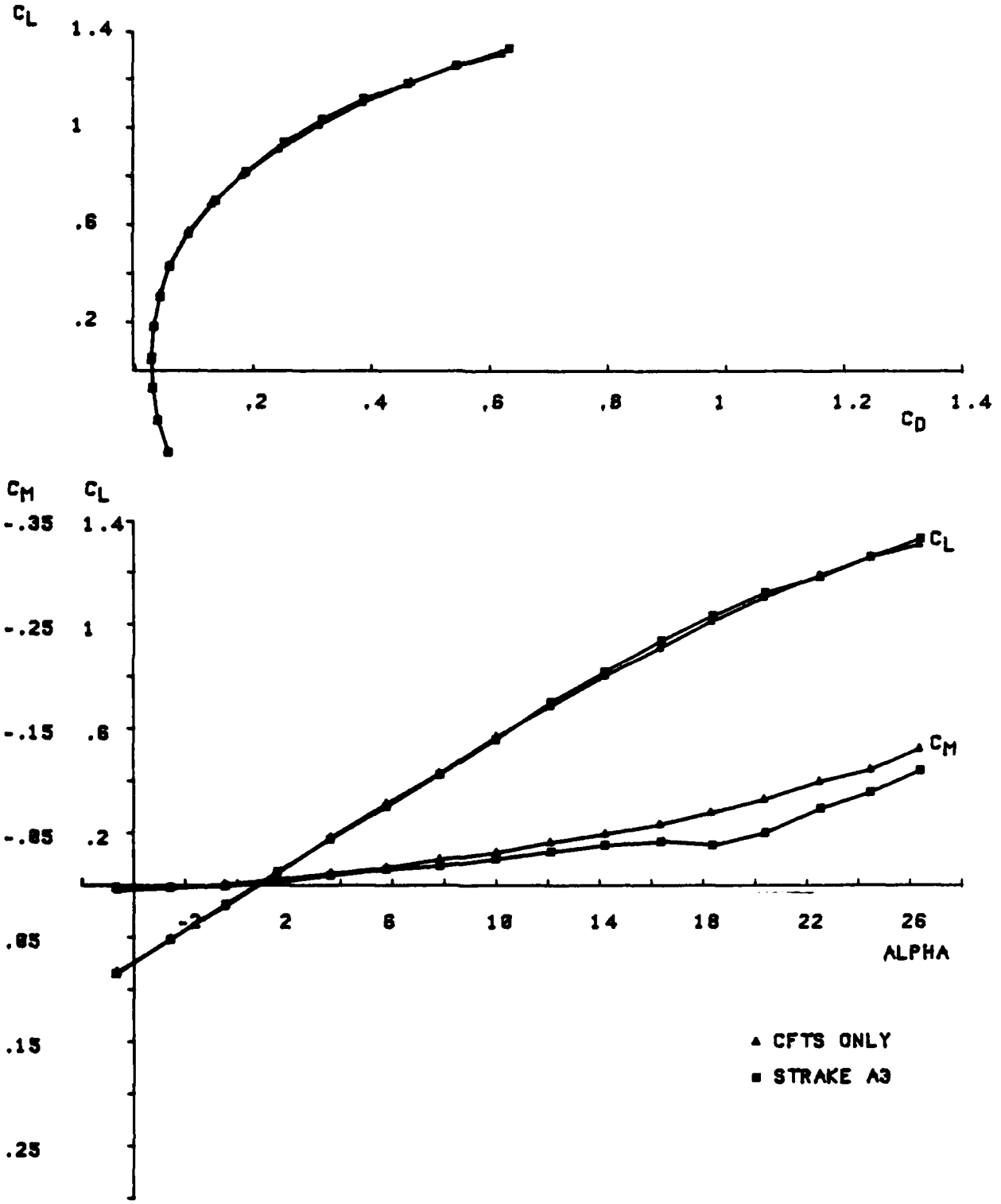

FIG B-2. LONGITUDINAL STABILITY DATA FOR AN F-15 WITH ONLY CFTS AND AN F-15 WITH CFTS AND F/B STRAKES.

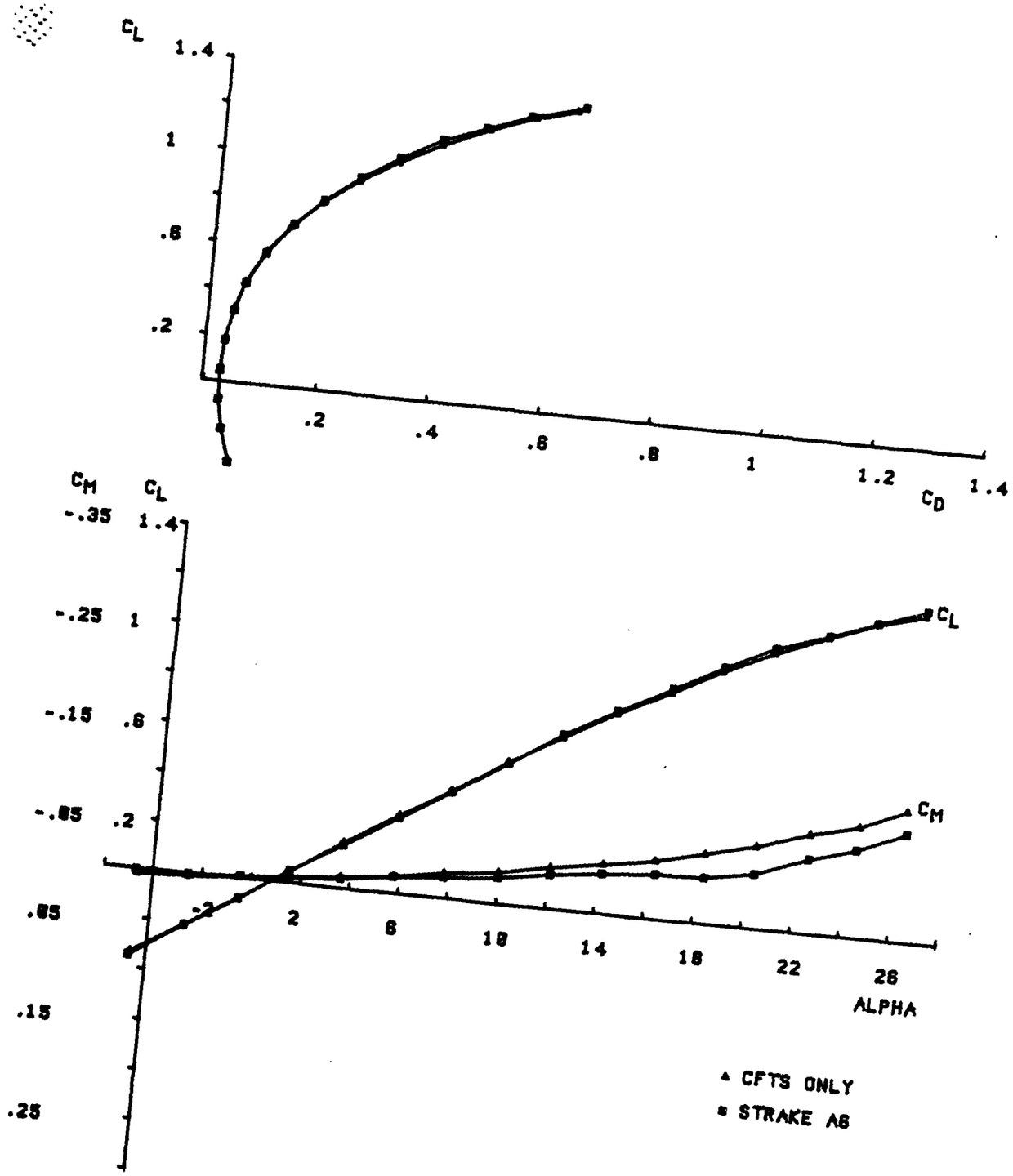

FIG B-3. LONGITUDINAL STABILITY DATA FOR AN F-15 WITH ONLY CFTS AND AN F-15 WITH CFTS AND F/B STRAKES.

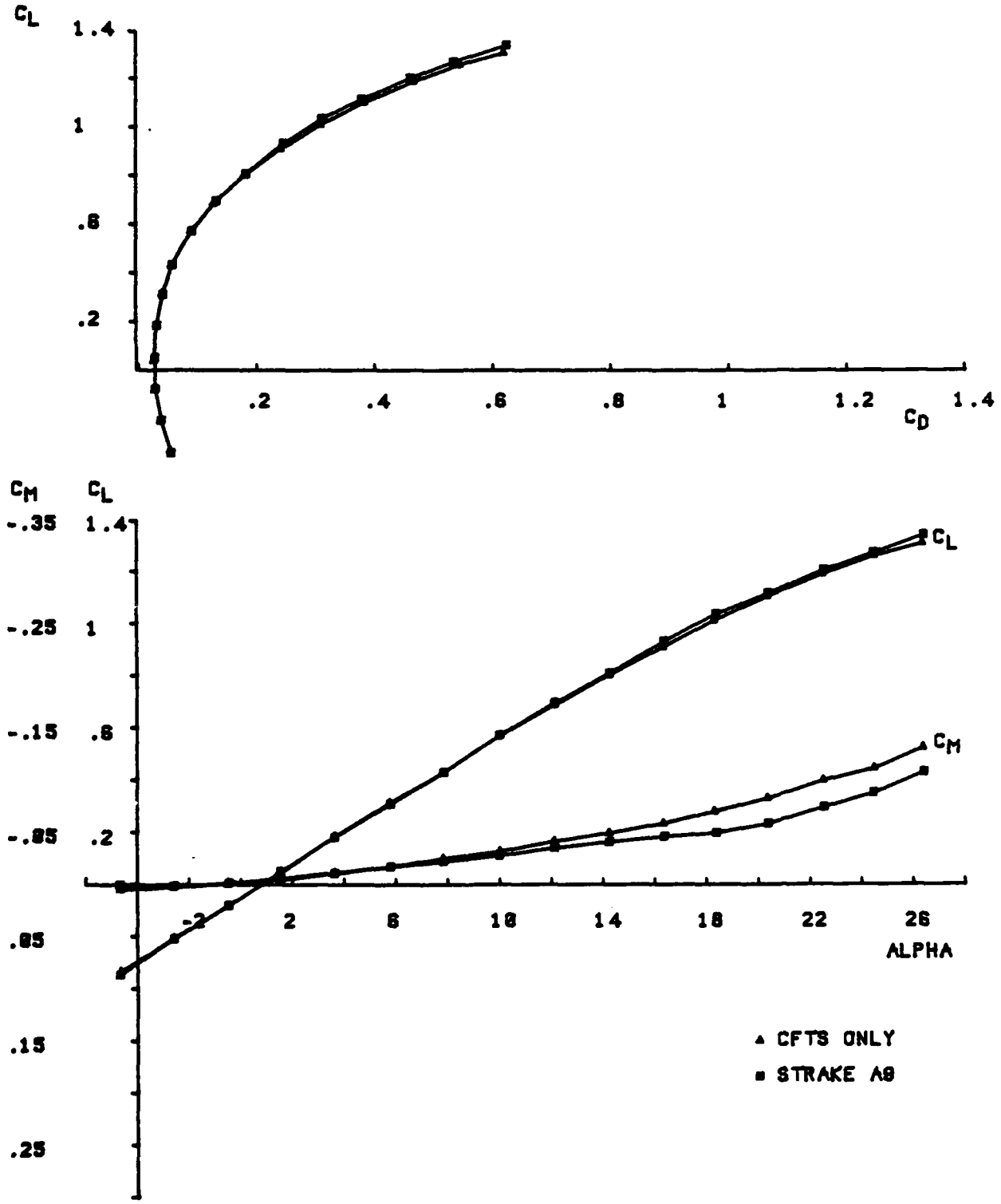

FIG 8-4. LONGITUDINAL STABILITY DATA FOR AN F-15 WITH ONLY CFTS AND AN F-15 WITH CFTS AND F/B STRAKES.

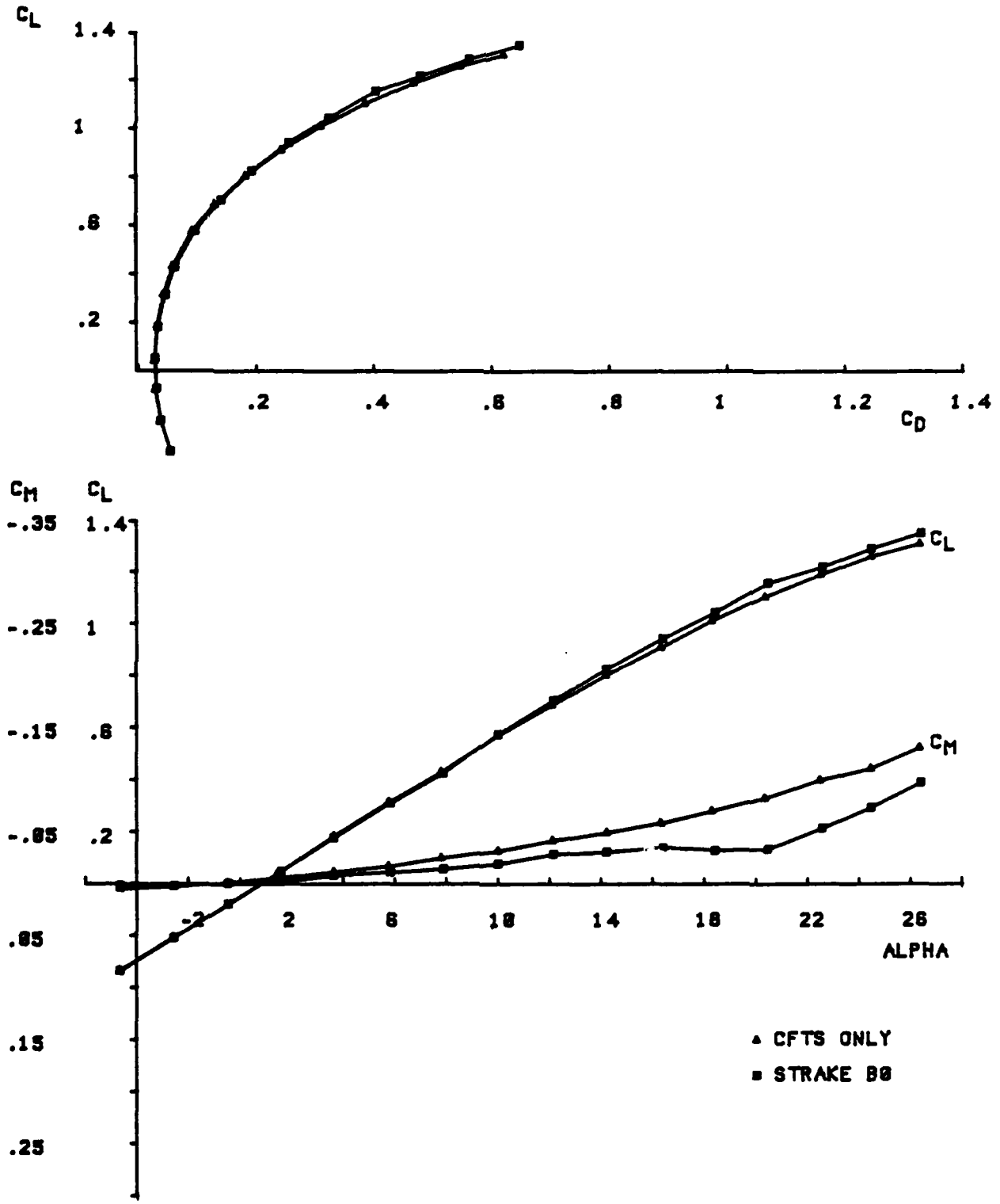

FIG B-5. LONGITUDINAL STABILITY DATA FOR AN F-15 WITH ONLY CFTS AND AN F-15 WITH CFTS AND F/B STRAKES.

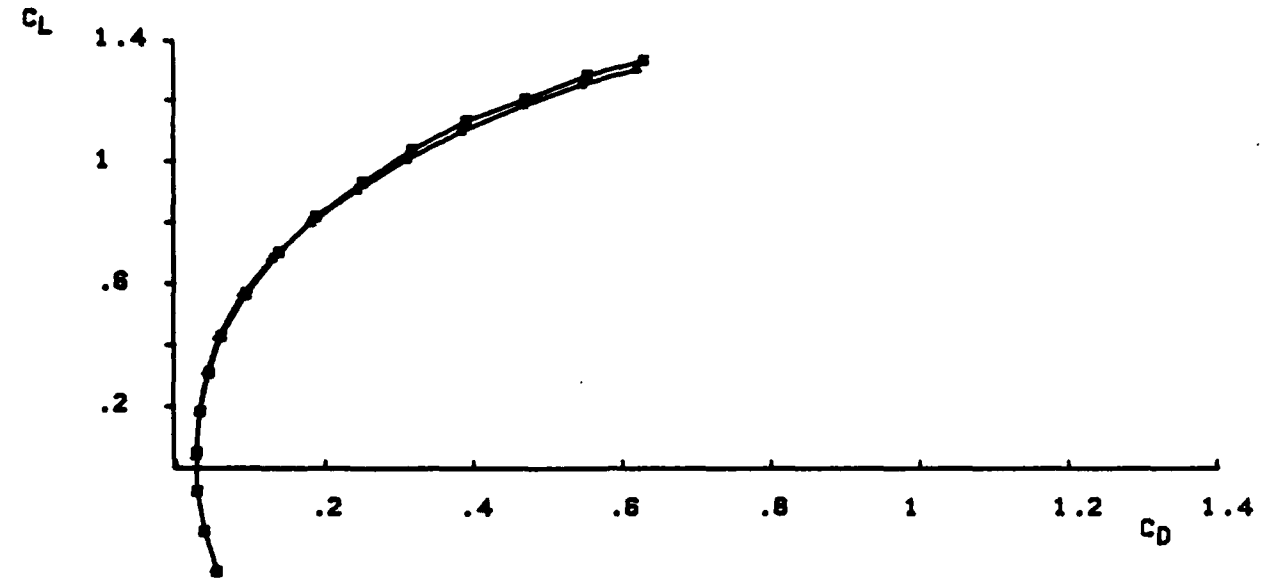

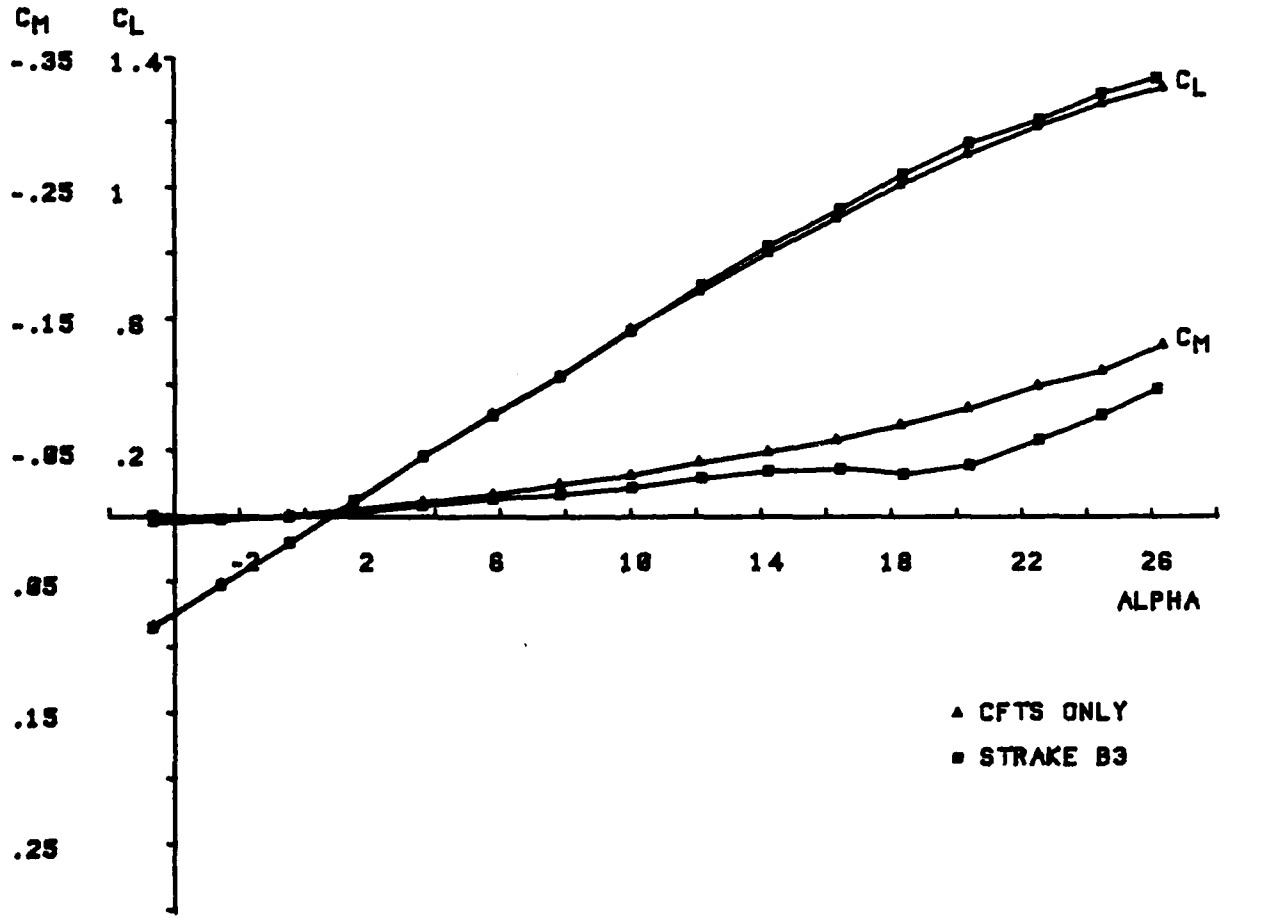

FIG B-6. LONGITUDINAL STABILITY DATA FOR AN F-15 WITH ONLY CFTS AND AN F-15 WITH CFTS AND F/B STRAKES.

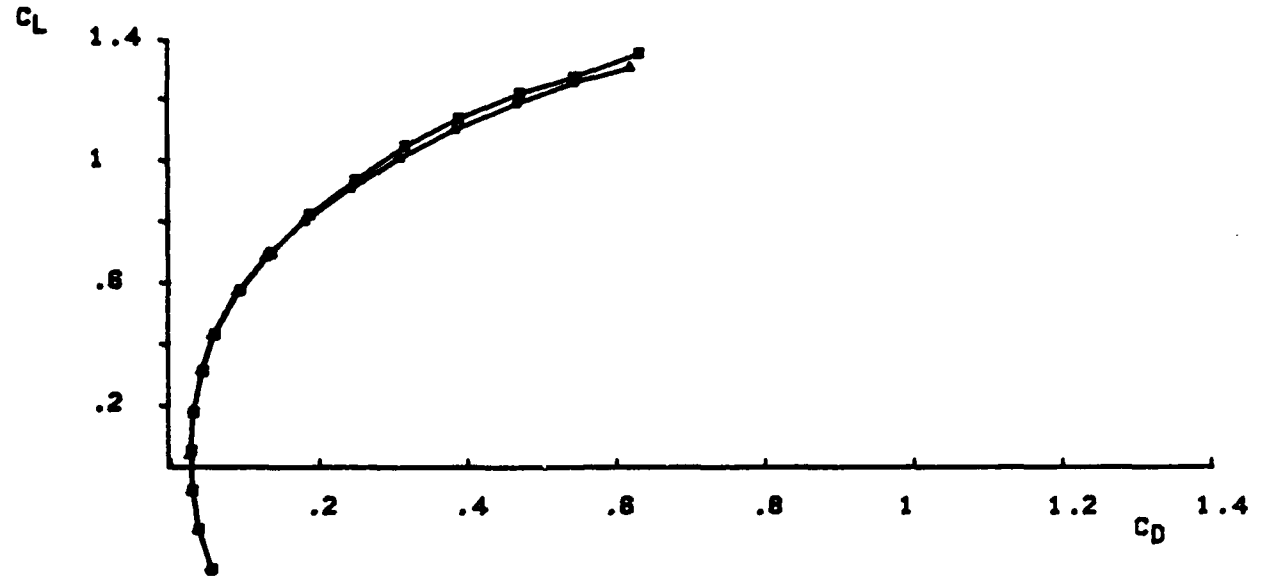

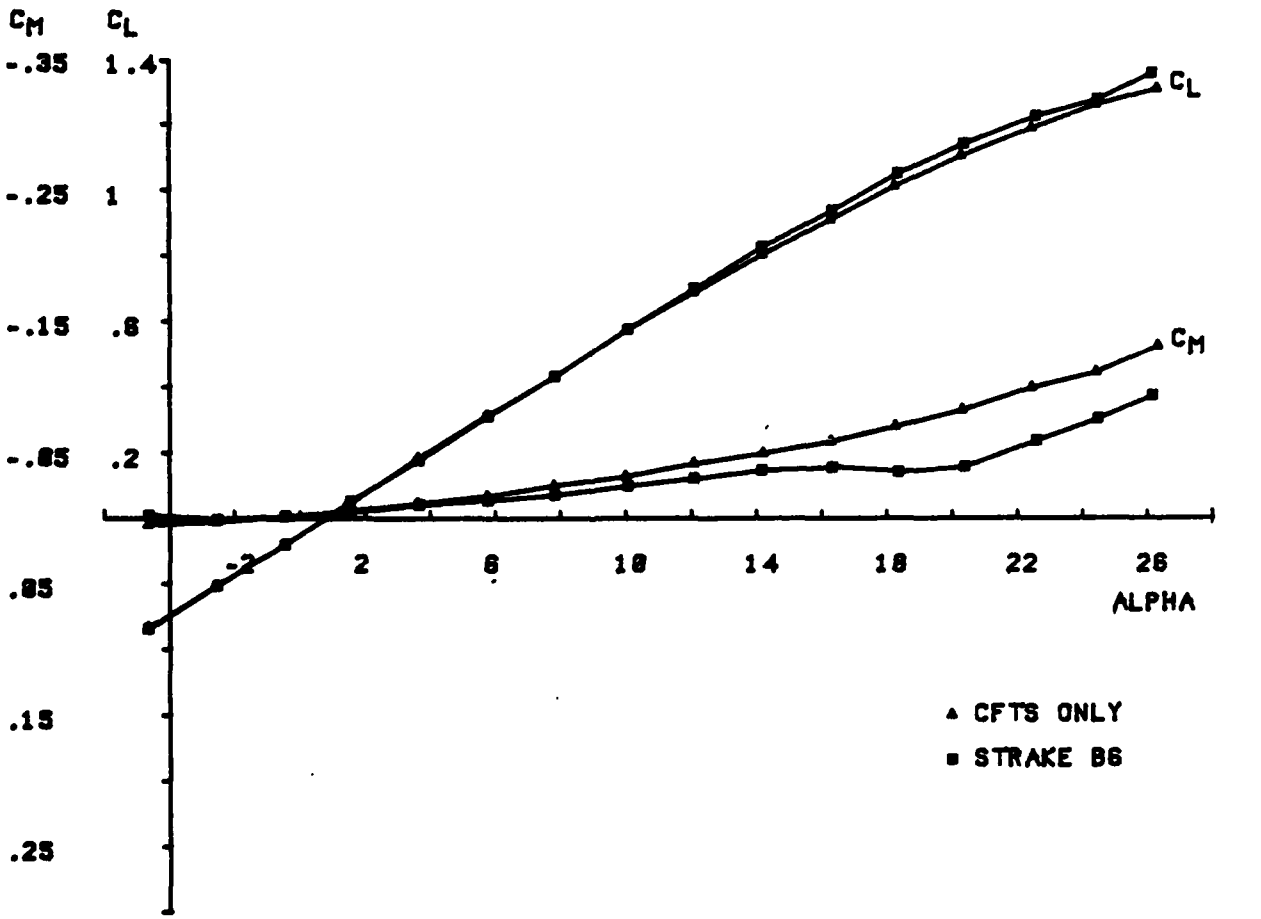

FIG B-7. LONGITUDINAL STABILITY DATA FOR AN F-15 WITH ONLY CFTS AND AN F-15 WITH CFTS AND F/B STRAKES.

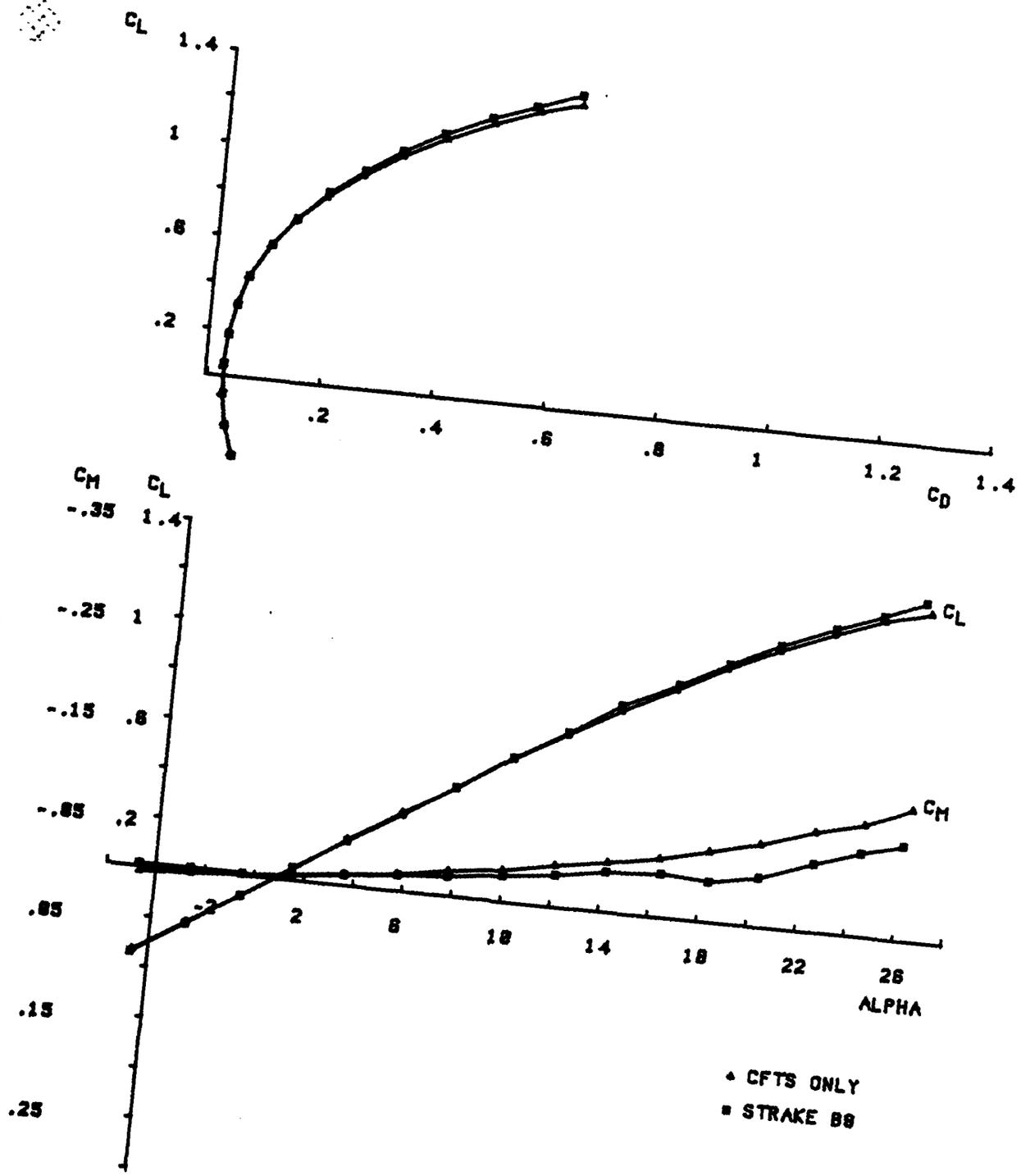

FIG 8-8. LONGITUDINAL STABILITY DATA FOR AN F-15 WITH ONLY CFTS AND AN F-15 WITH CFTS AND F/8 STRAKES.

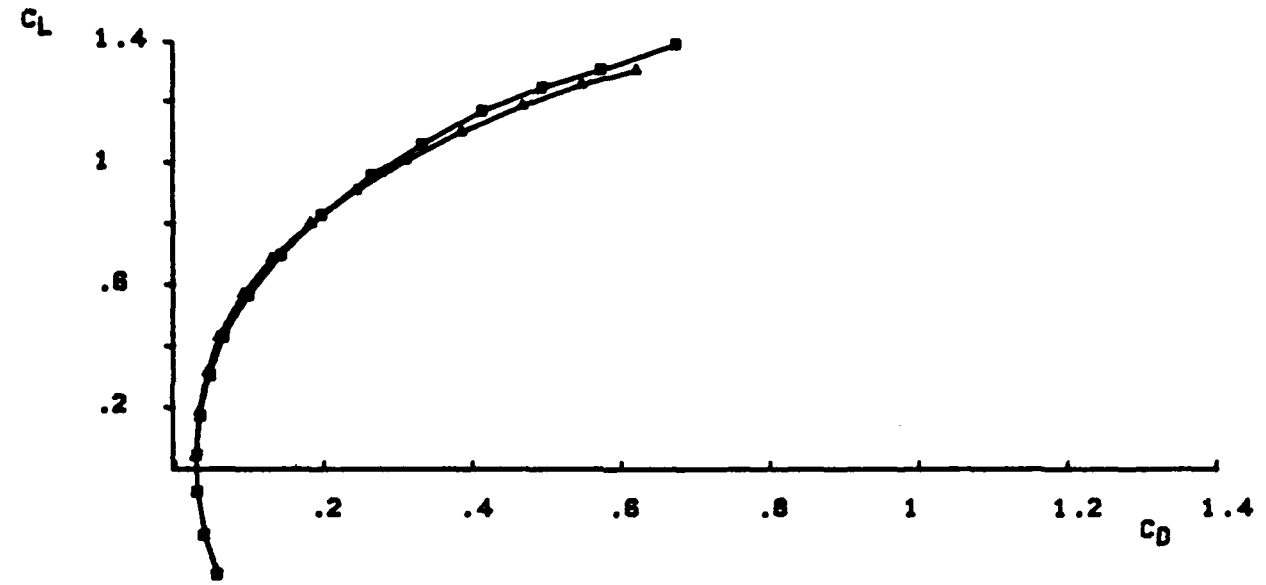

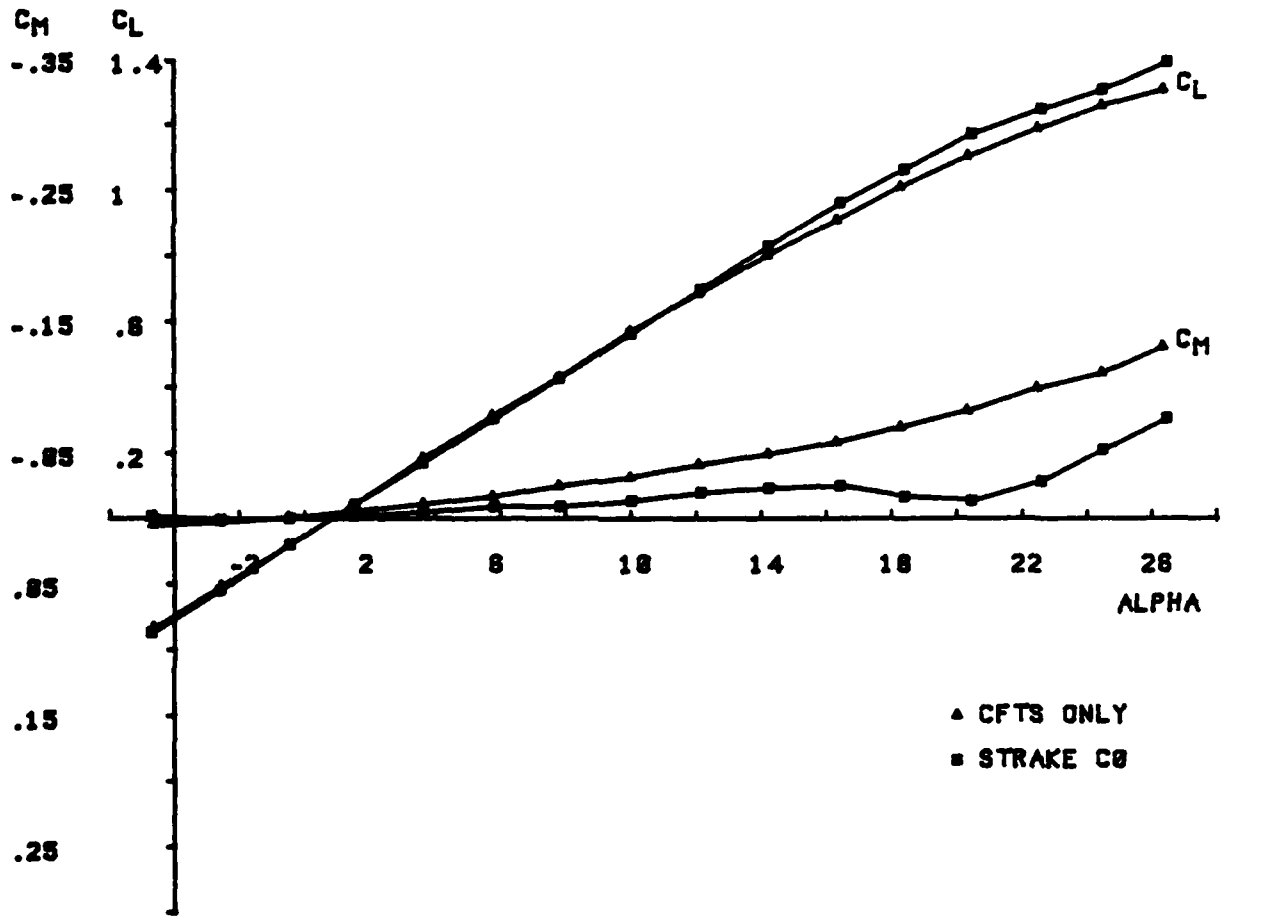

FIG B-9. LONGITUDINAL STABILITY DATA FOR AN F-15 WITH ONLY CFTS AND AN F-15 WITH CFTS AND F/B STRAKES.

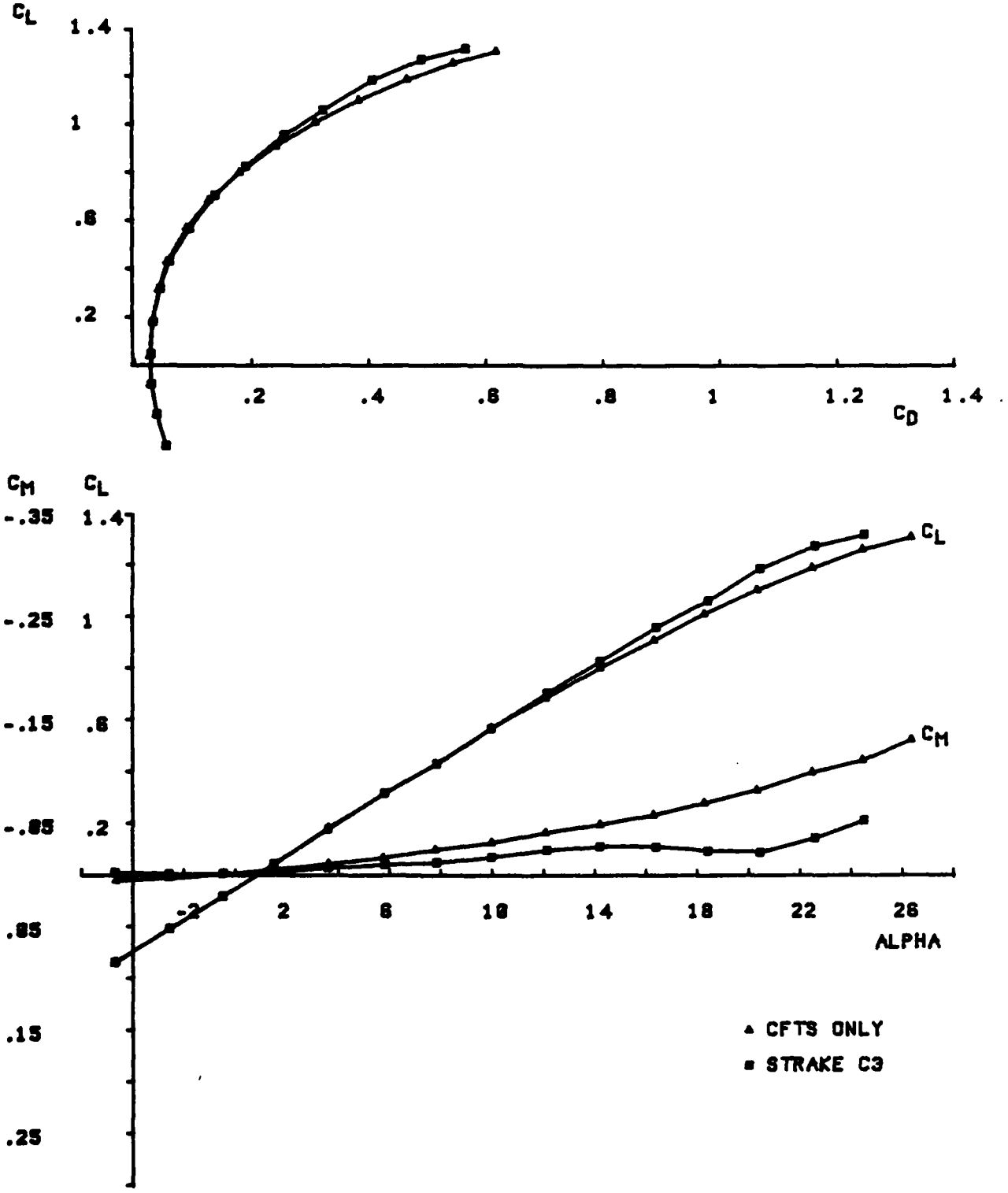

FIG B-10. LONGITUDINAL STABILITY DATA FOR AN F-15 WITH ONLY CFTS AND AN F-15 WITH CFTS AND F/B STRAKES.

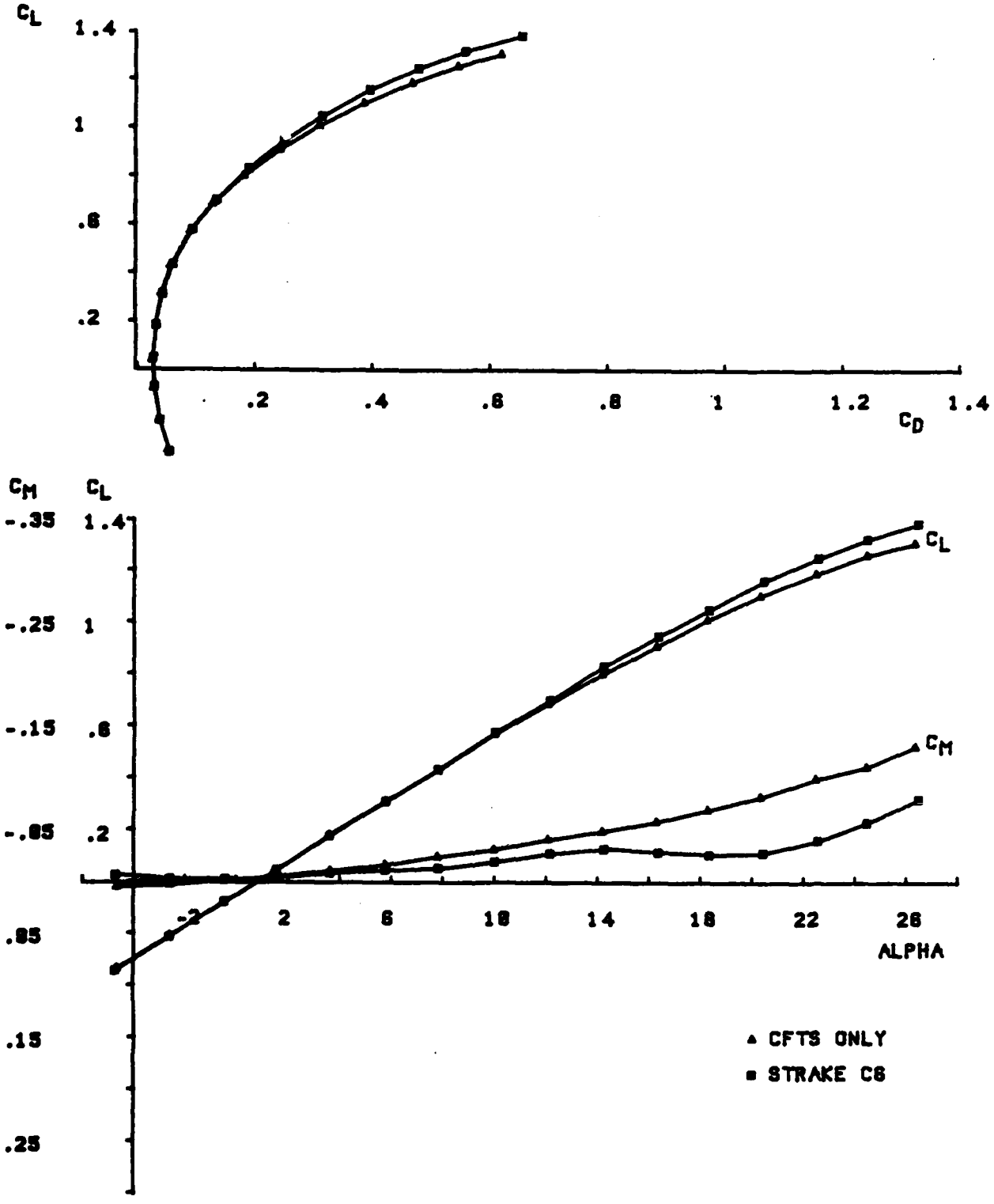

FIG B-11. LONGITUDINAL STABILITY DATA FOR AN F-15 WITH ONLY CFTS AND AN F-15 WITH CFTS AND F/B STRAKES.

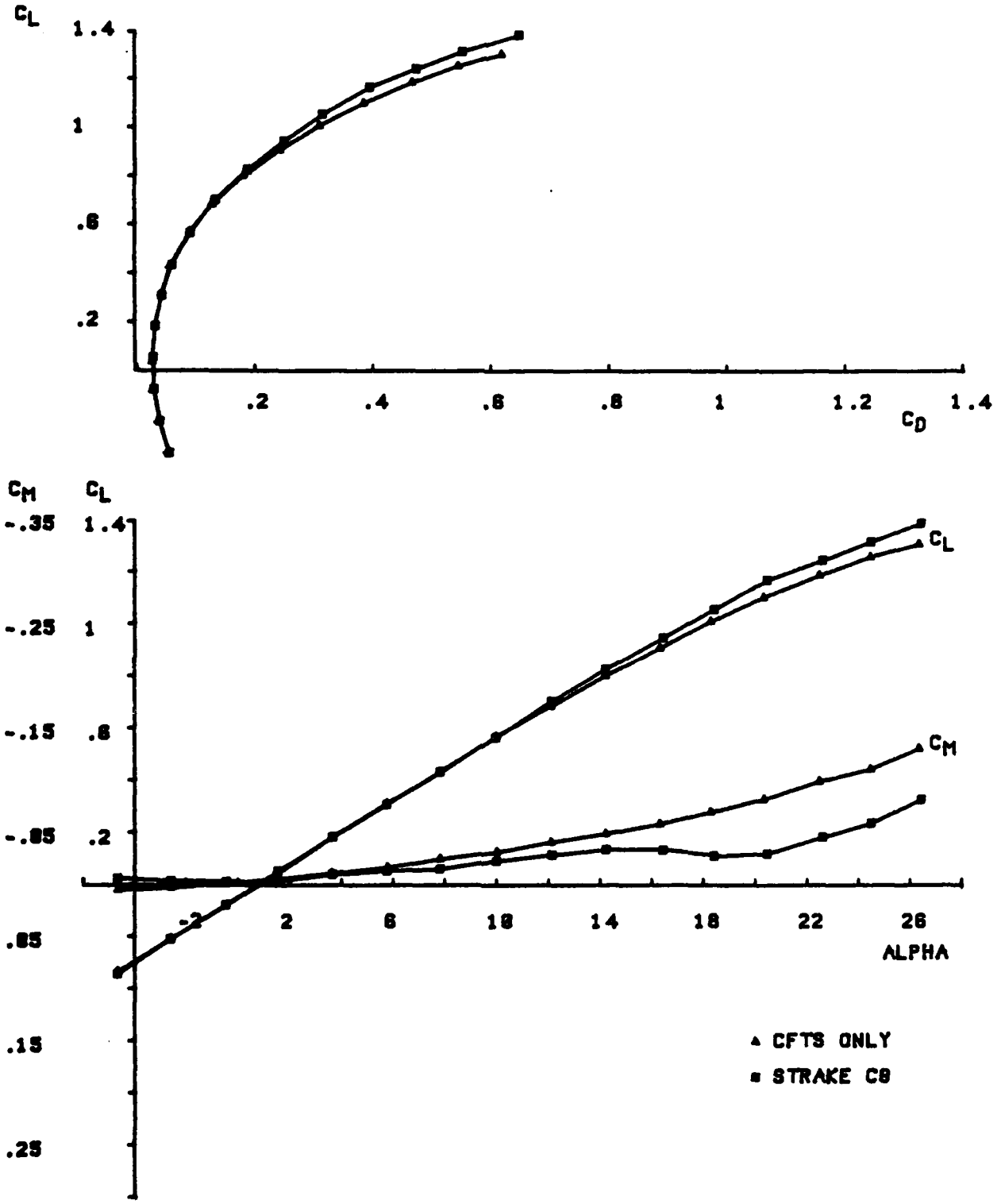

FIG 8-12. LONGITUDINAL STABILITY DATA FOR AN F-15 WITH ONLY CFTS AND AN F-15 WITH CFTS AND F/8 STRAKES.

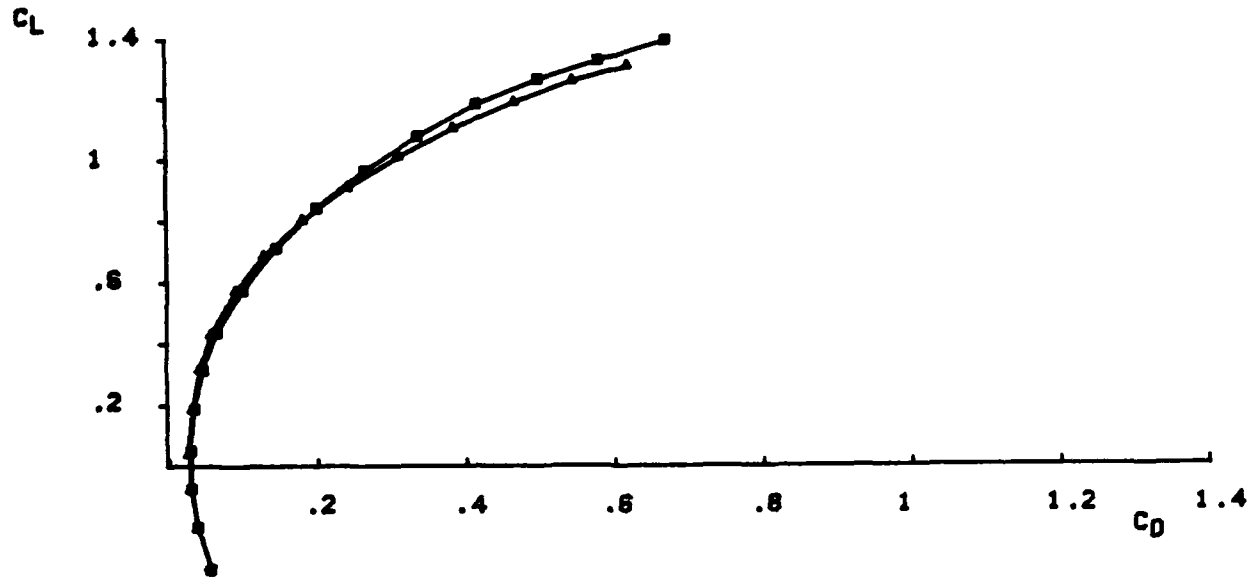

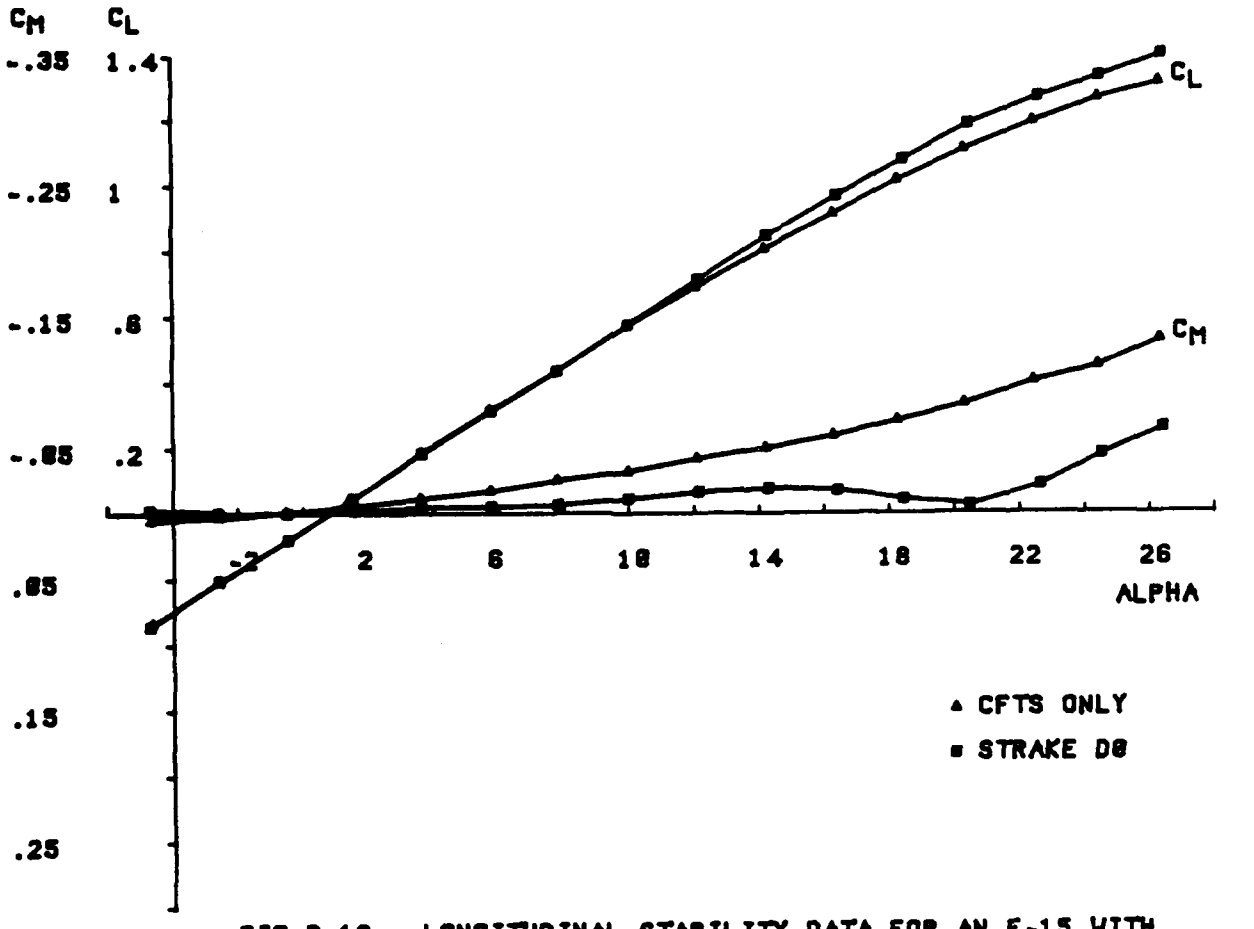

FIG B-13. LONGITUDINAL STABILITY DATA FOR AN F-15 WITH ONLY CFTS AND AN F-15 WITH CFTS AND F/B STRAKES.

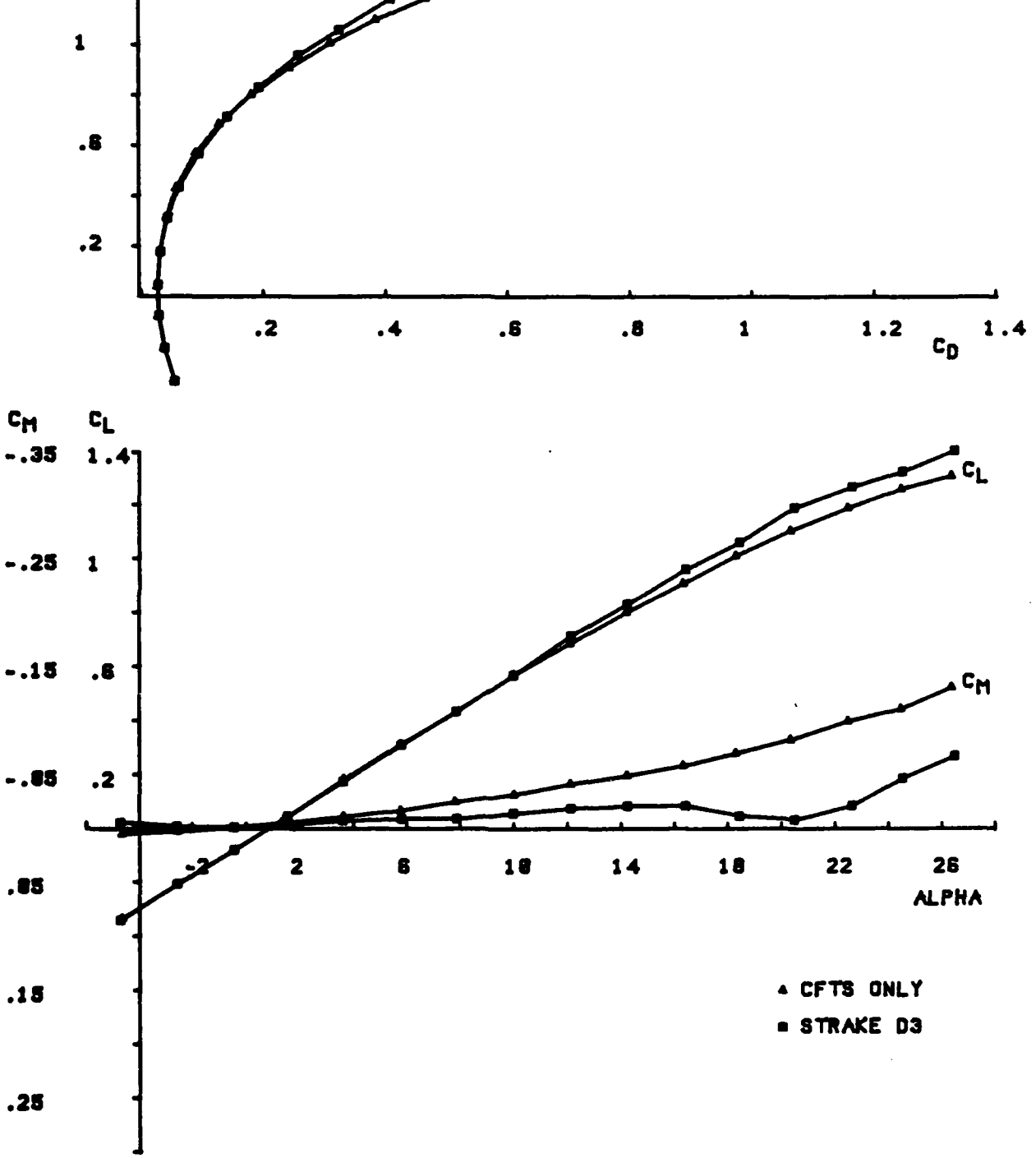

FIG B-14. LONGITUDINAL STABILITY DATA FOR AN F-15 WITH ONLY CFTS AND AN F-15 WITH CFTS AND F/B STRAKES.

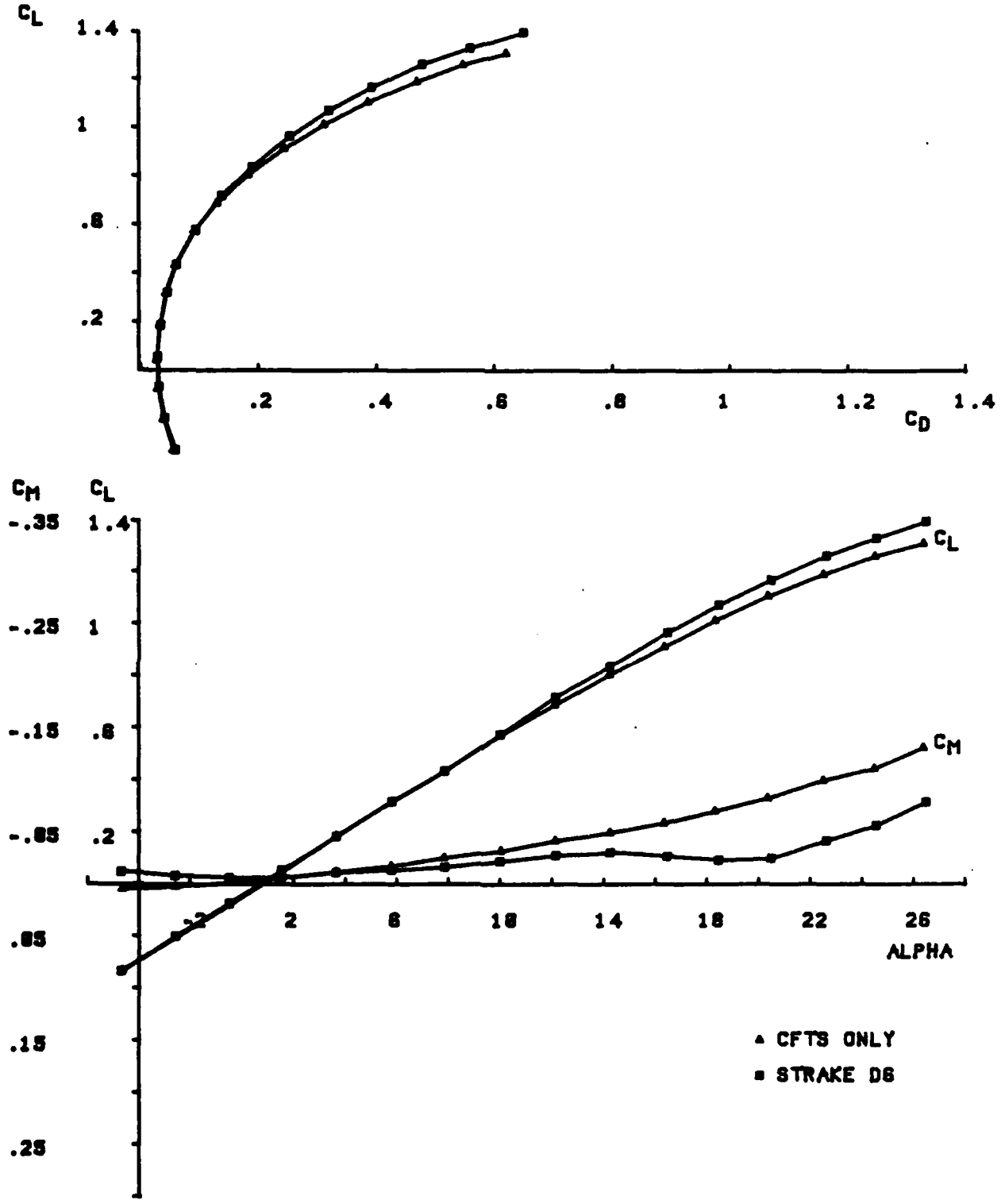

FIG B-15. LONGITUDINAL STABILITY DATA FOR AN F-15 WITH ONLY CFTS AND AN F-15 WITH CFTS AND F/B STRAKES.

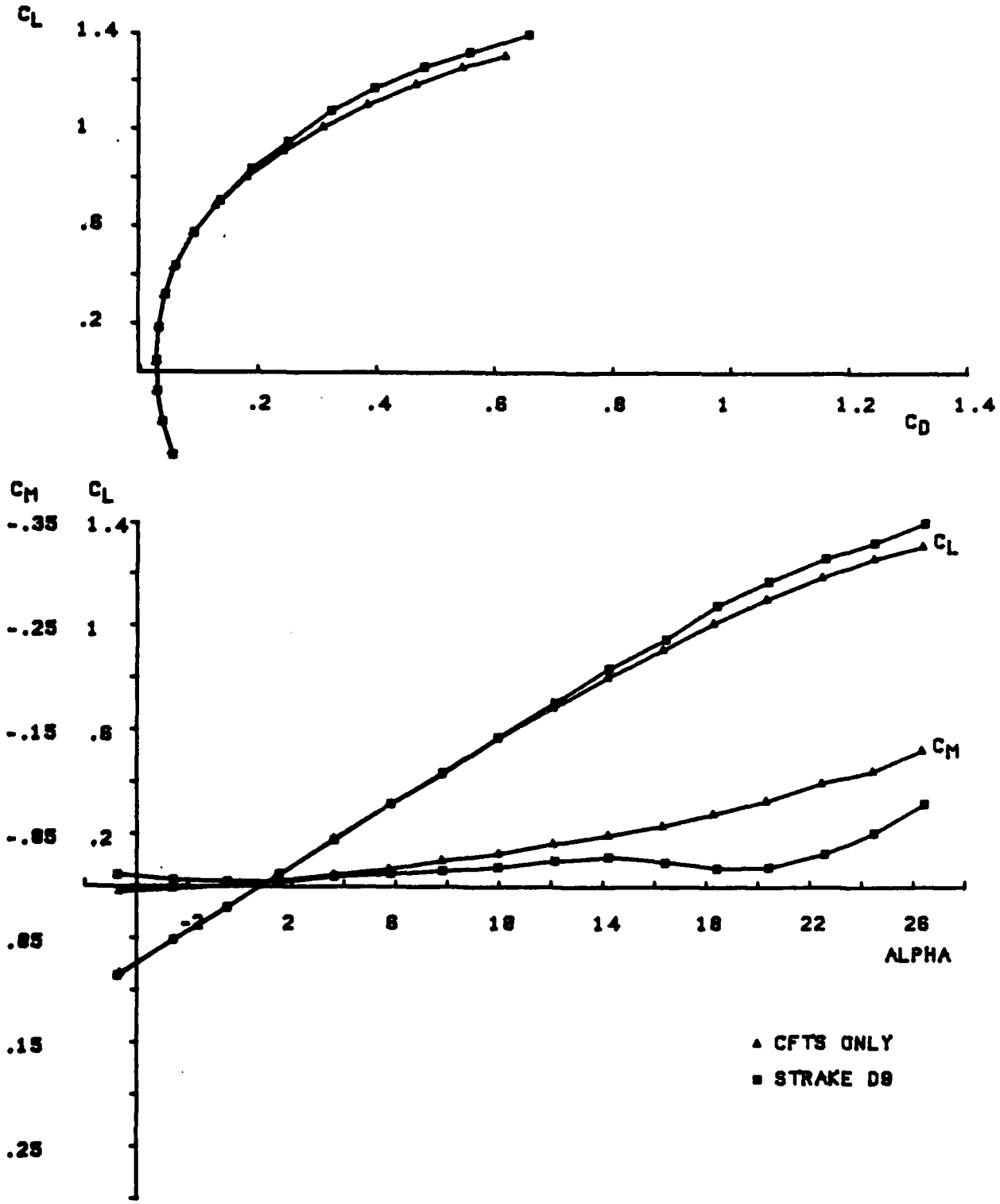

FIG B-16. LONGITUDINAL STABILITY DATA FOR AN F-15 WITH ONLY CFTS AND AN F-15 WITH CFTS AND F/B STRAKES.

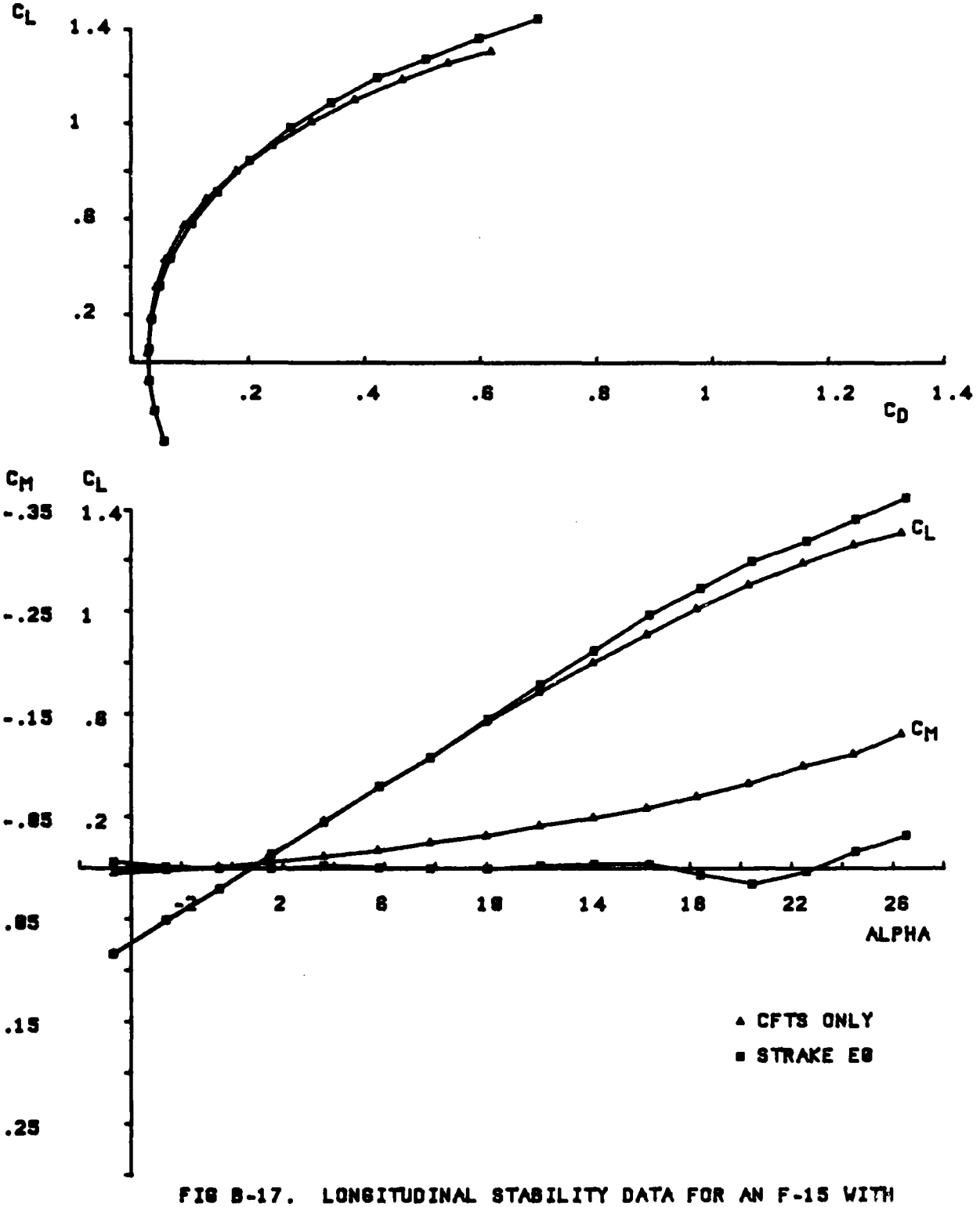

FIG 8-17. LONGITUDINAL STABILITY DATA FOR AN F-15 WITH ONLY CFTS AND AN F-15 WITH CFTS AND F/8 STRAKES.

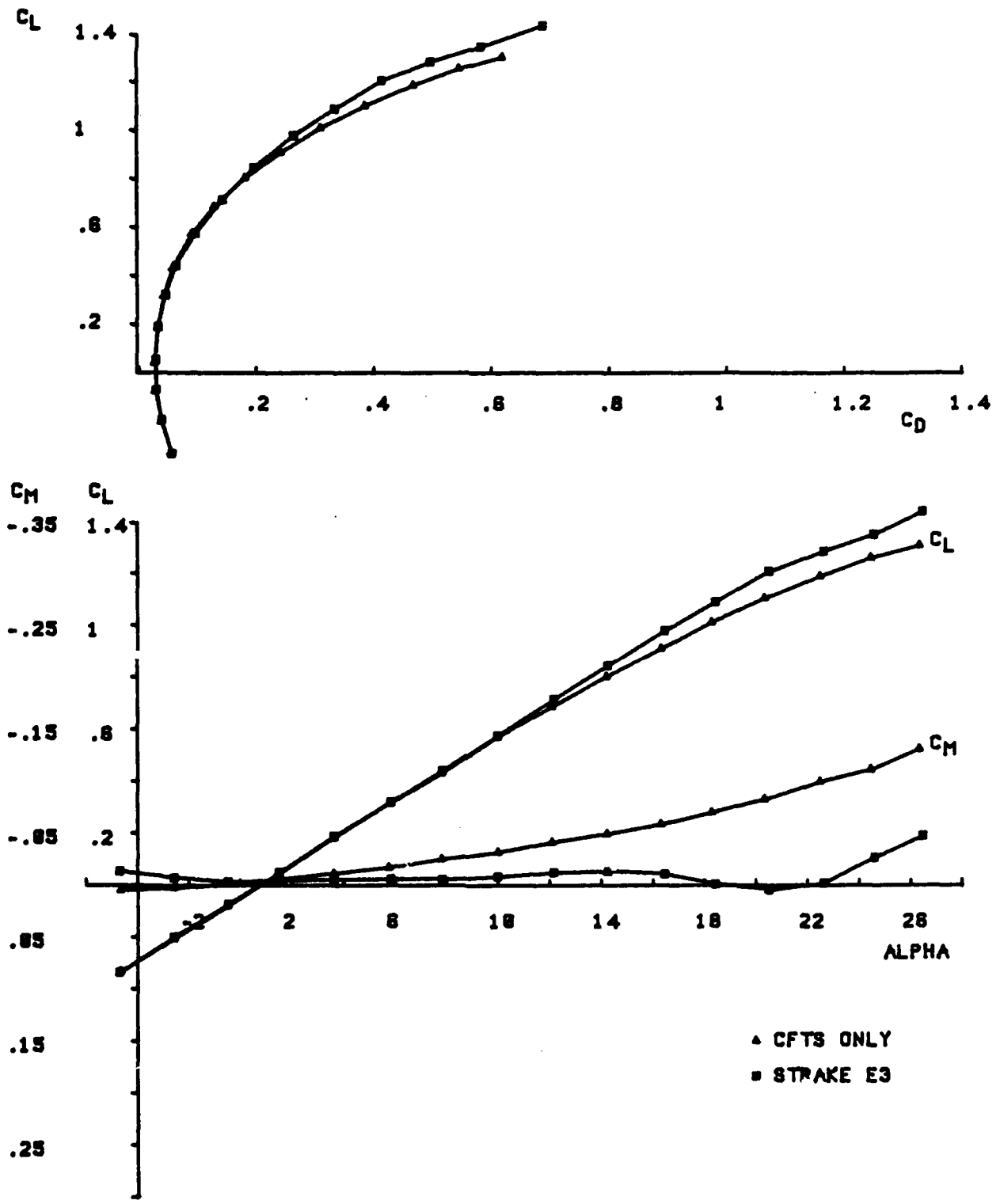

FIG B-18. LONGITUDINAL STABILITY DATA FOR AN F-15 WITH ONLY CFTS AND AN F-15 WITH CFTS AND F/B STRAKES.

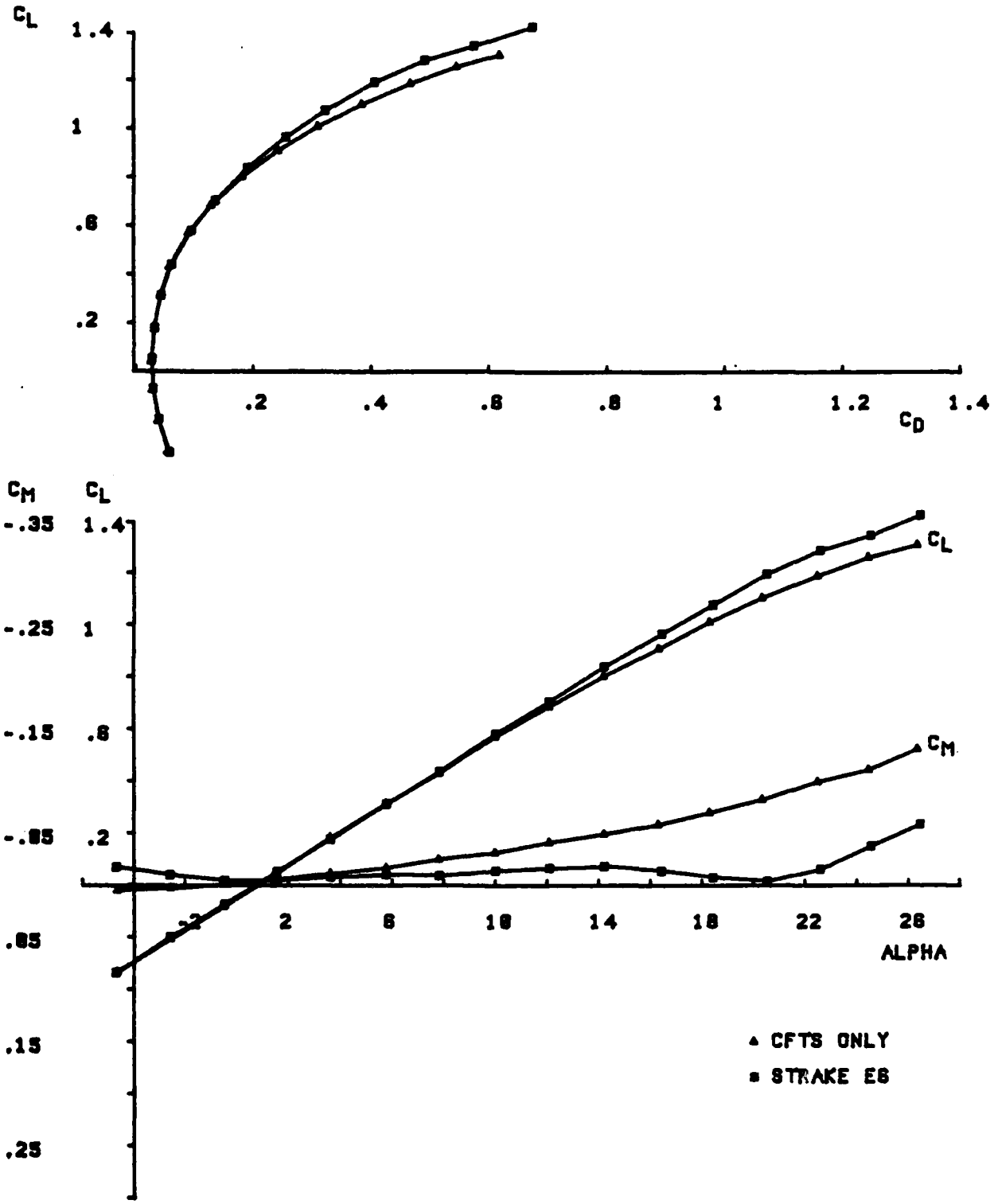

FIG 8-19. LONGITUDINAL STABILITY DATA FOR AN F-15 WITH ONLY CFTS AND AN F-15 WITH CFTS AND F/B STRAKES.

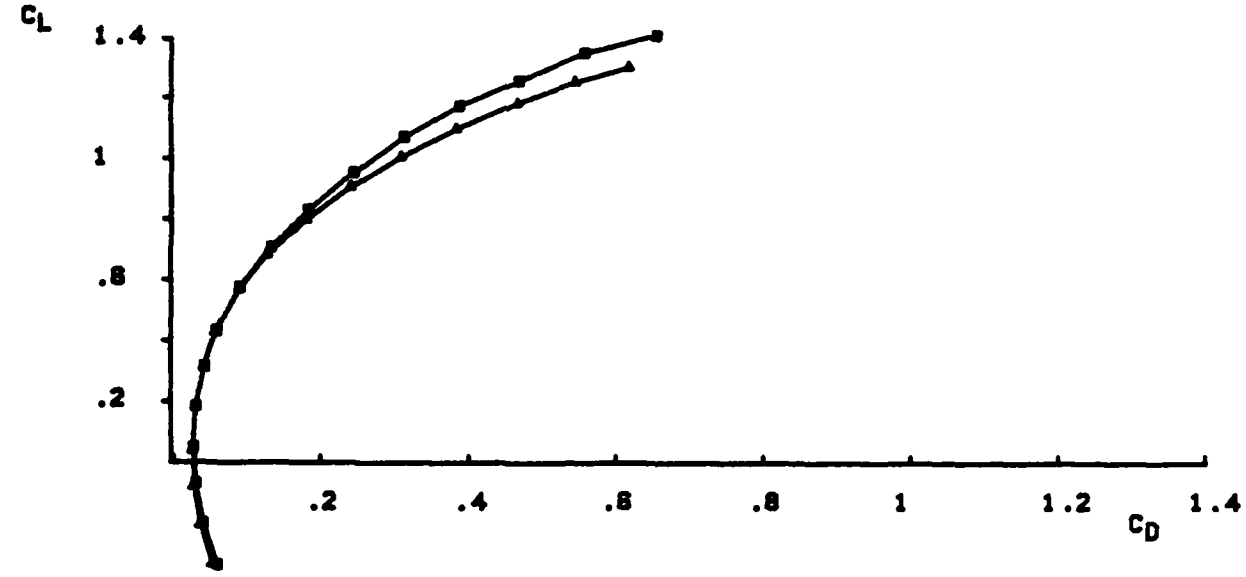

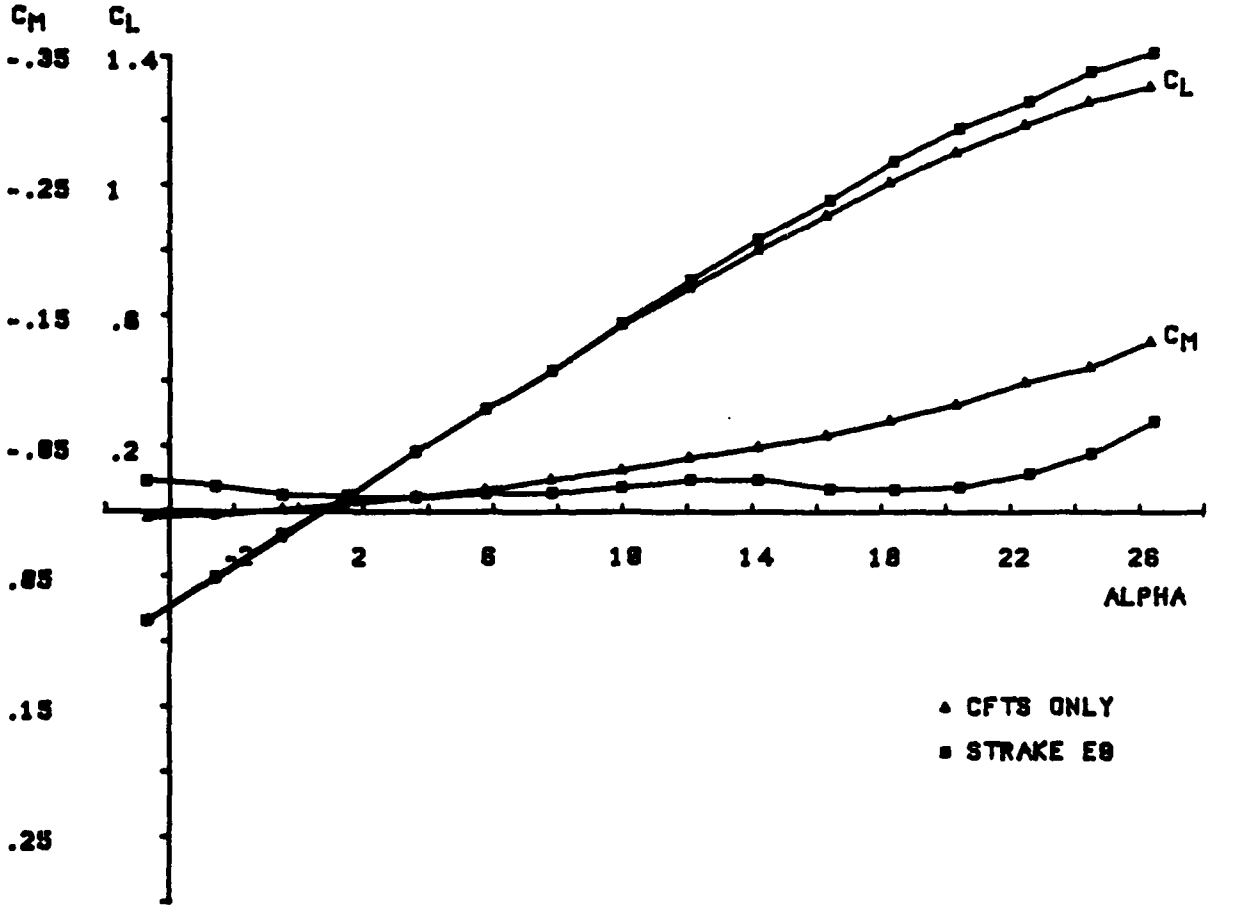

FIG B-28. LONGITUDINAL STABILITY DATA FOR AN F-15 WITH ONLY CFTS AND AN F-15 WITH CFTS AND F/B STRAKES.

Longitudinal Data

at

High Angle of Attack

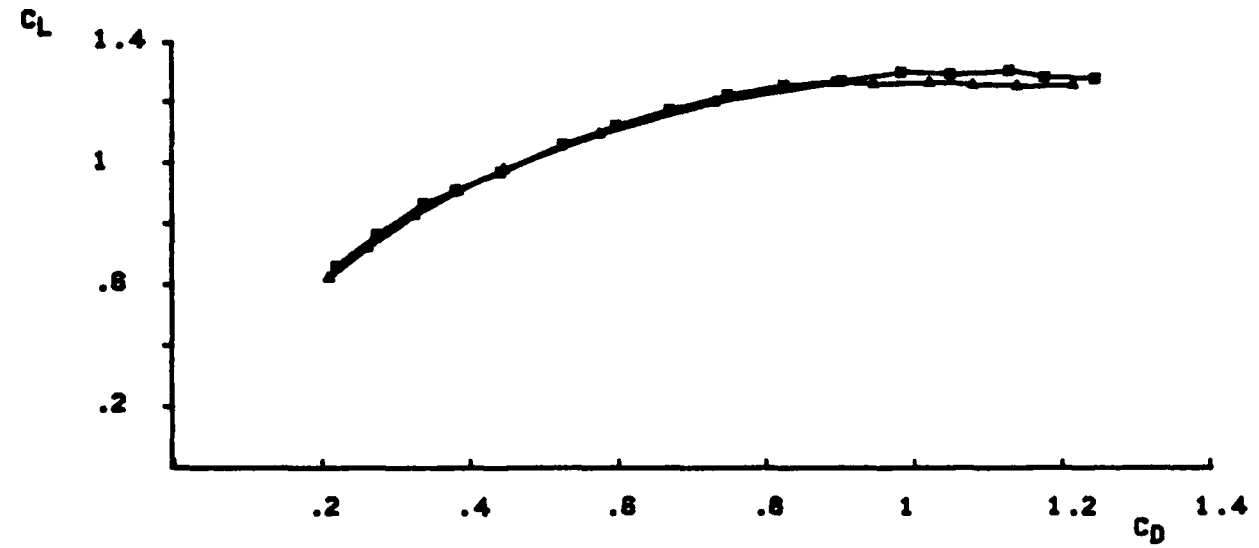

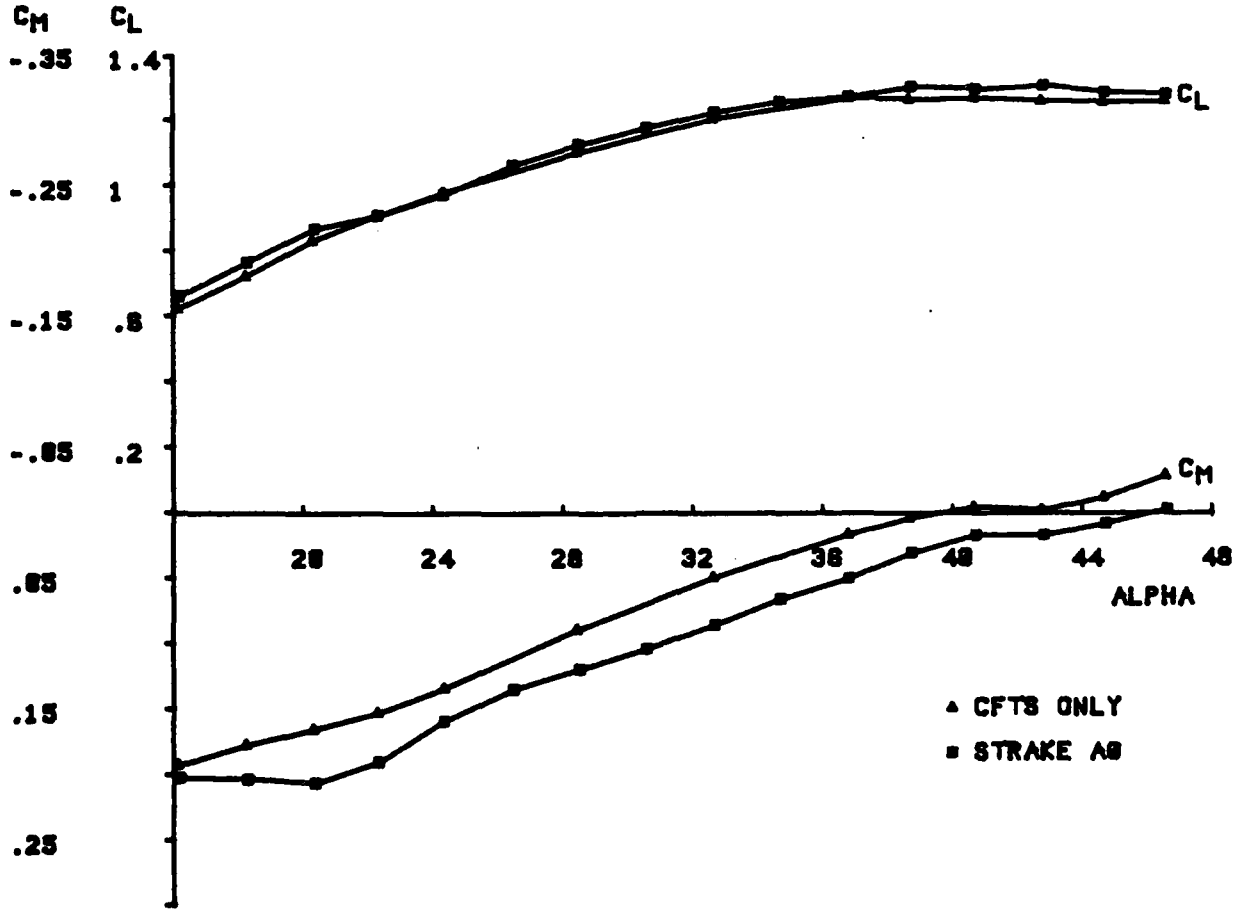

FIG B-21. LONGITUDINAL STABILITY DATA FOR AN F-15 WITH ONLY CFTS AND AN F-15 WITH CFTS AND F/B STRAKES.

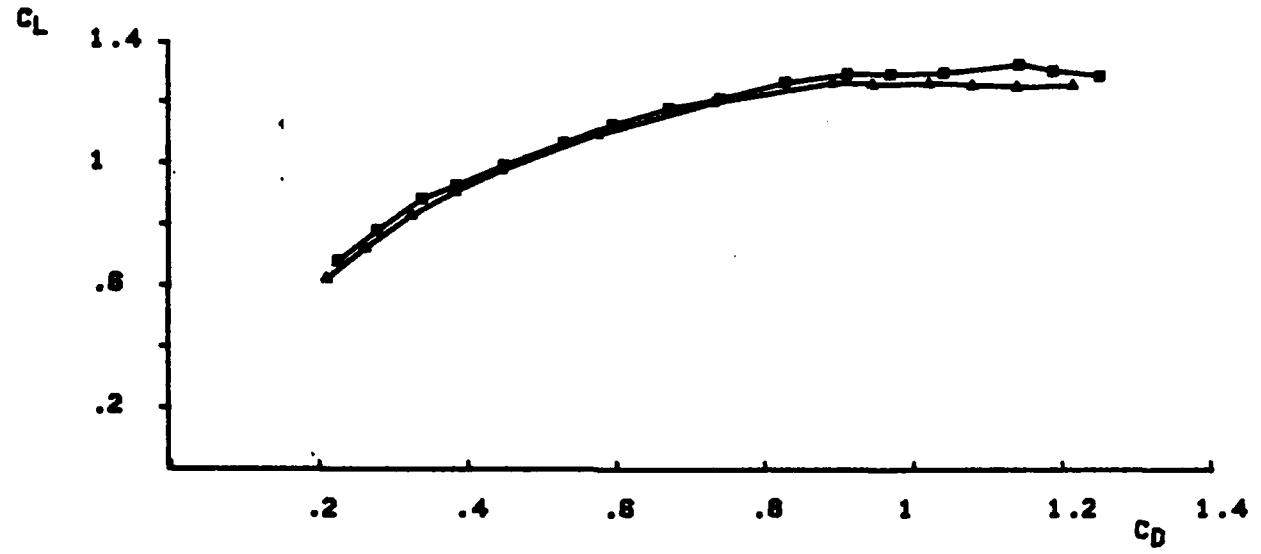

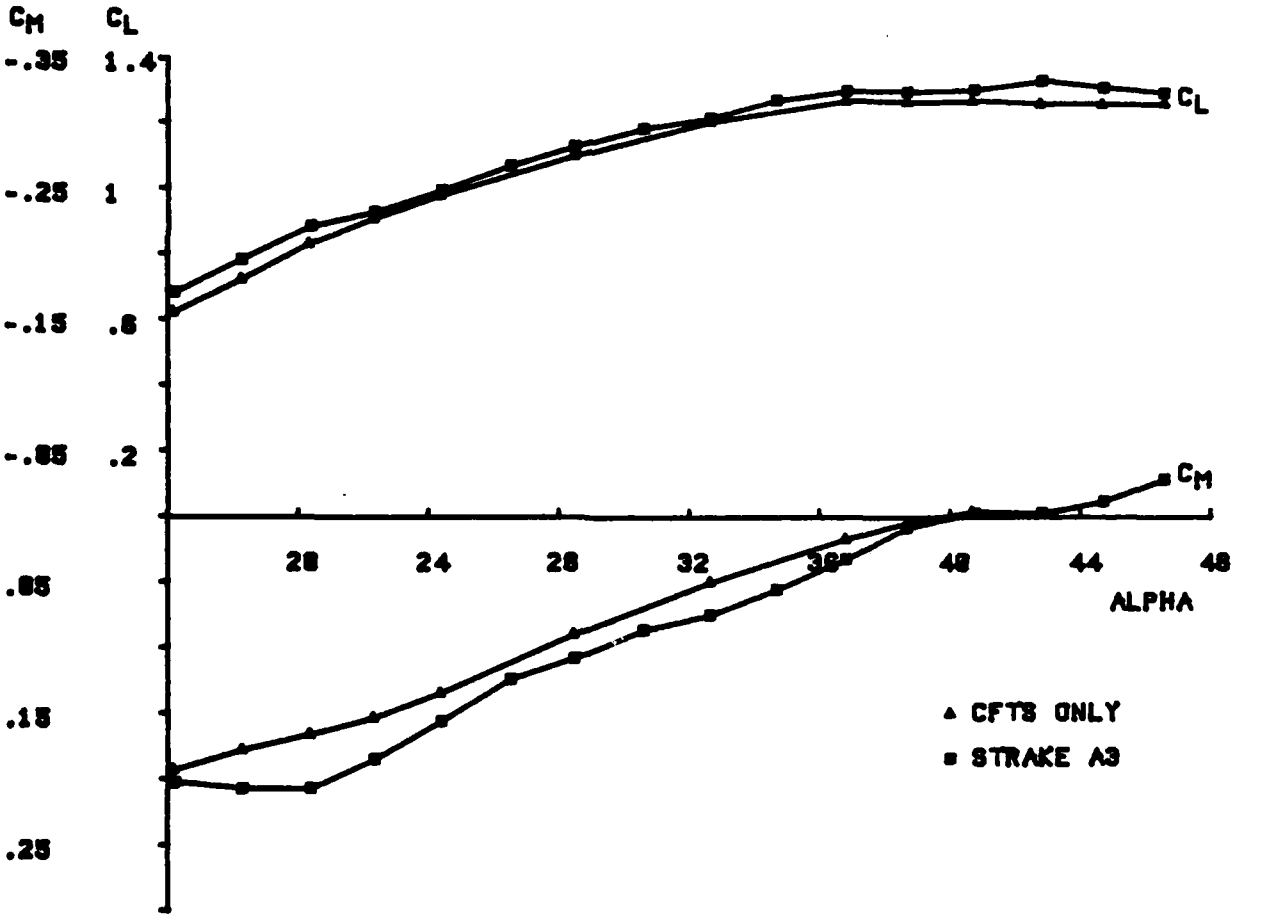

FIG B-22. LONGITUDINAL STABILITY DATA FOR AN F-15 WITH ONLY CFTS AND AN F-15 WITH CFTS AND F/B STRAKES.

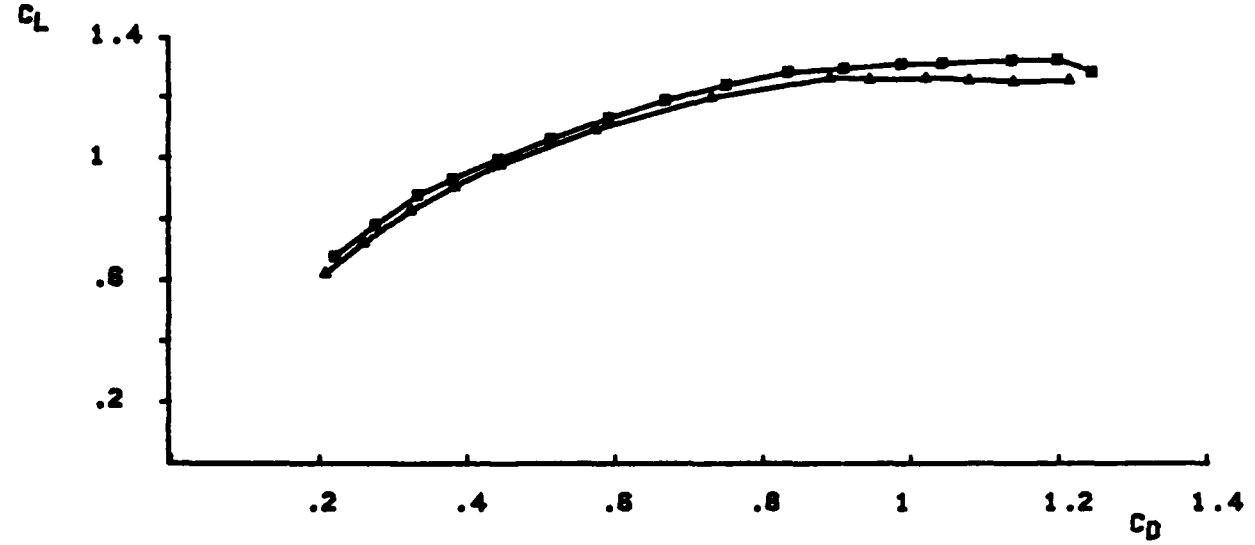

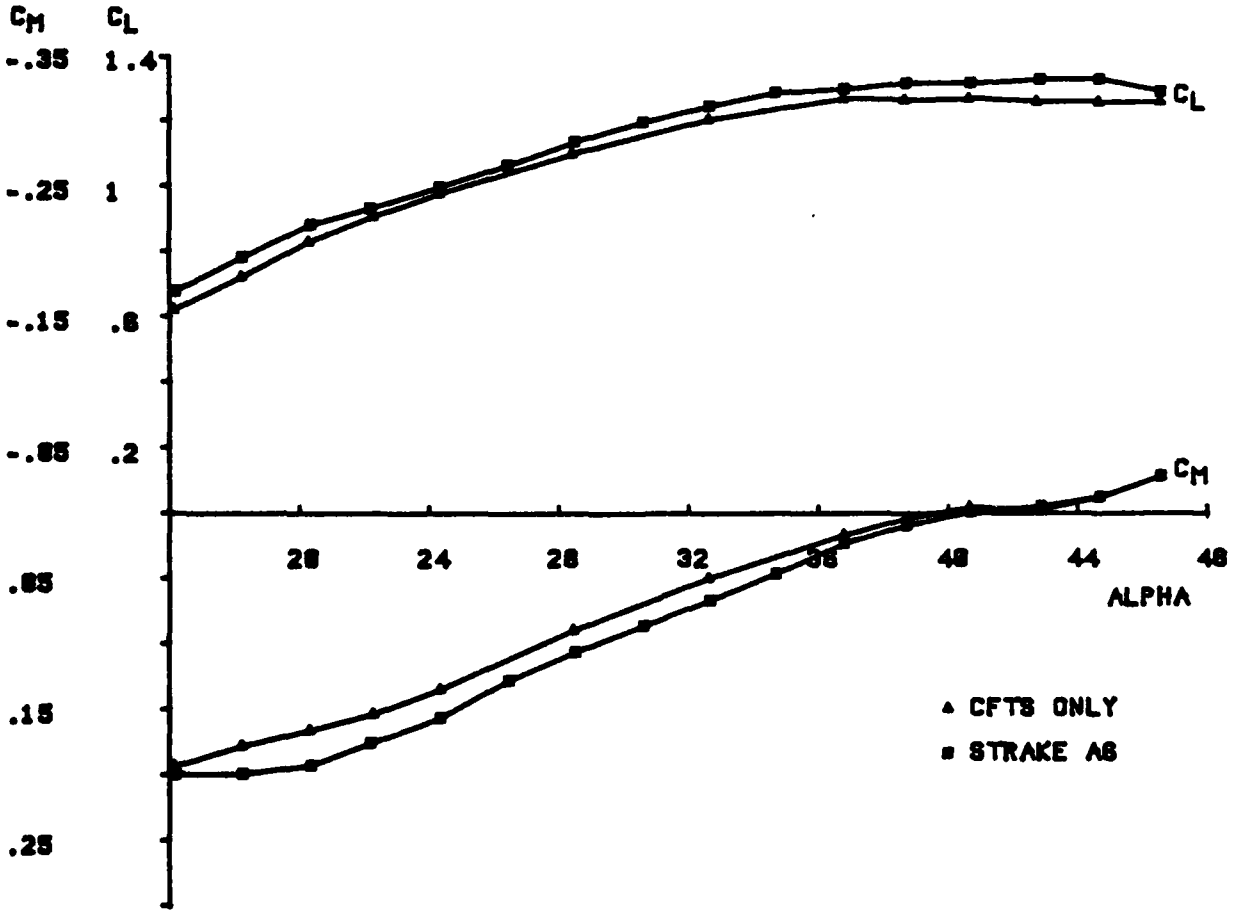

FIG B-23. LONGITUDINAL STABILITY DATA FOR AN F-15 WITH ONLY CFTS AND AN F-15 WITH CFTS AND F/B STRAKES.

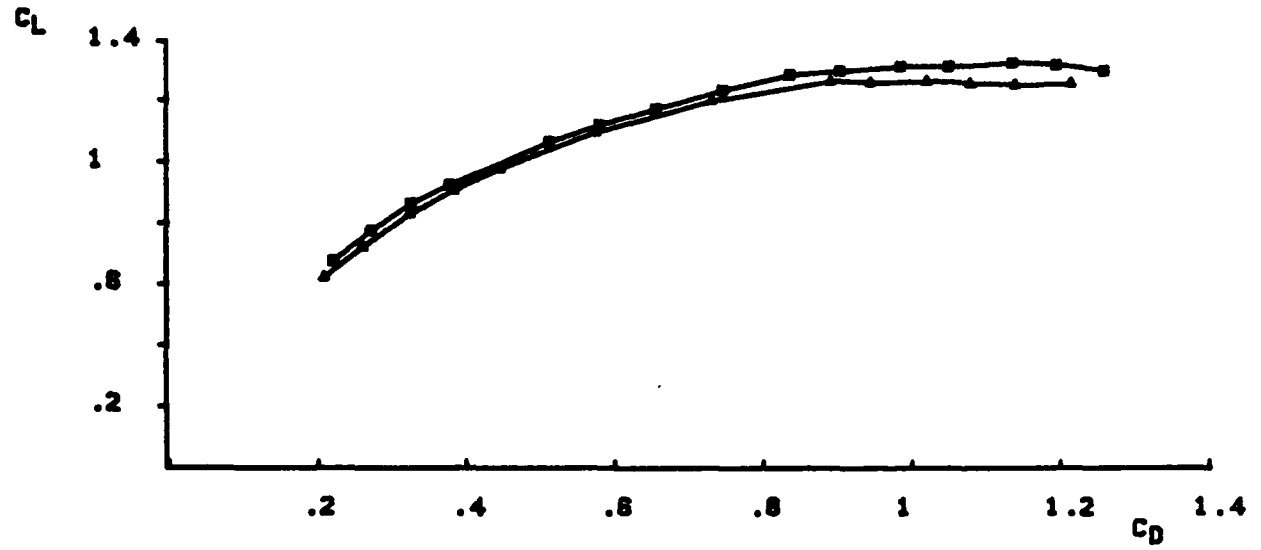

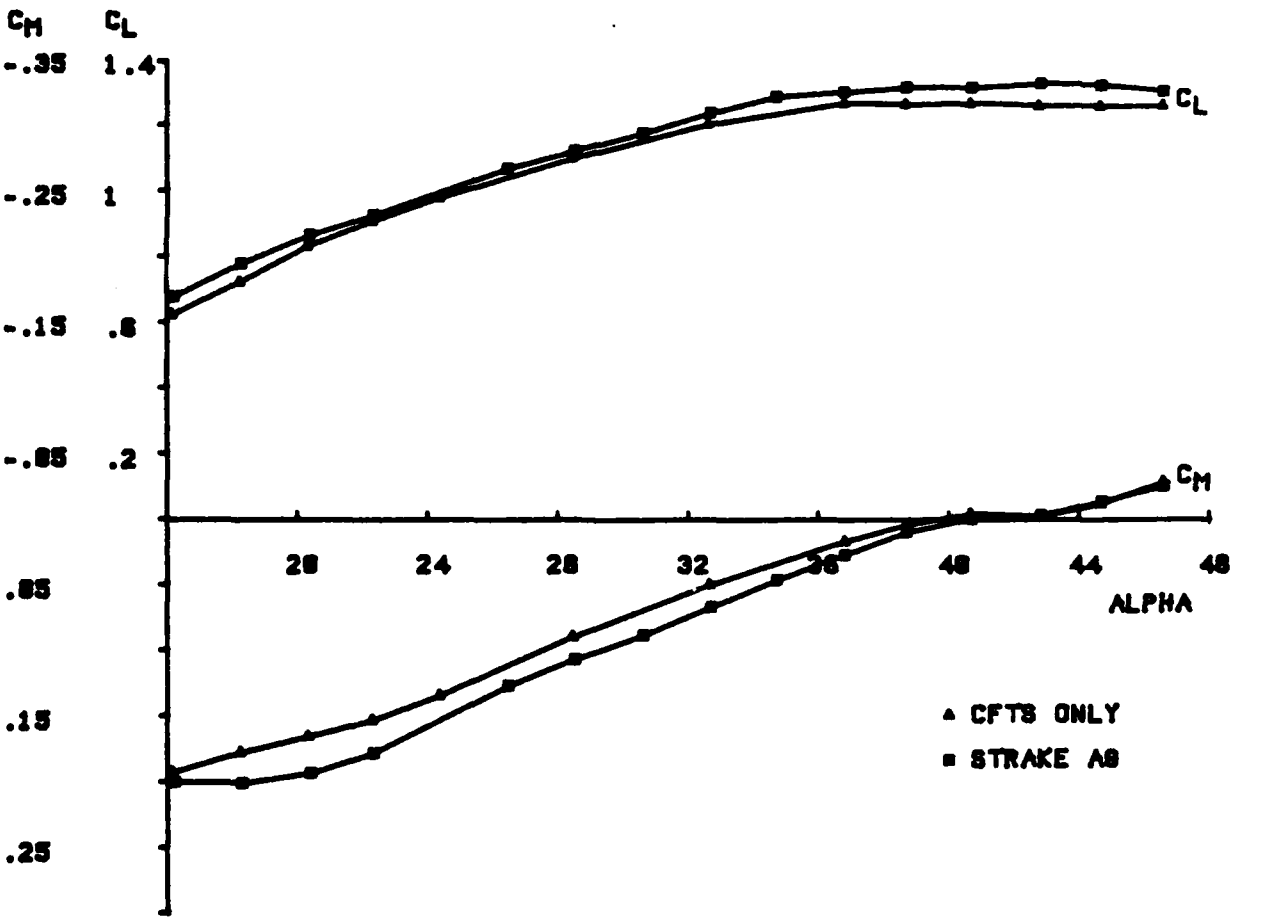

FIG B-24. LONGITUDINAL STABILITY DATA FOR AN F-15 WITH ONLY CFTS AND AN F-15 WITH CFTS AND F/B STRAKES.

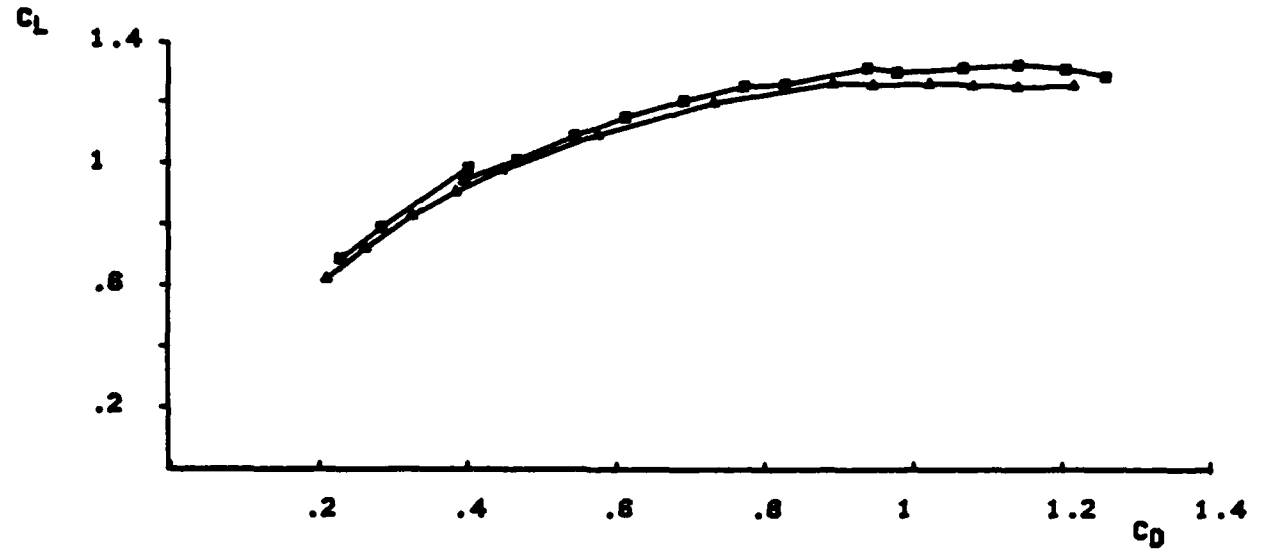

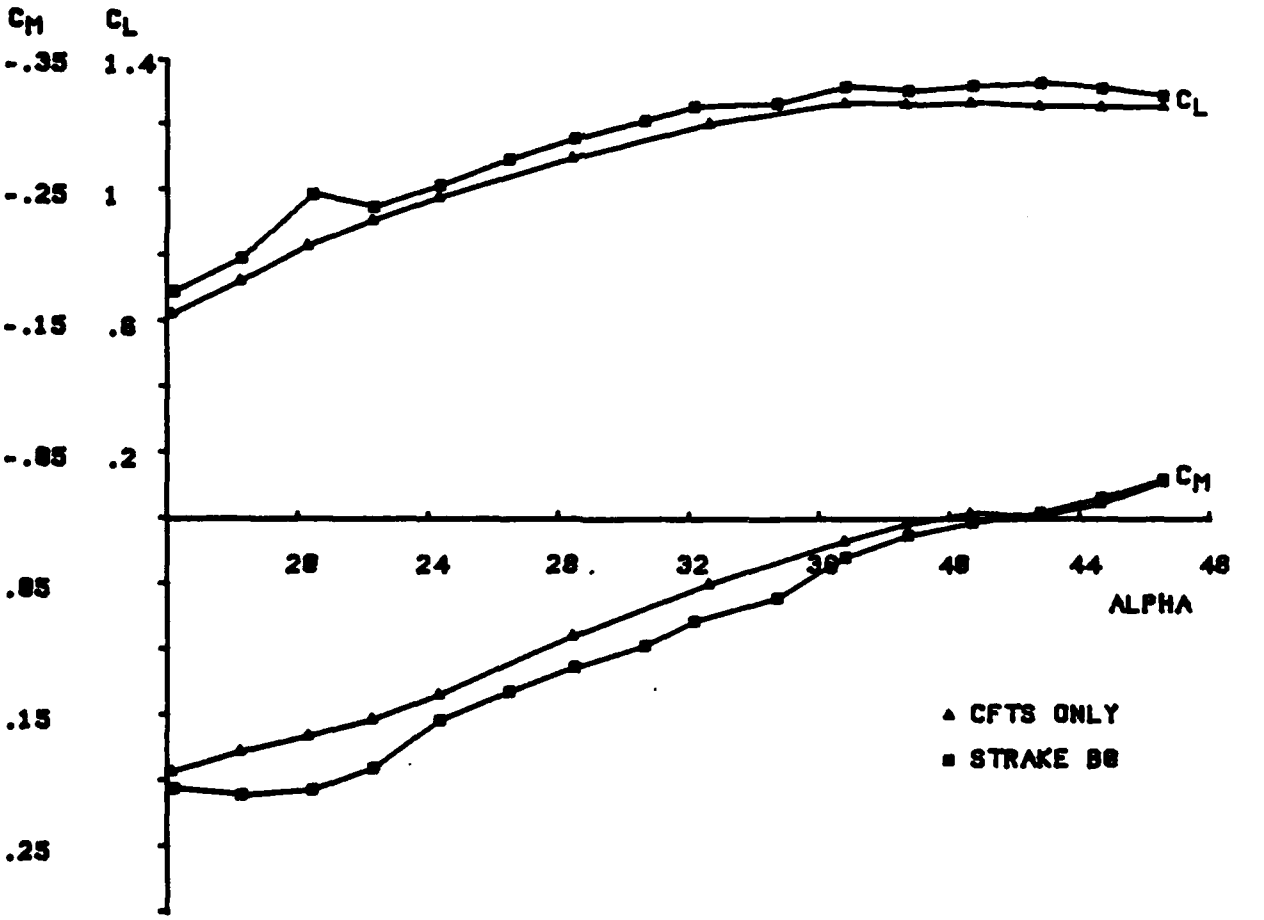

FIG B-25. LONGITUDINAL STABILITY DATA FOR AN F-15 WITH ONLY CFTS AND AN F-15 WITH CFTS AND F/B STRAKES.

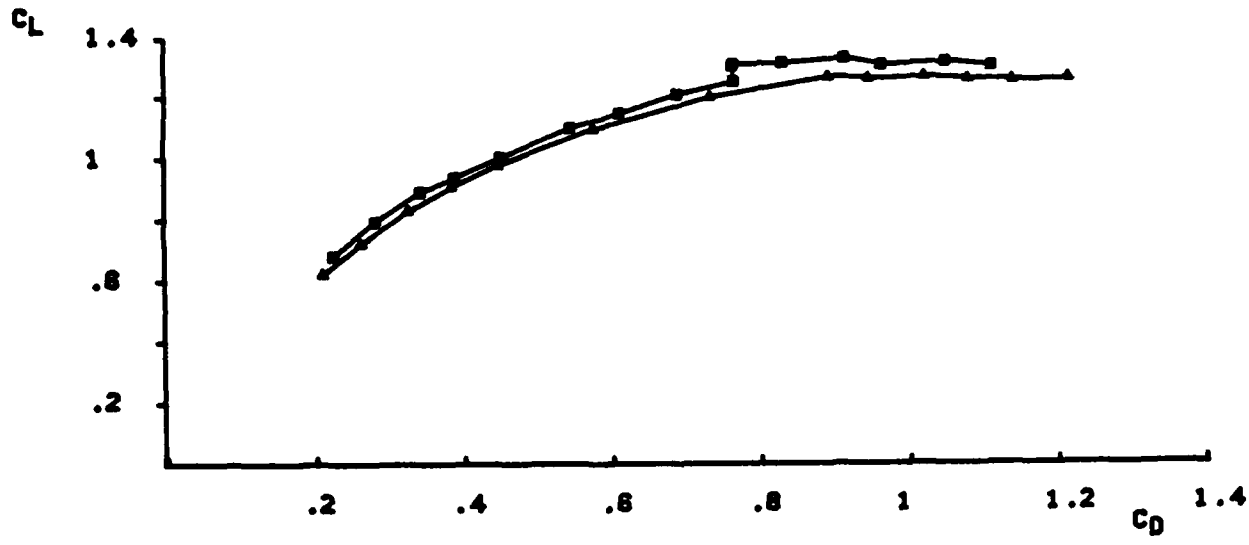

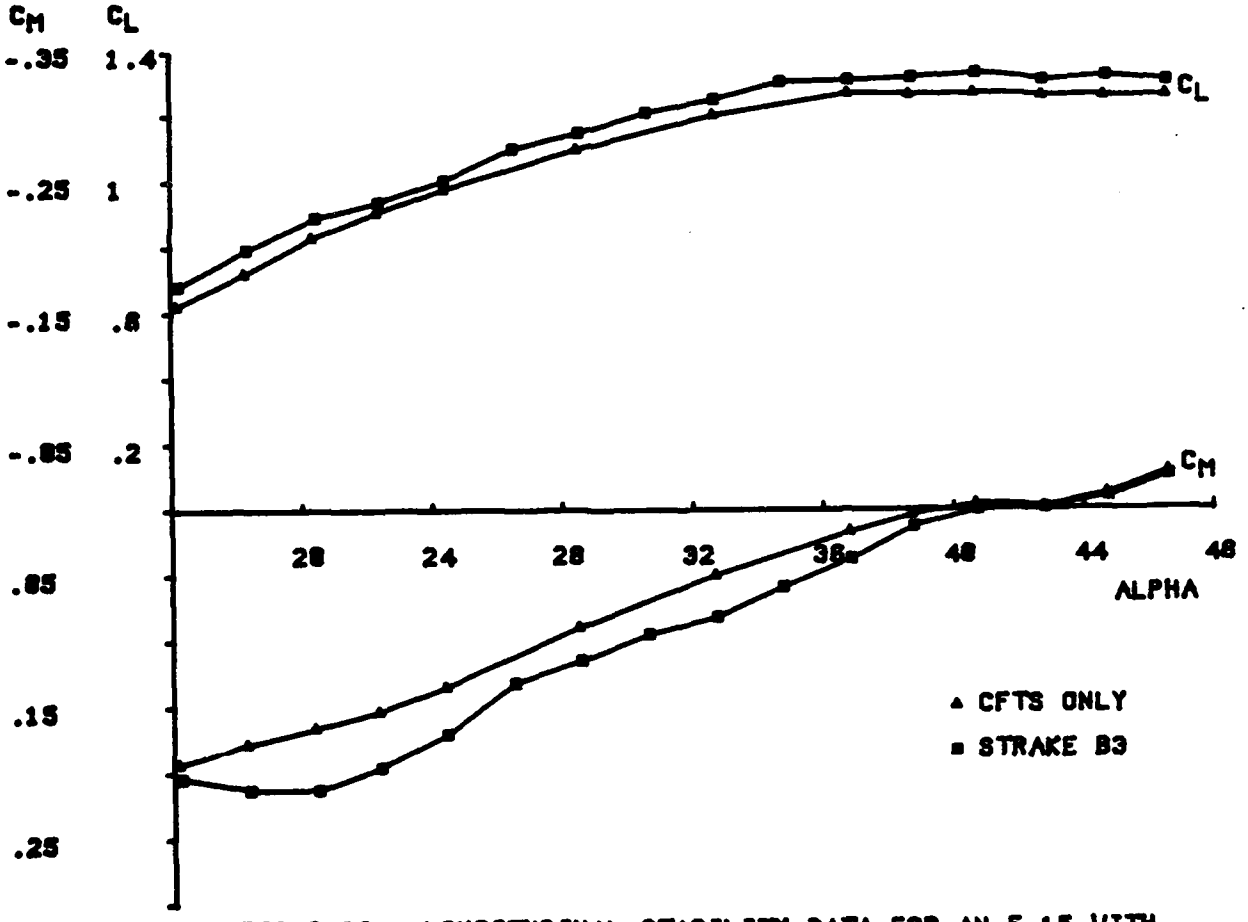

FIG B-26. LONGITUDINAL STABILITY DATA FOR AN F-15 WITH ONLY CFTS AND AN F-15 WITH CFTS AND F/B STRAKES.

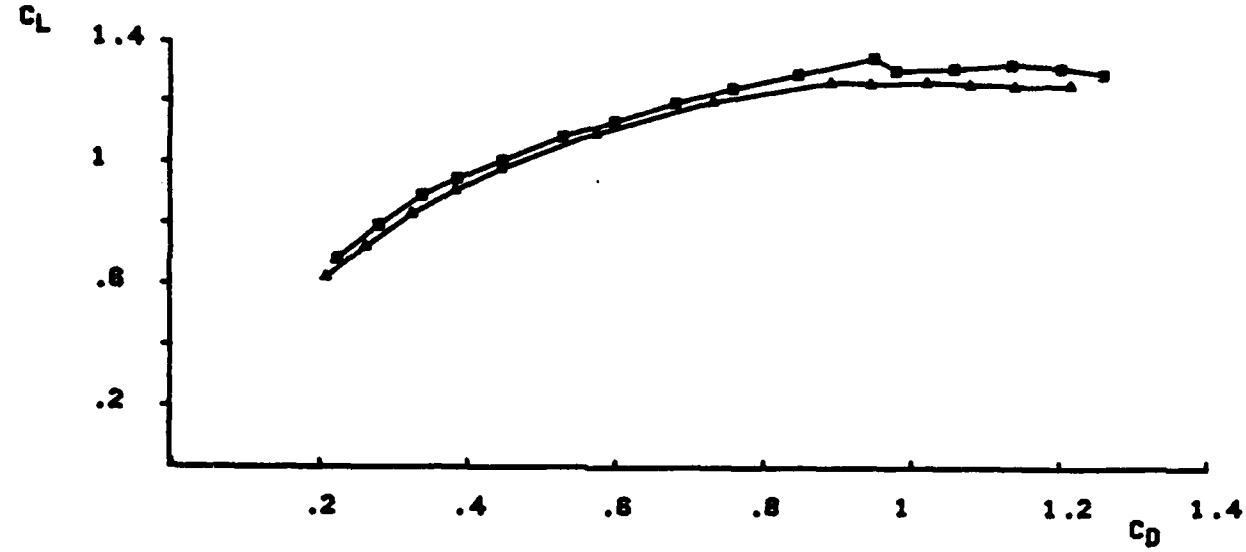

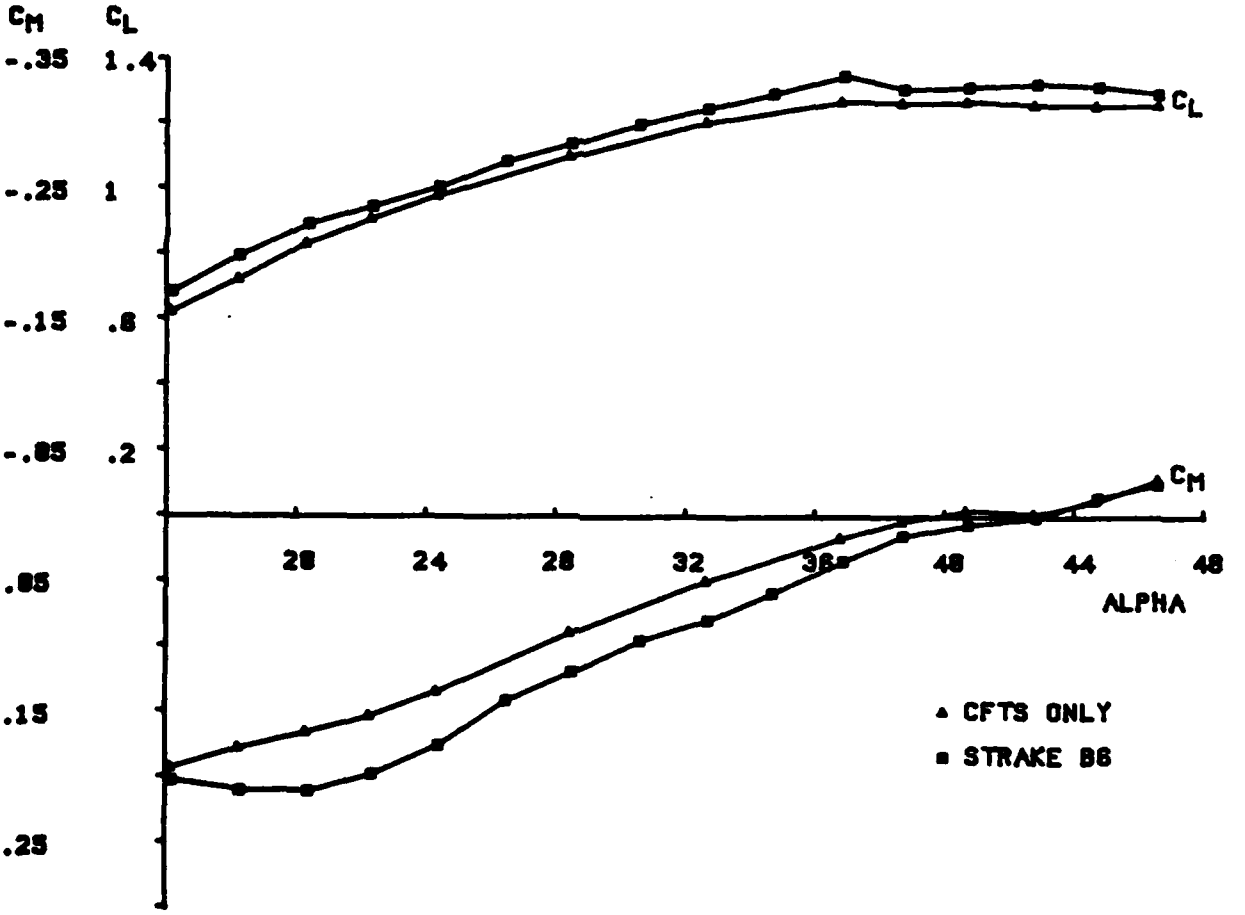

FIG B-27. LONGITUDINAL STABILITY DATA FOR AN F-15 WITH ONLY CFTS AND AN F-15 WITH CFTS AND F/B STRAKES.

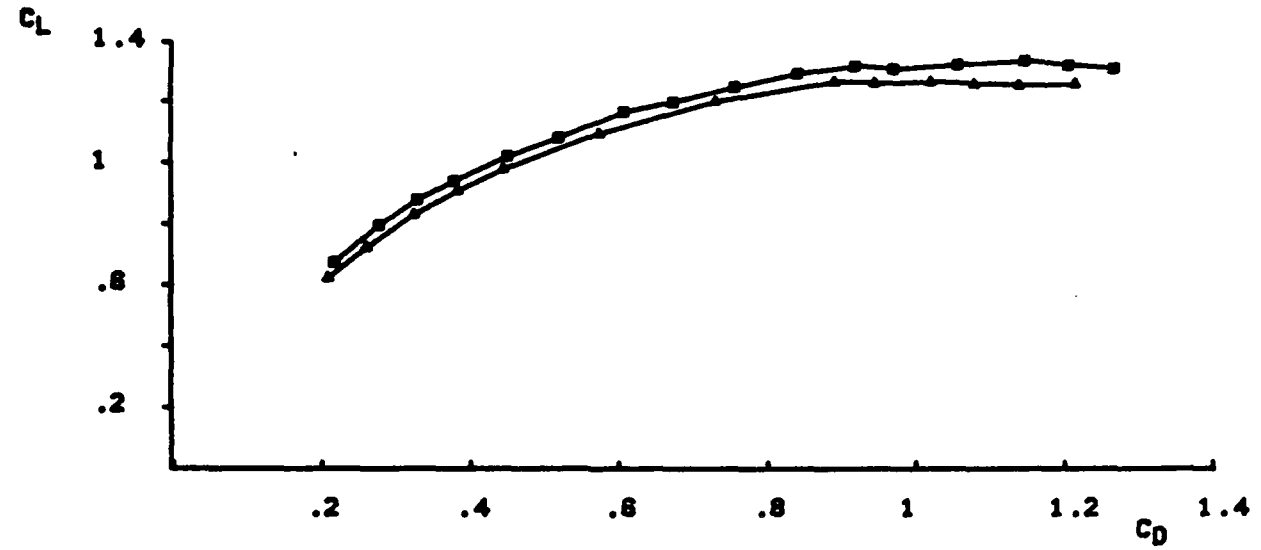

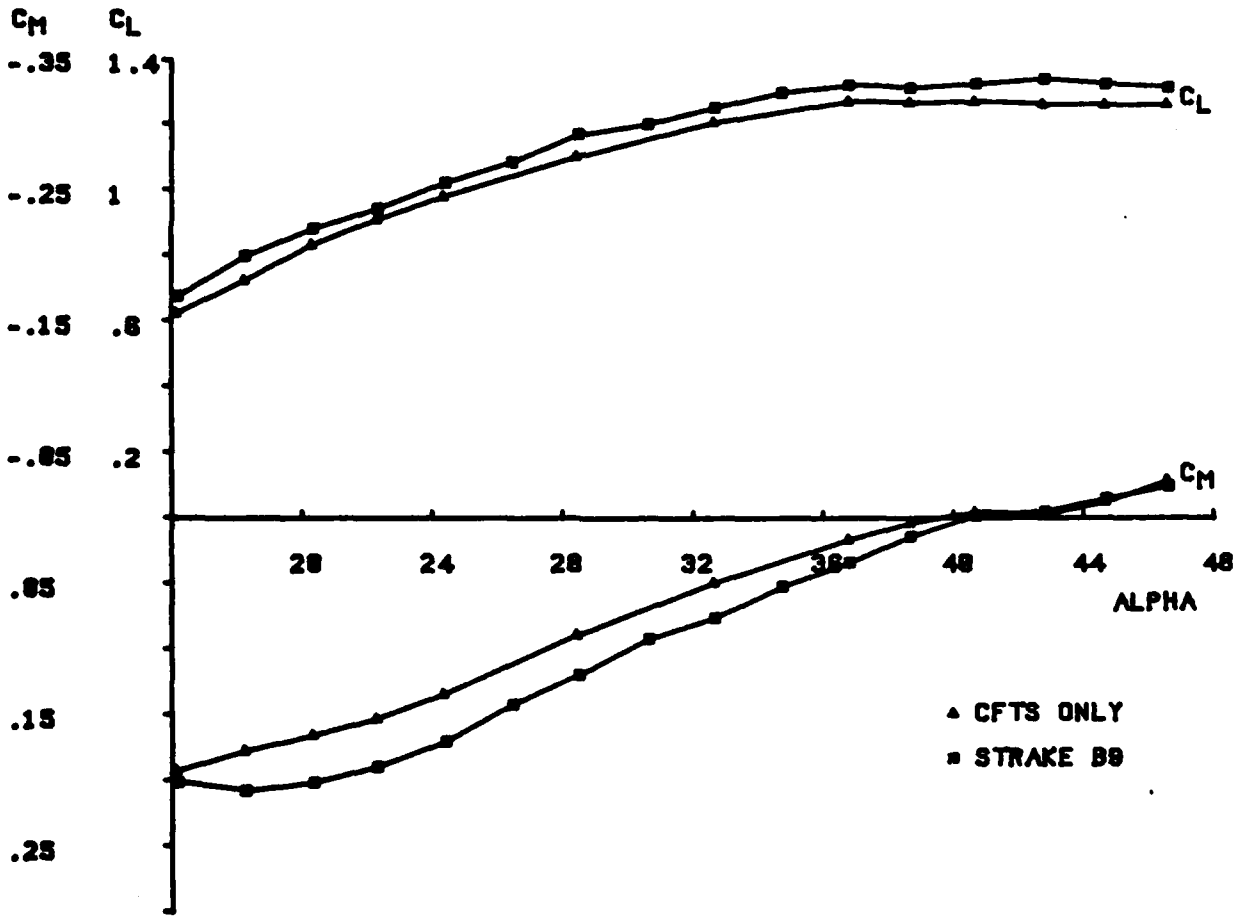

FIG B-28. LONGITUDINAL STABILITY DATA FOR AN F-15 WITH ONLY CFTS AND AN F-15 WITH CFTS AND F/B STRAKES.

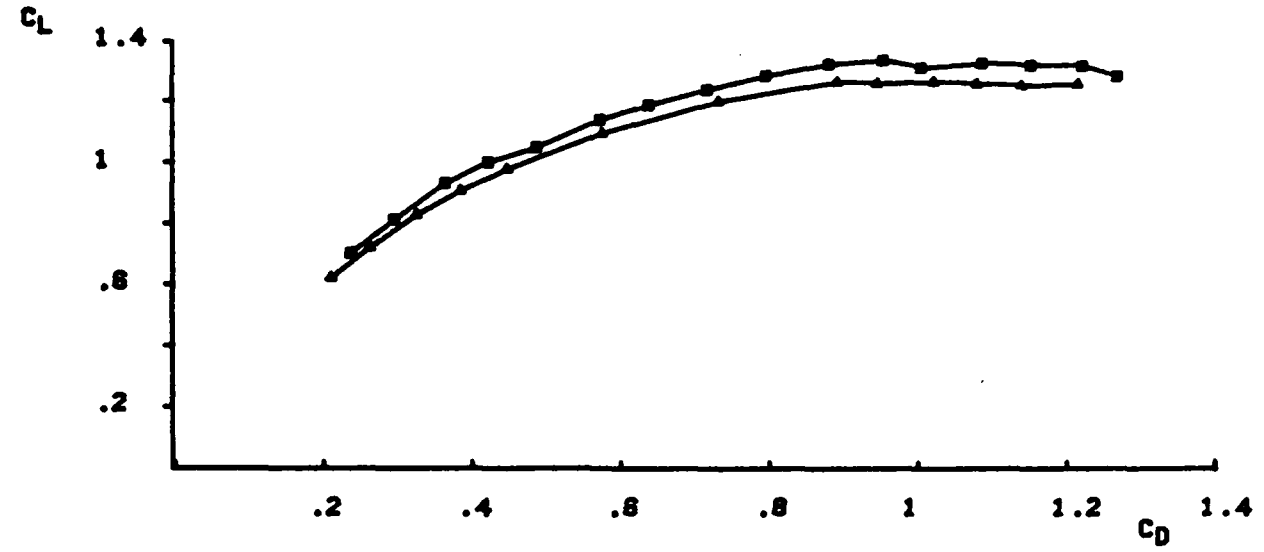

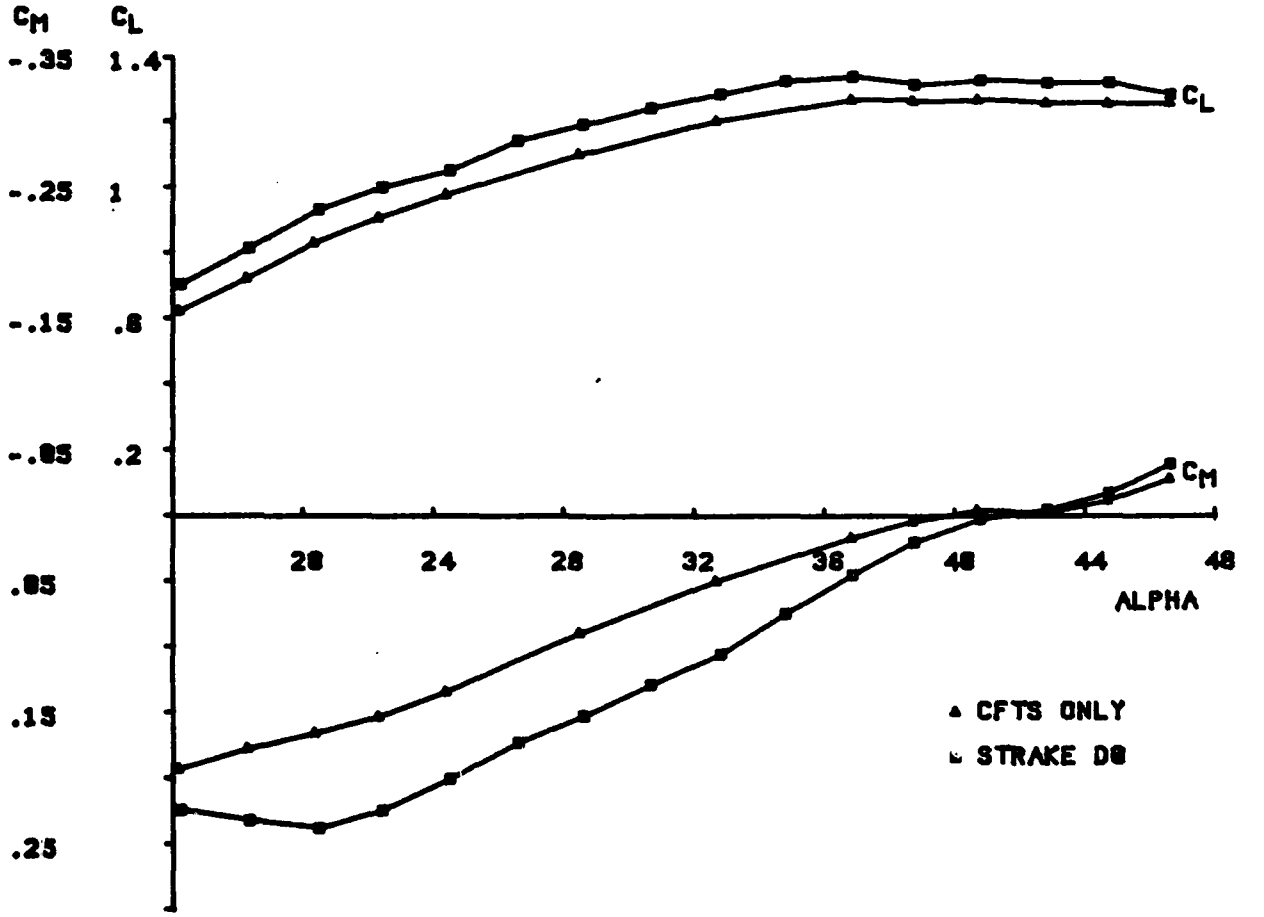

FIG B-28. LONGITUDINAL STABILITY DATA FOR AN F-15 WITH ONLY CFTS AND AN F-15 WITH CFTS AND F/B STRAKES.

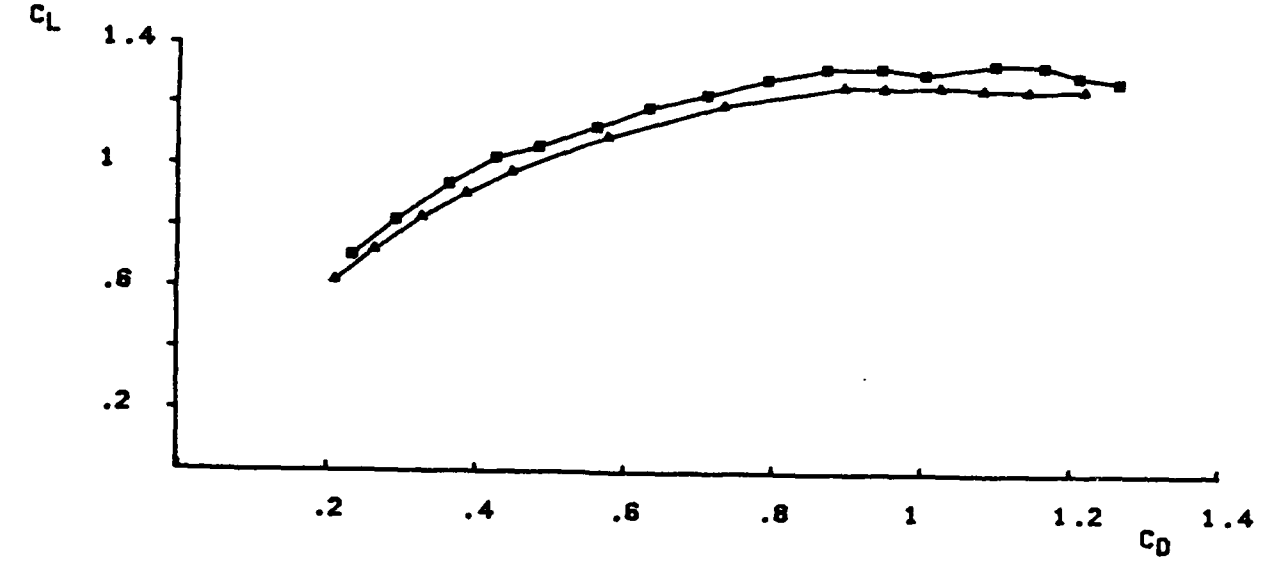

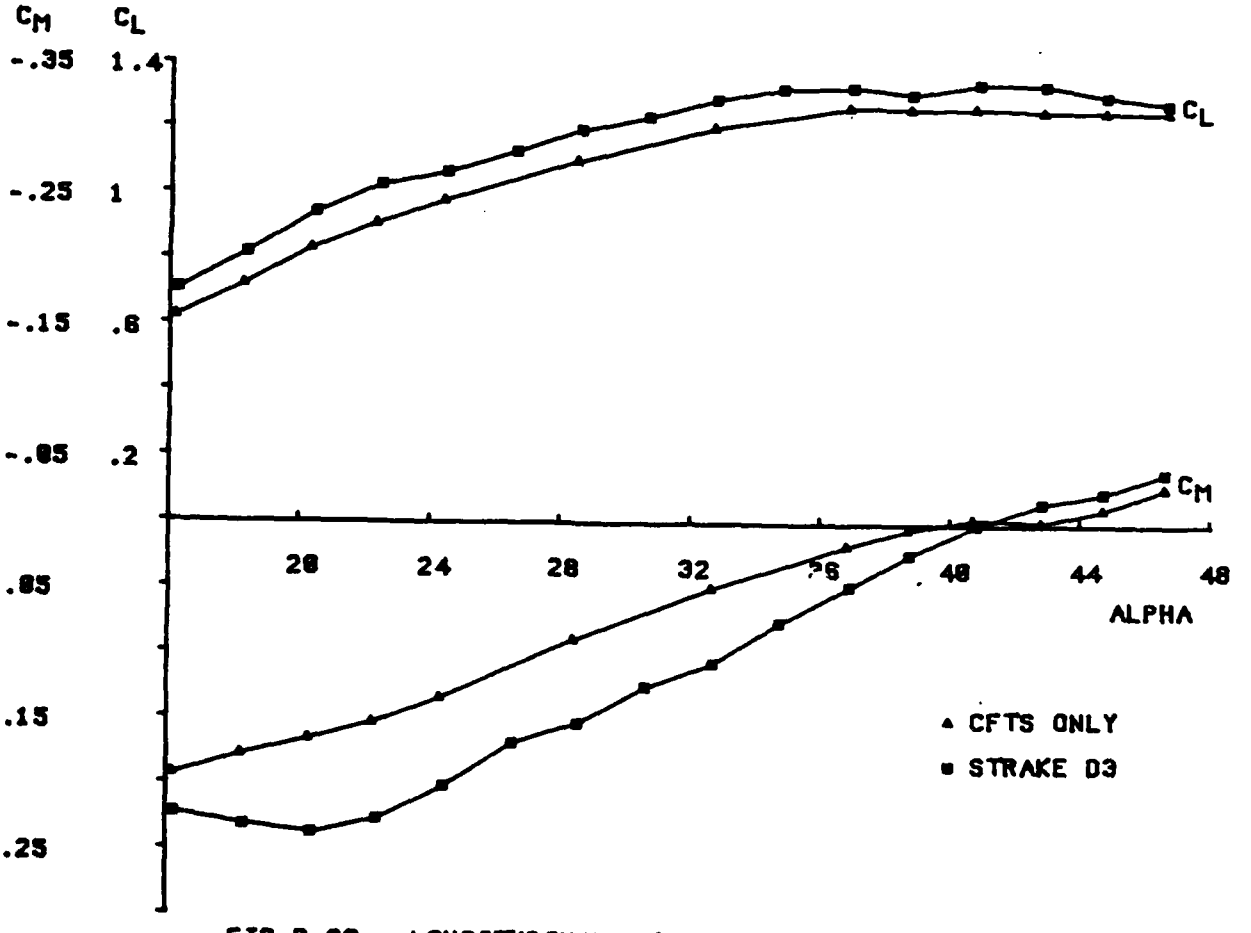

FIG B-30. LONGITUDINAL STABILITY DATA FOR AN F-15 WITH ONLY CFTS AND AN F-15 WITH CFTS AND F/B STRAKES.

AD-A136 912 A WIND TUNNEL INVESTIGATION TO DETERMINE DOMINANT FOREBODY STRAKE DESIGN..(U) AIR FORCE INST OF TECH WRIGHT-PATTERSON AFB OH SCHOOL OF ENGI.. T A DUNCAN 2/2

UNCLASSIFIED DEC 83 AFIT/GAE/AA/83D-7 F/G 20/4 NL

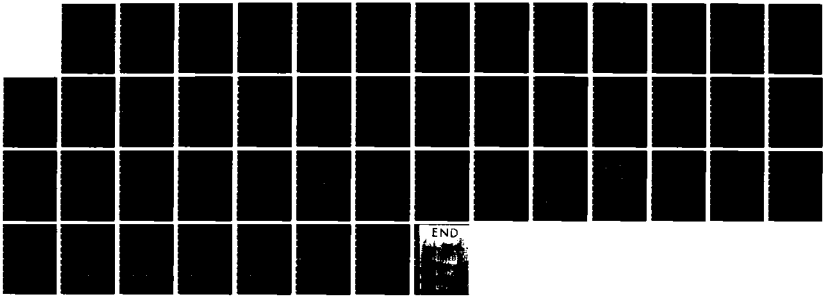

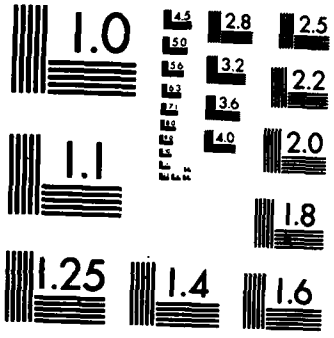

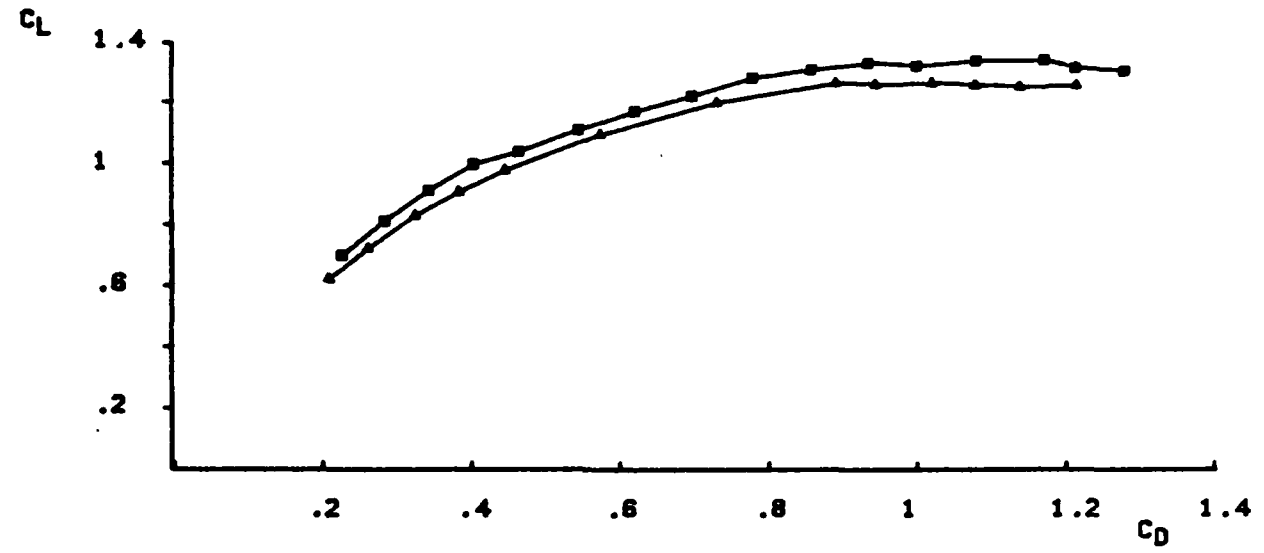

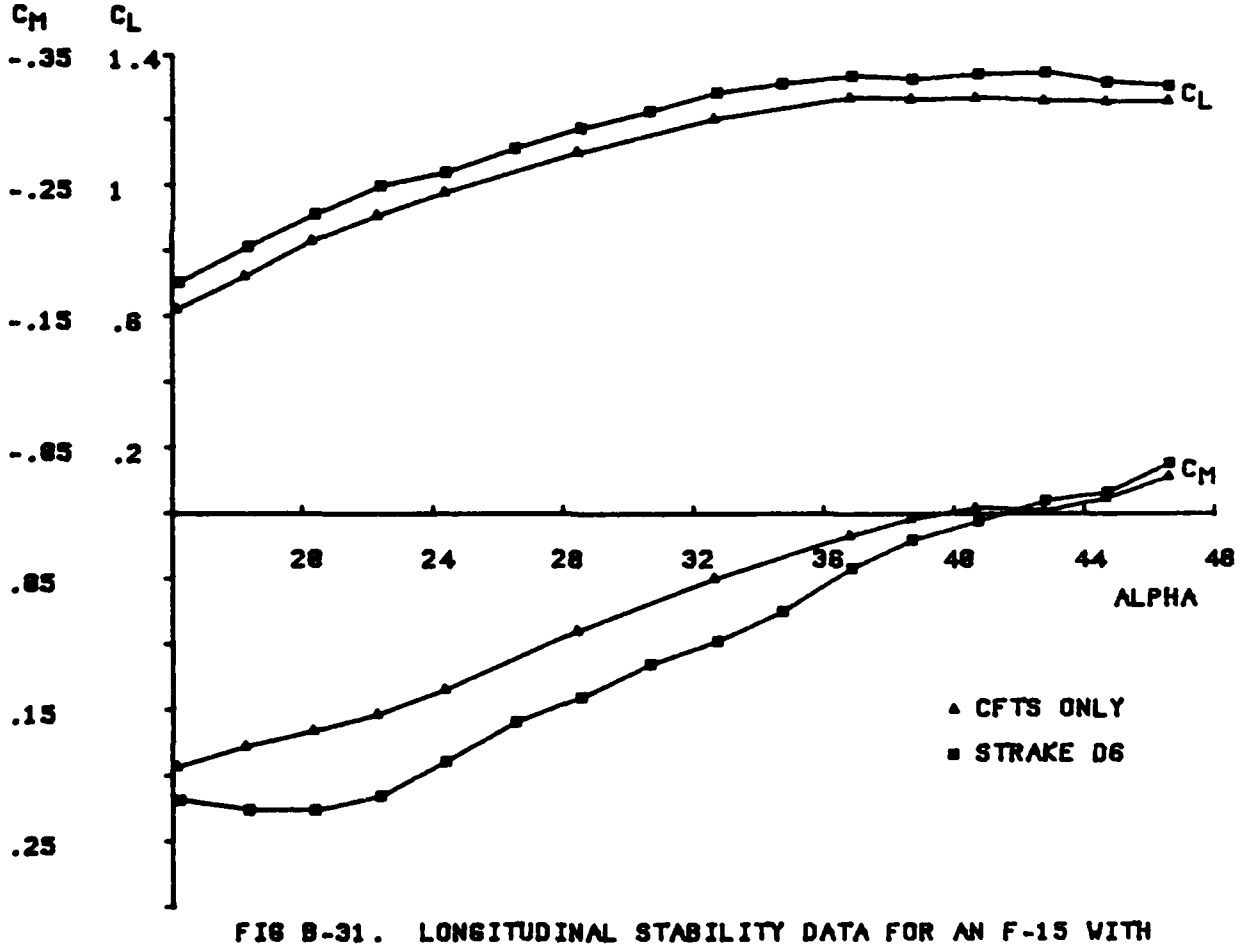

FIG B-31. LONGITUDINAL STABILITY DATA FOR AN F-15 WITH ONLY CFTS AND AN F-15 WITH CFTS AND F/B STRAKES.

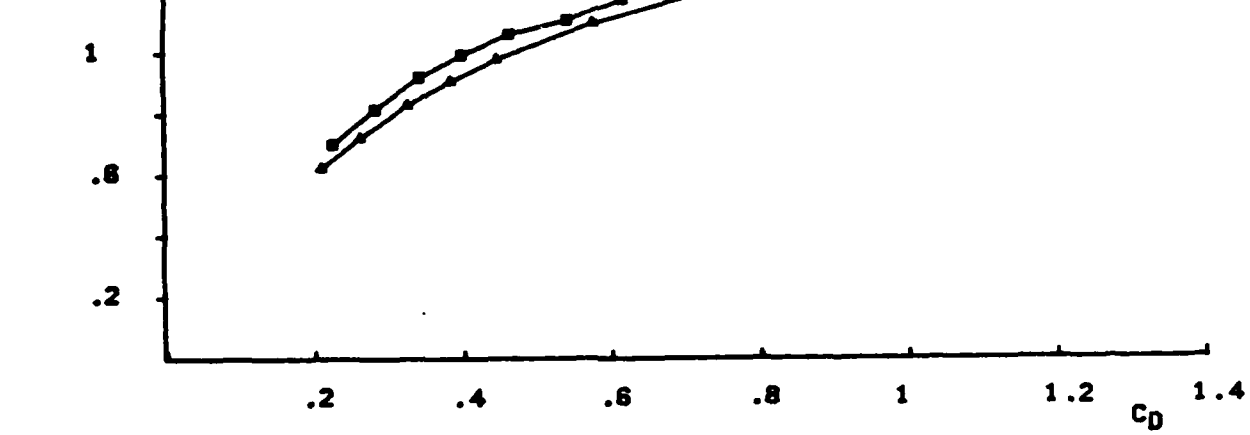

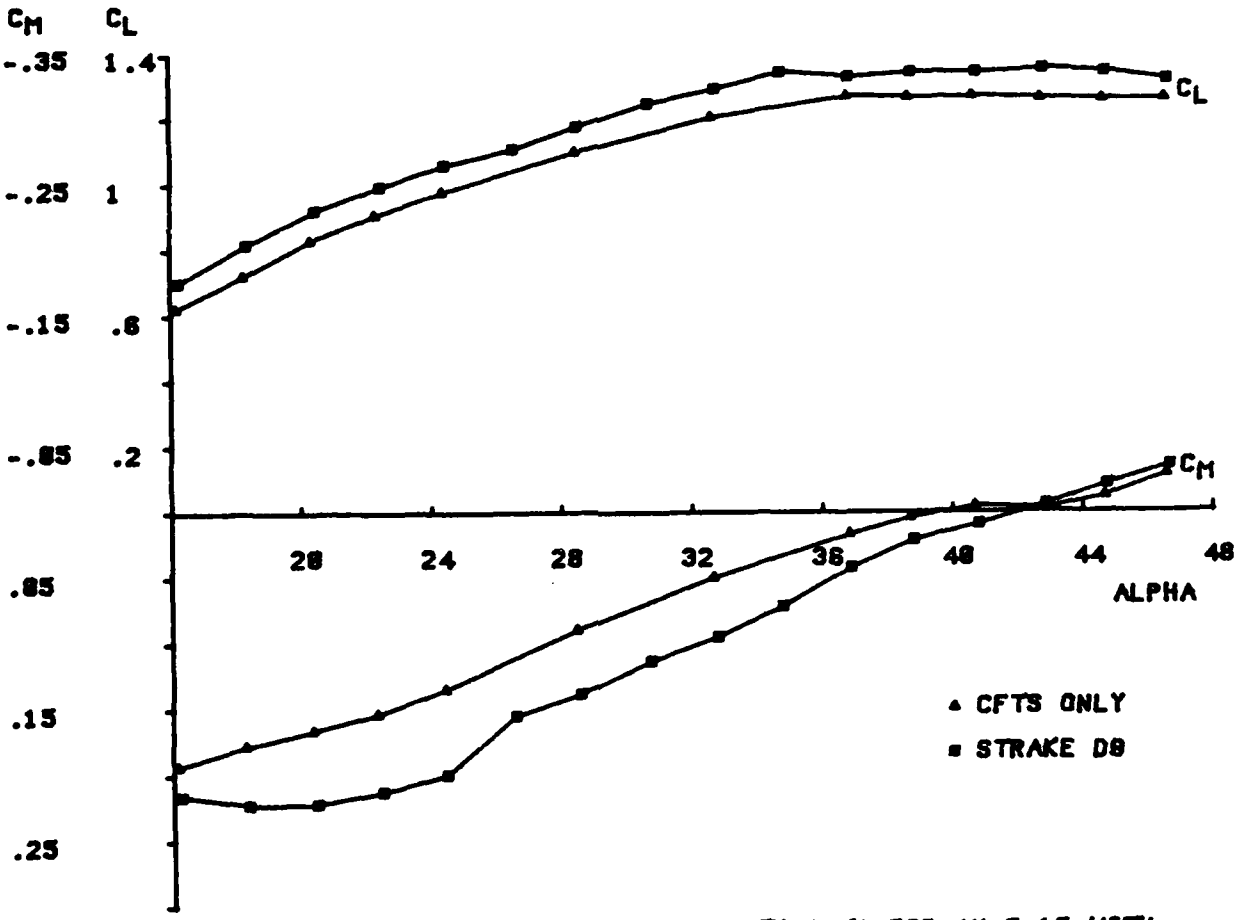

FIG B-32. LONGITUDINAL STABILITY DATA FOR AN F-15 WITH ONLY CFTS AND AN F-15 WITH CFTS AND F/B STRAKES.

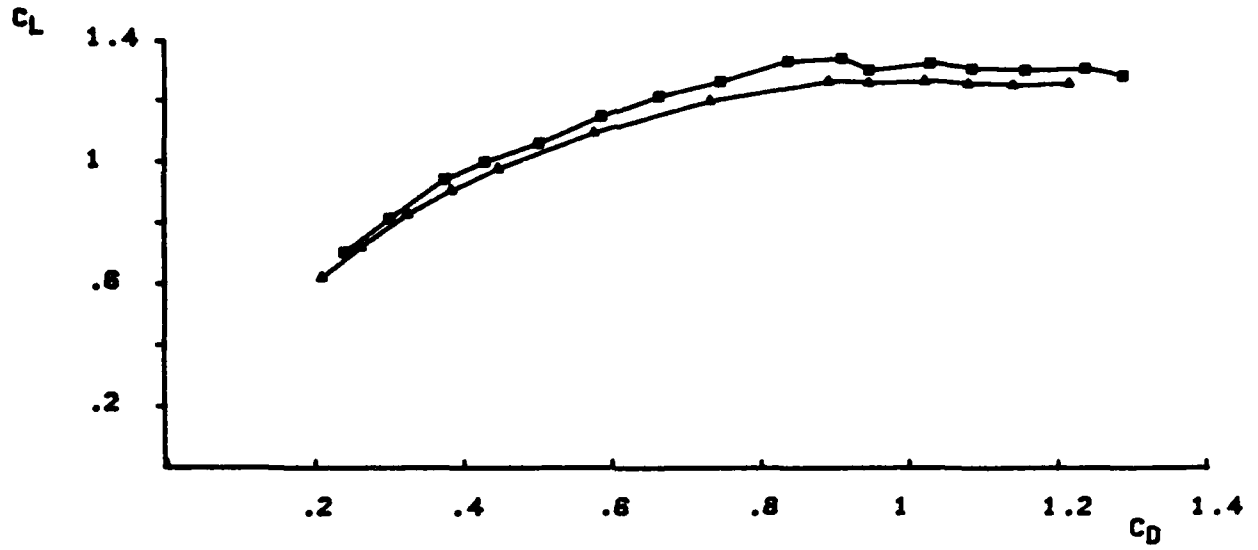

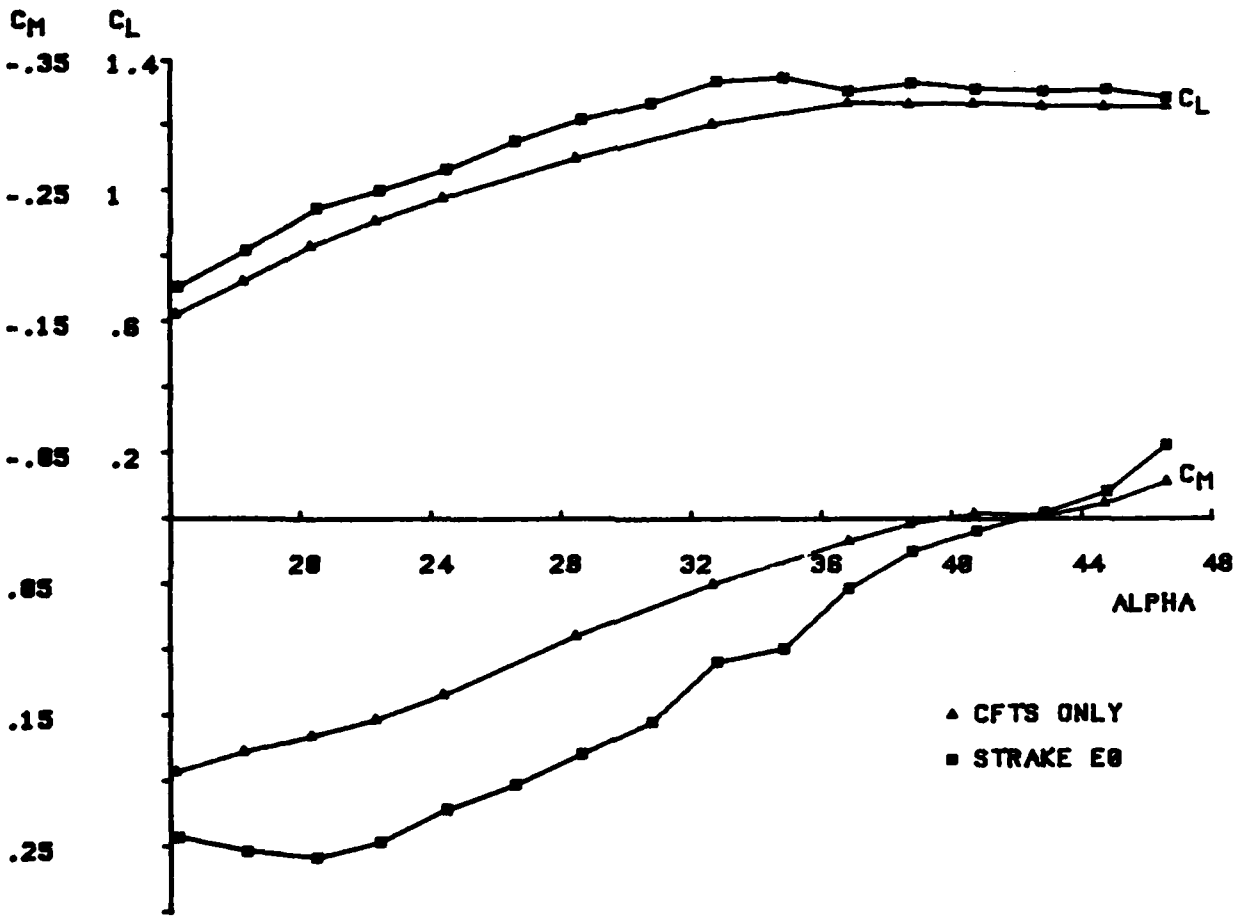

FIG B-33. LONGITUDINAL STABILITY DATA FOR AN F-15 WITH ONLY CFTS AND AN F-15 WITH CFTS AND F/B STRAKES.

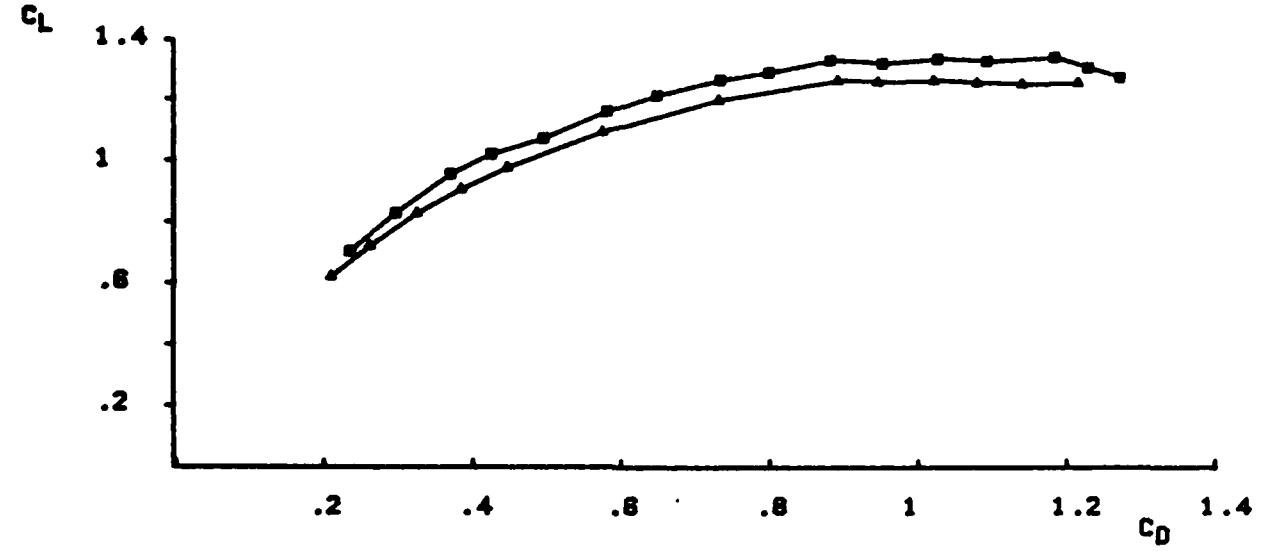

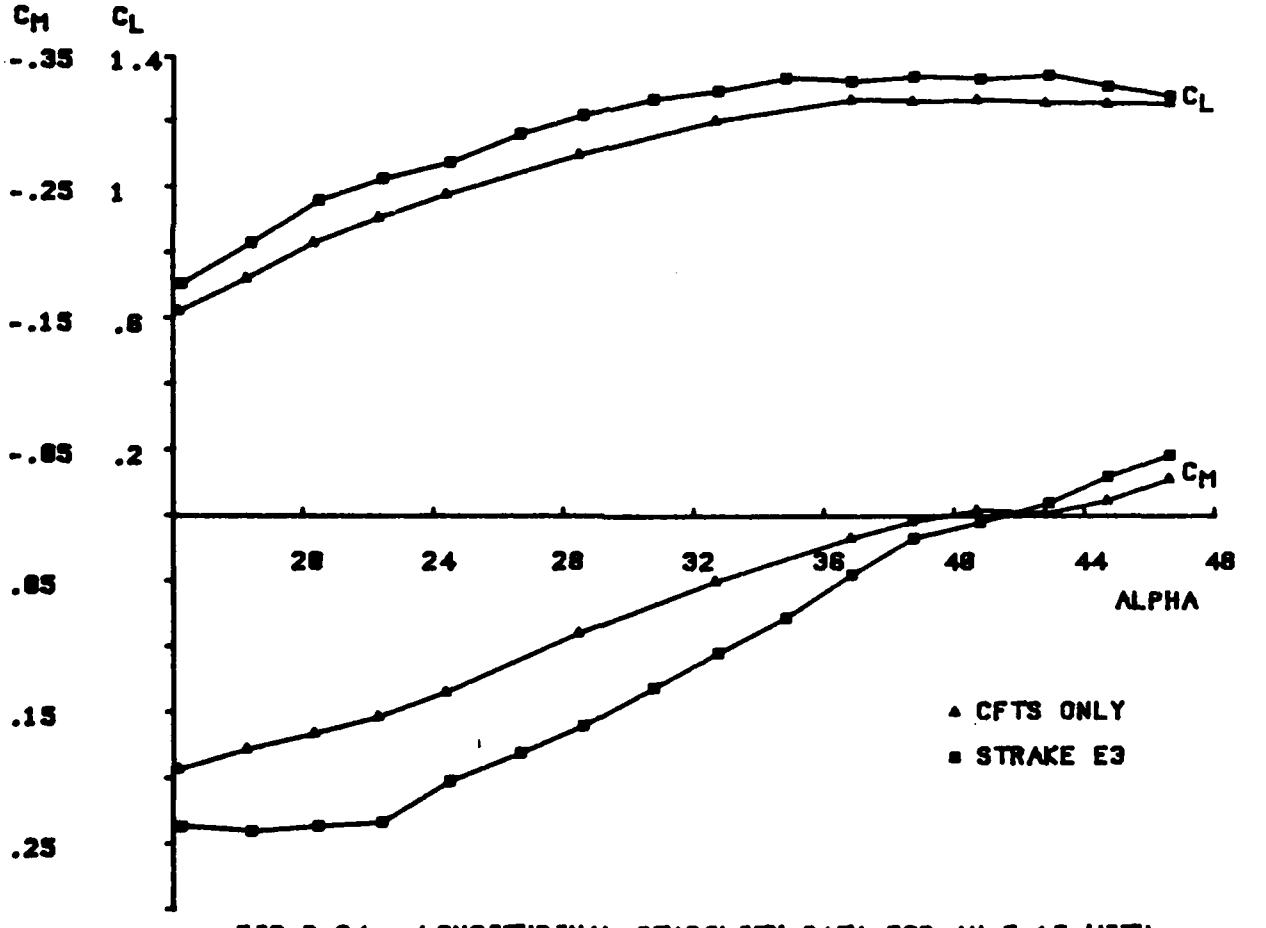

FIG B-34. LONGITUDINAL STABILITY DATA FOR AN F-15 WITH ONLY CFTS AND AN F-15 WITH CFTS AND F/B STRAKES.

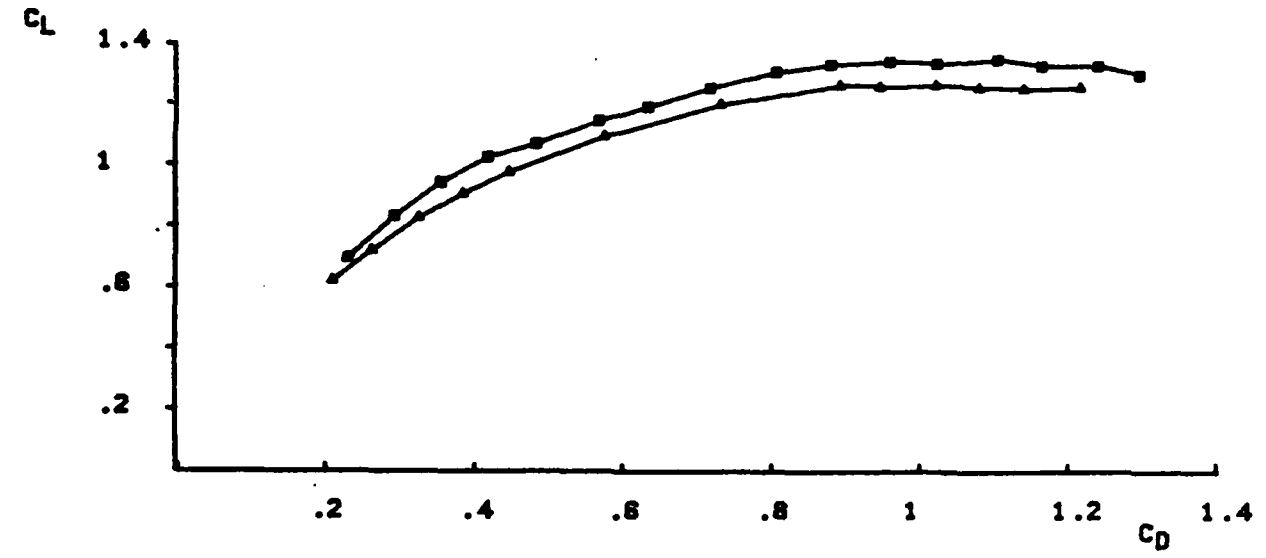

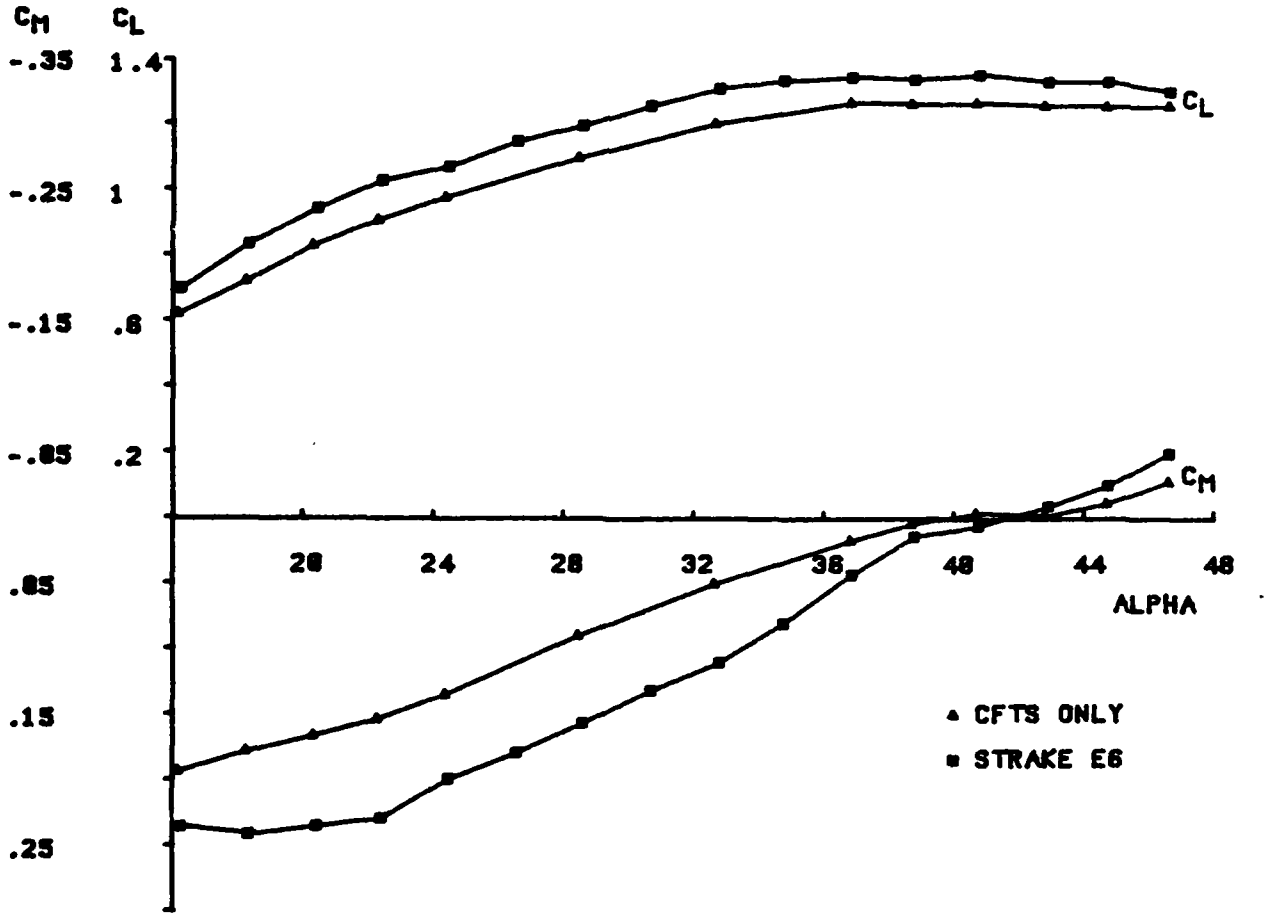

FIG B-35. LONGITUDINAL STABILITY DATA FOR AN F-15 WITH ONLY CFTS AND AN F-15 WITH CFTS AND F/B STRAKES.

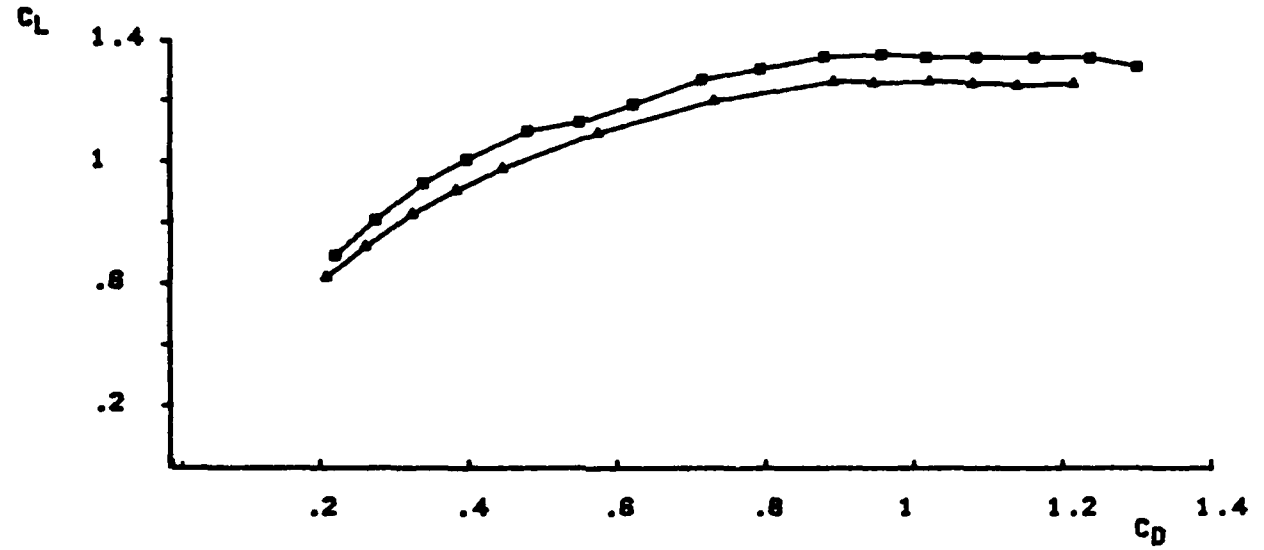

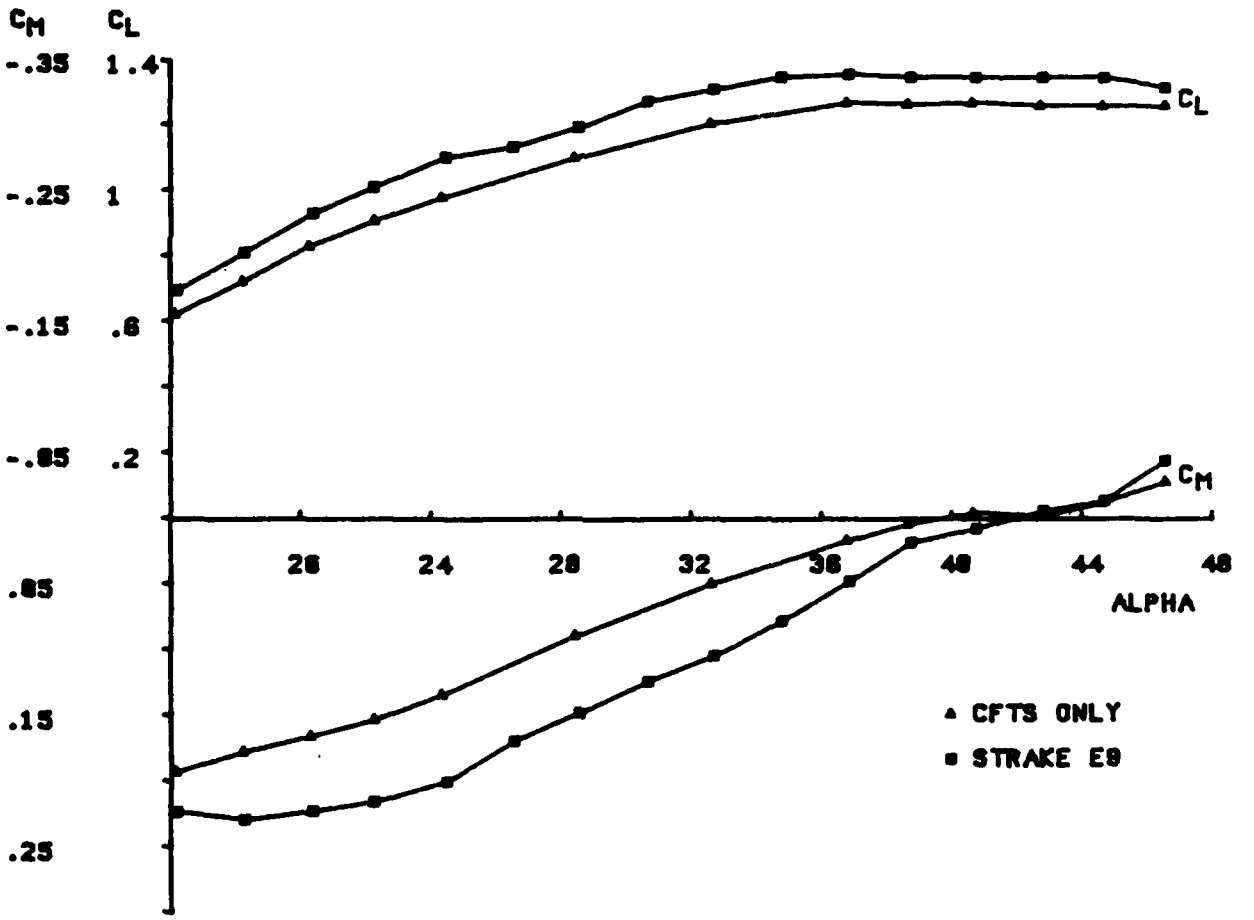

FIG B-36. LONGITUDINAL STABILITY DATA FOR AN F-15 WITH ONLY CFTS AND AN F-15 WITH CFTS AND F/B STRAKES.

Appendix C

Lateral Data

This section contains the high angle of attack (16 to 44 degrees) lateral stability data. The stability parameter, $C_{N_{\beta\ DYN}}$ (see Section III), is plotted versus side slip angle (β) for eight angles of attack (α). Also contained in this appendix are plots of the parameters C_N vs β and C_ℓ vs β. The CFT Only data is shown on each plot for comparison.

The following grid can be used to identify model configurations with strakes. Areas are in percent of wing area, spans in percent of wind span, and strake incidence angle in degrees.

CONF.	AREA	SPAN	ANGLE
A0	.65%	2.5%	0
A3	.65%	2.5%	-3
A6	.65%	2.5%	-6
A9	.65%	2.5%	-9
B0	1.0 %	3.7%	0
B3	1.0 %	3.7%	-3
B6	1.0 %	3.7%	-6
B9	1.0 %	3.7%	-9
C0	1.4 %	5.0%	0
C3	1.4 %	5.0%	-3
C6	1.4 %	5.0%	-6
C9	1.4 %	5.0%	-9
D0	1.8 %	6.2%	0
D3	1.8 %	6.2%	-3
D6	1.8 %	6.2%	-6
D9	1.8 %	6.2%	-9
E0	2.2 %	7.5%	0
E3	2.2 %	7.5%	-3
E6	2.2 %	7.5%	-6
E9	2.2 %	7.5%	-9

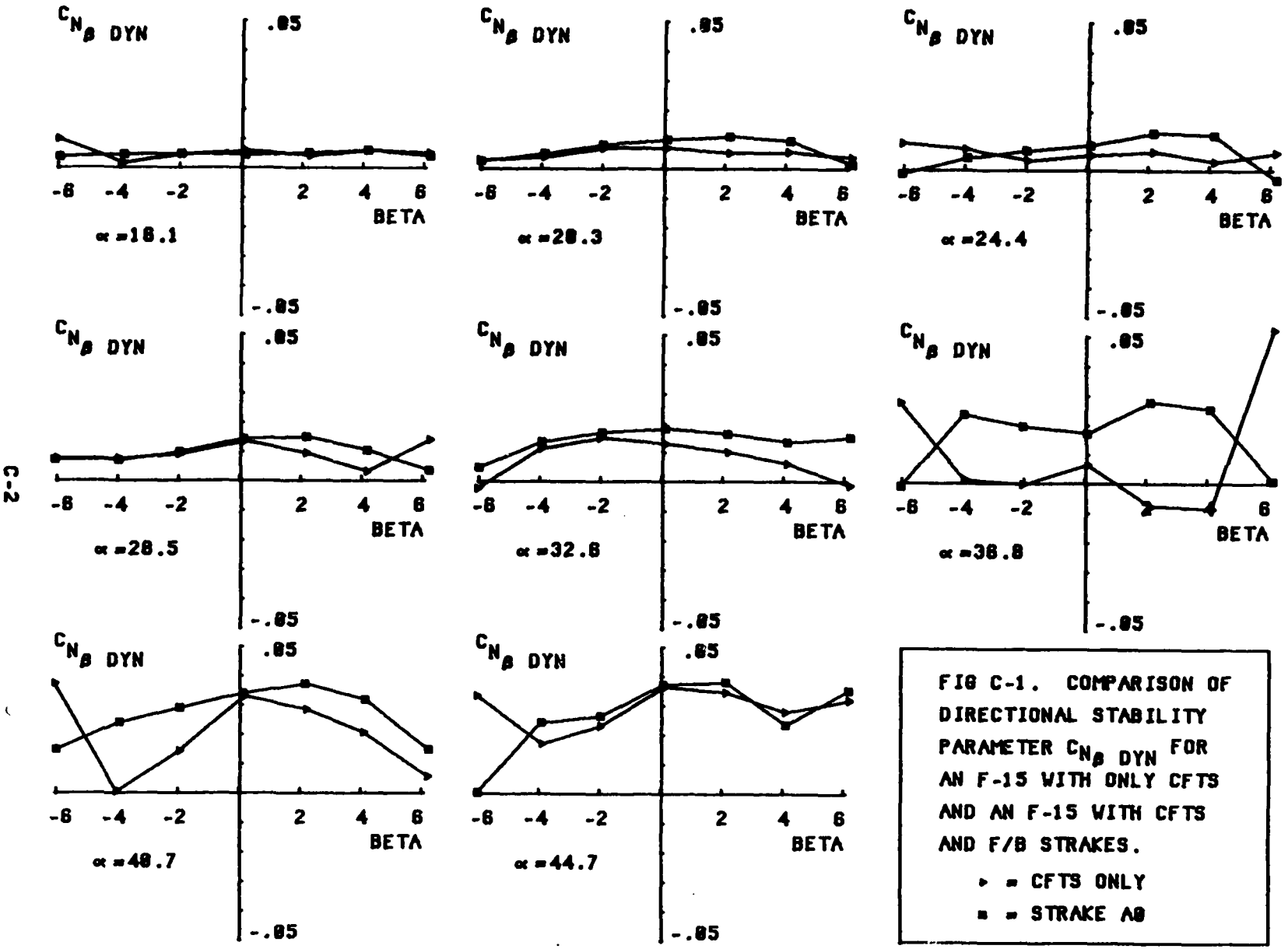

FIG C-1. COMPARISON OF DIRECTIONAL STABILITY PARAMETER C_{N_β} DYN FOR AN F-15 WITH ONLY CFTS AND AN F-15 WITH CFTS AND F/B STRAKES.

▸ = CFTS ONLY

▪ = STRAKE A8

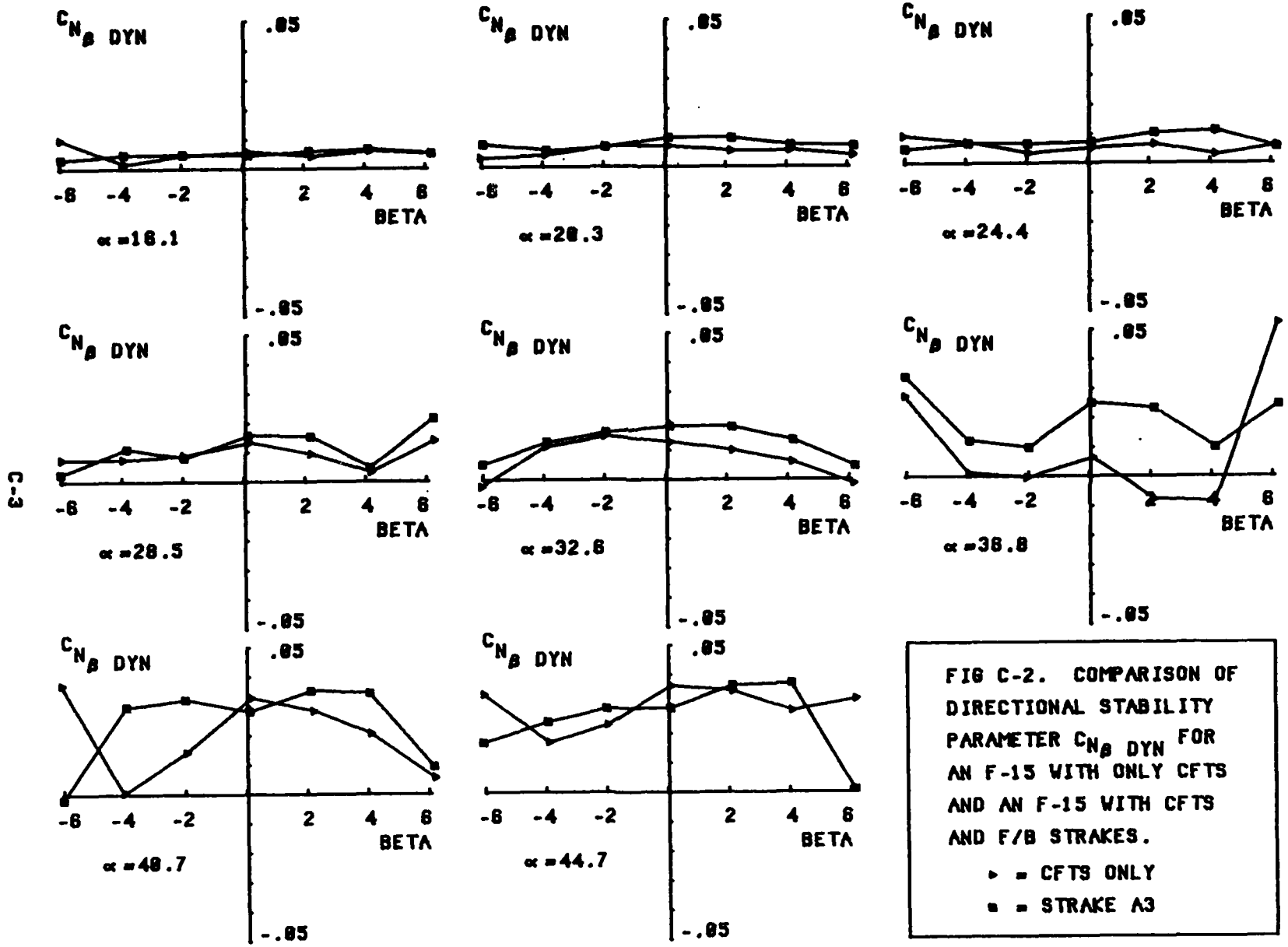

FIG C-2. COMPARISON OF DIRECTIONAL STABILITY PARAMETER $C_{N_\beta\ DYN}$ FOR AN F-15 WITH ONLY CFTS AND AN F-15 WITH CFTS AND F/B STRAKES.

▸ = CFTS ONLY

▪ = STRAKE A3

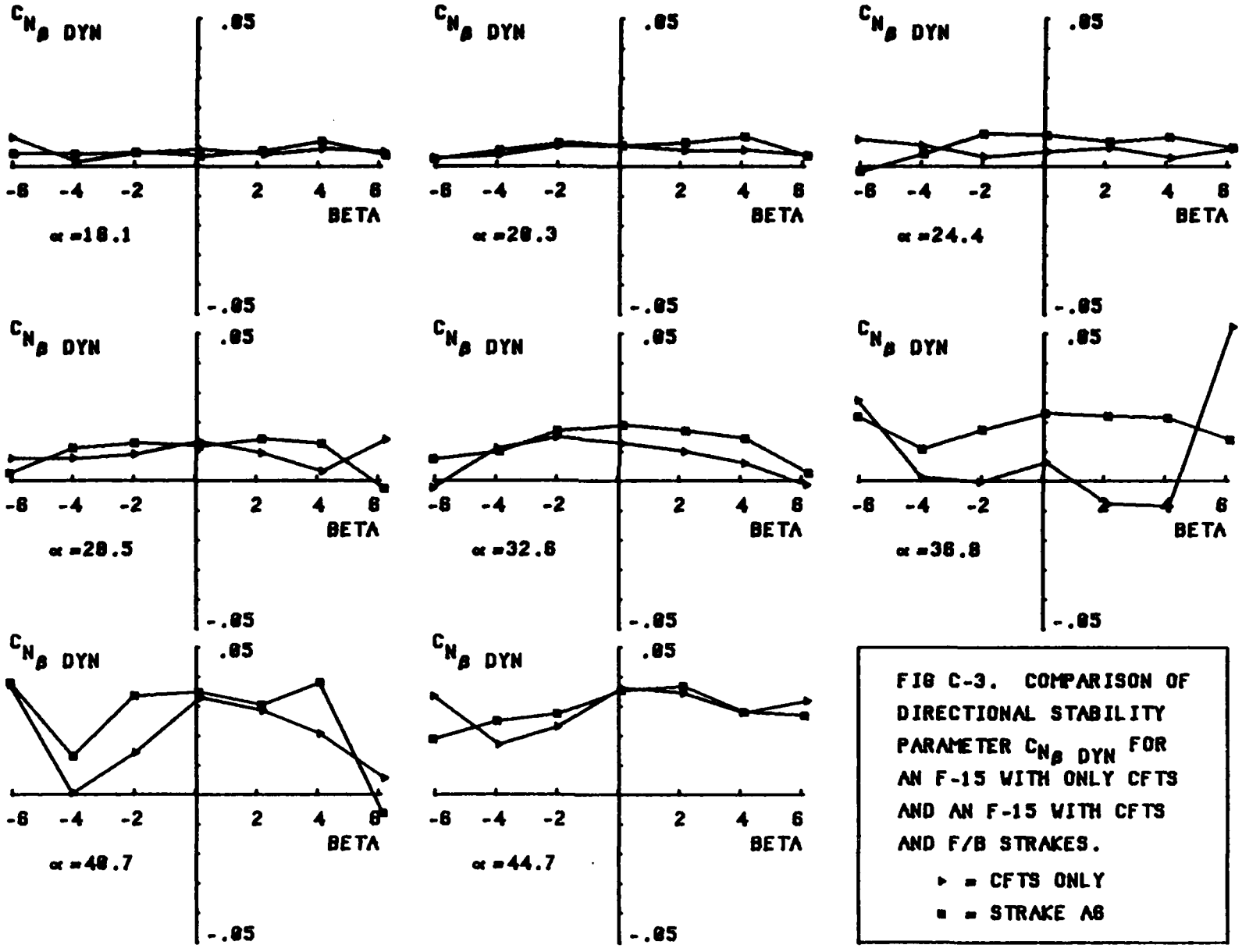

FIG C-3. COMPARISON OF DIRECTIONAL STABILITY PARAMETER $C_{N_\beta\ DYN}$ FOR AN F-15 WITH ONLY CFTS AND AN F-15 WITH CFTS AND F/B STRAKES.

▸ = CFTS ONLY

▪ = STRAKE A8

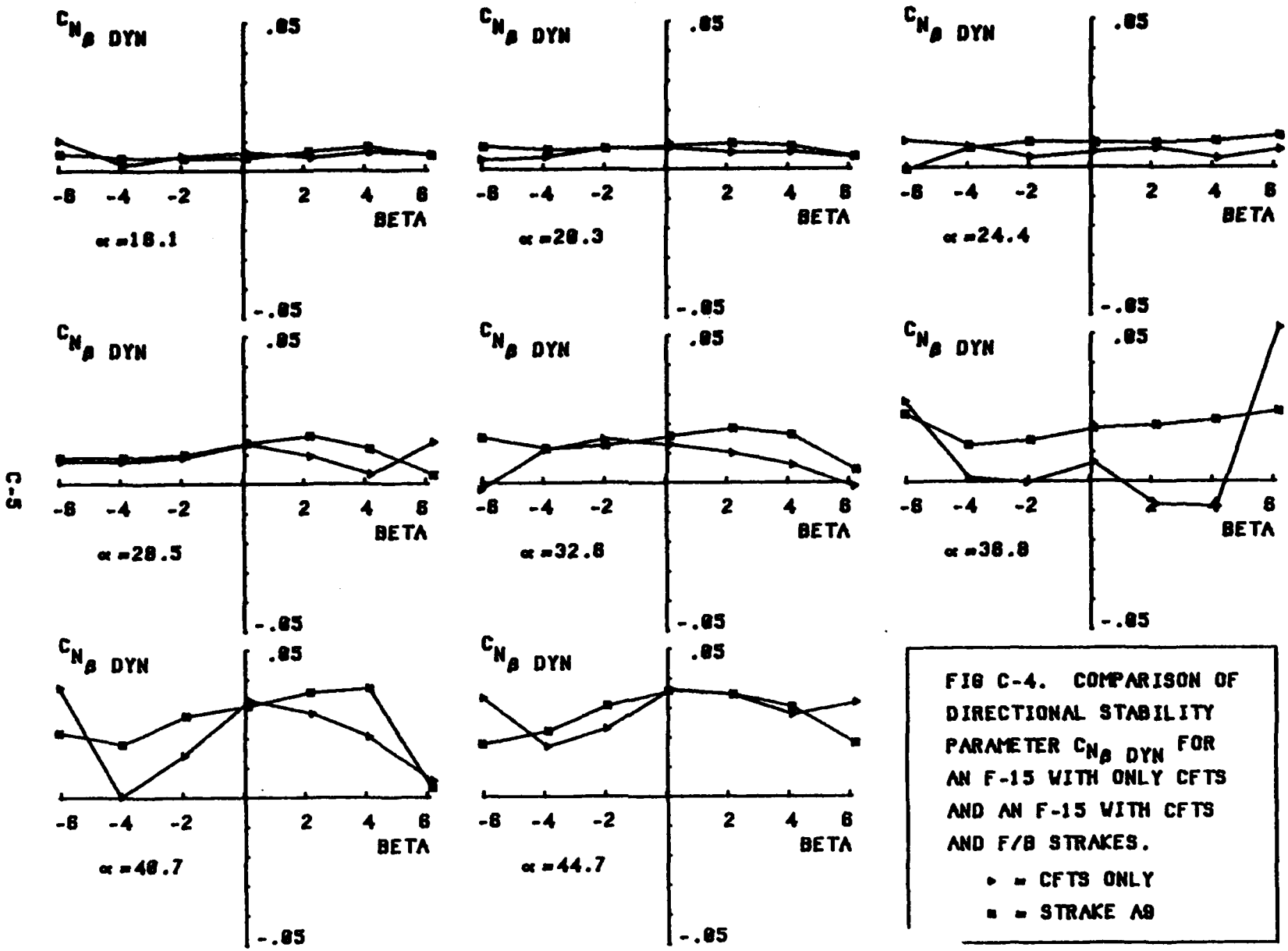

FIG C-4. COMPARISON OF DIRECTIONAL STABILITY PARAMETER $C_{N_\beta\ DYN}$ FOR AN F-15 WITH ONLY CFTS AND AN F-15 WITH CFTS AND F/B STRAKES.

▸ = CFTS ONLY

▪ = STRAKE A9

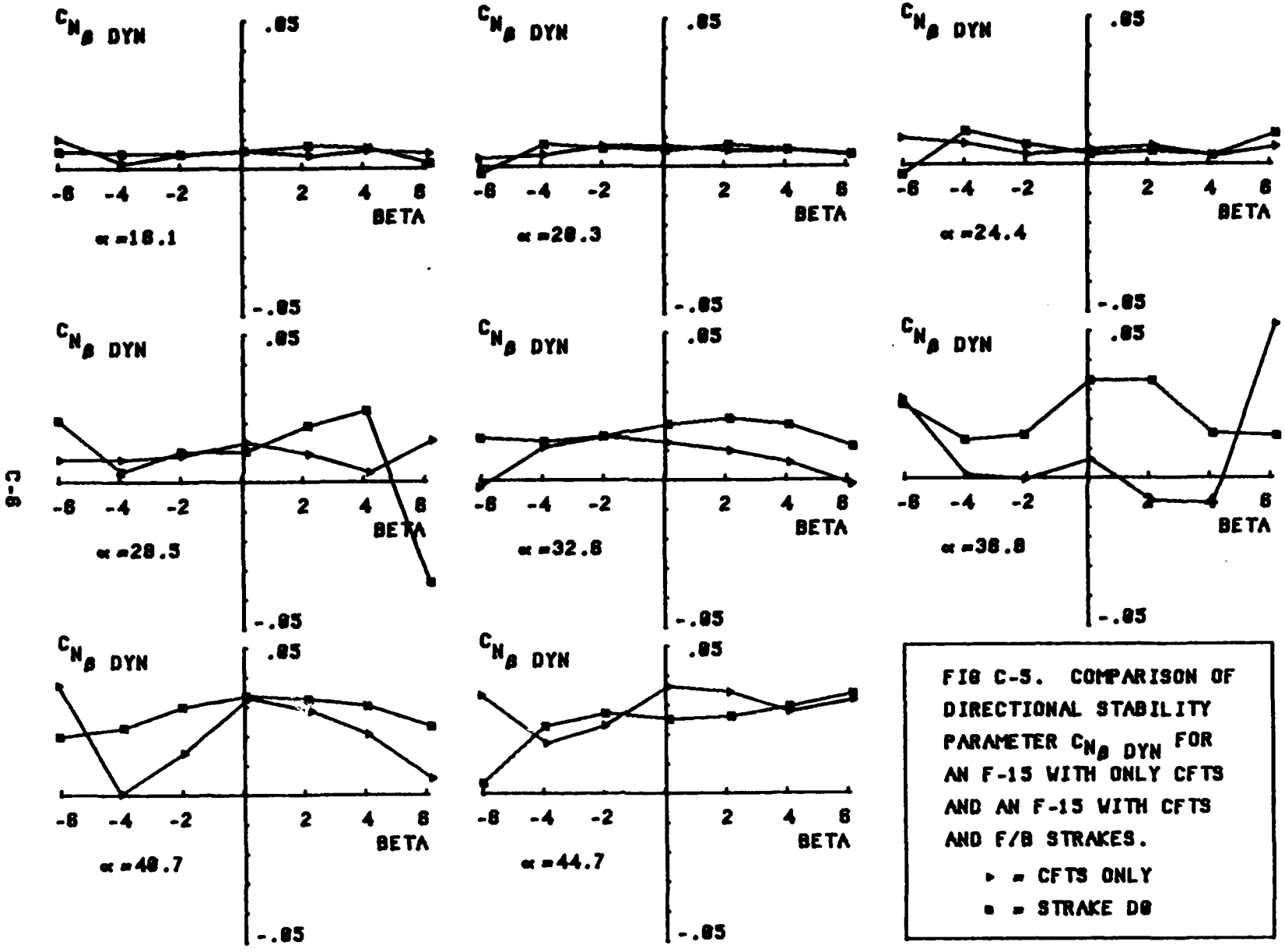

C-8

FIG C-5. COMPARISON OF DIRECTIONAL STABILITY PARAMETER $C_{N_\beta\ DYN}$ FOR AN F-15 WITH ONLY CFTS AND AN F-15 WITH CFTS AND F/B STRAKES.

▸ = CFTS ONLY

▪ = STRAKE DB

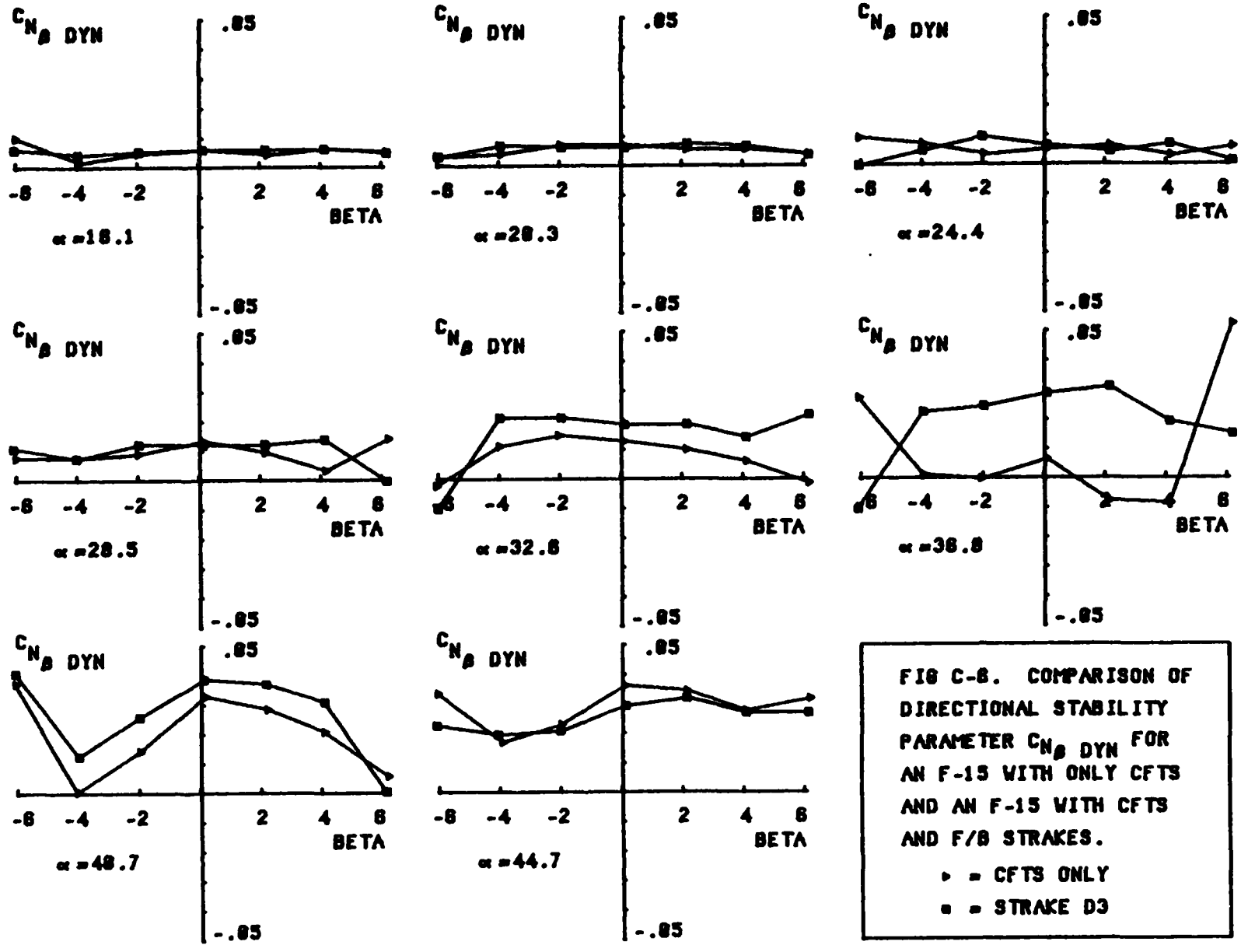

FIG C-8. COMPARISON OF DIRECTIONAL STABILITY PARAMETER C_{N_β} DYN FOR AN F-15 WITH ONLY CFTS AND AN F-15 WITH CFTS AND F/8 STRAKES.

▸ = CFTS ONLY

▪ = STRAKE D3

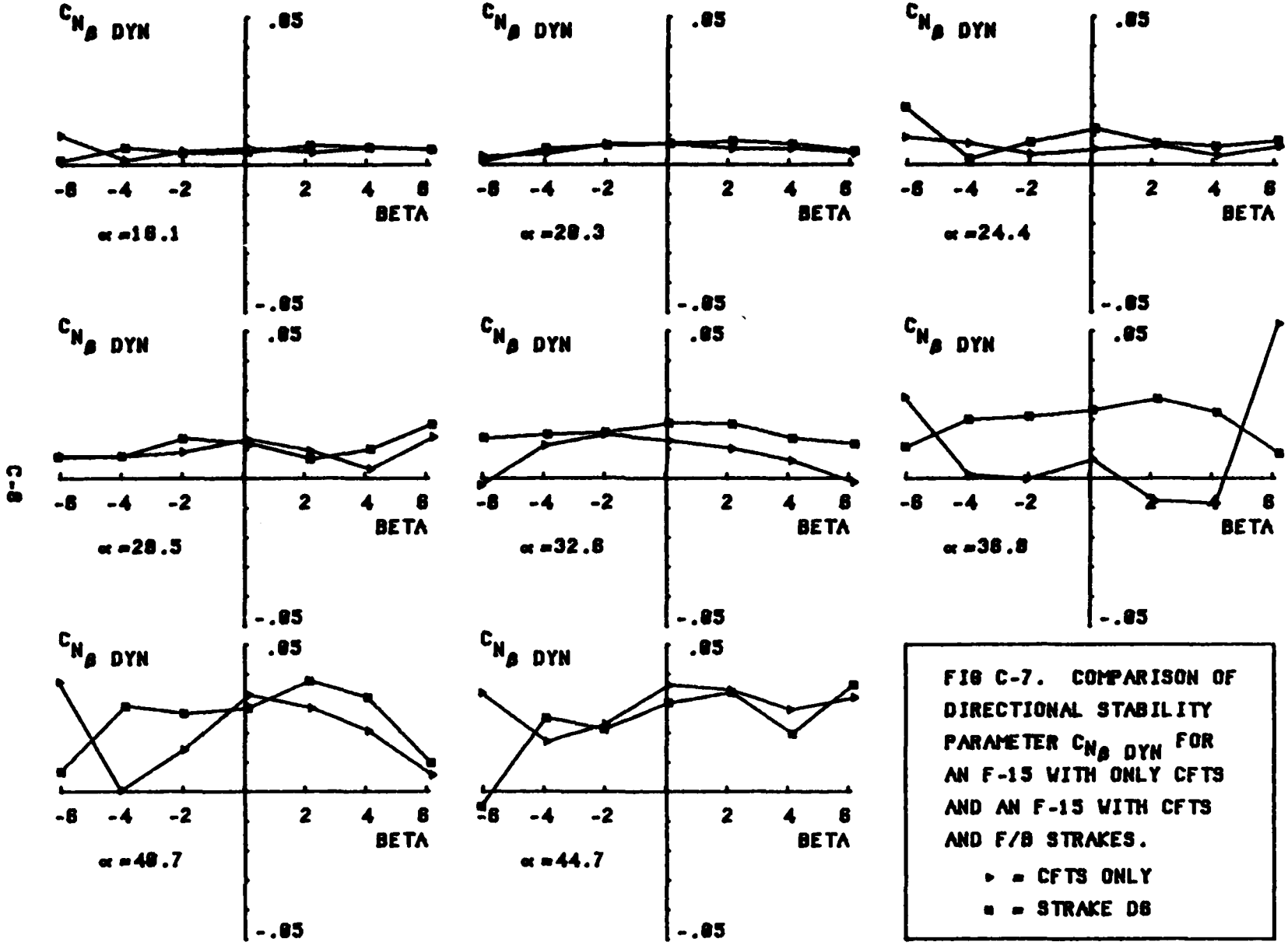

FIG C-7. COMPARISON OF DIRECTIONAL STABILITY PARAMETER $C_{N_\beta\ DYN}$ FOR AN F-15 WITH ONLY CFTS AND AN F-15 WITH CFTS AND F/B STRAKES.

▸ = CFTS ONLY

▪ = STRAKE DB

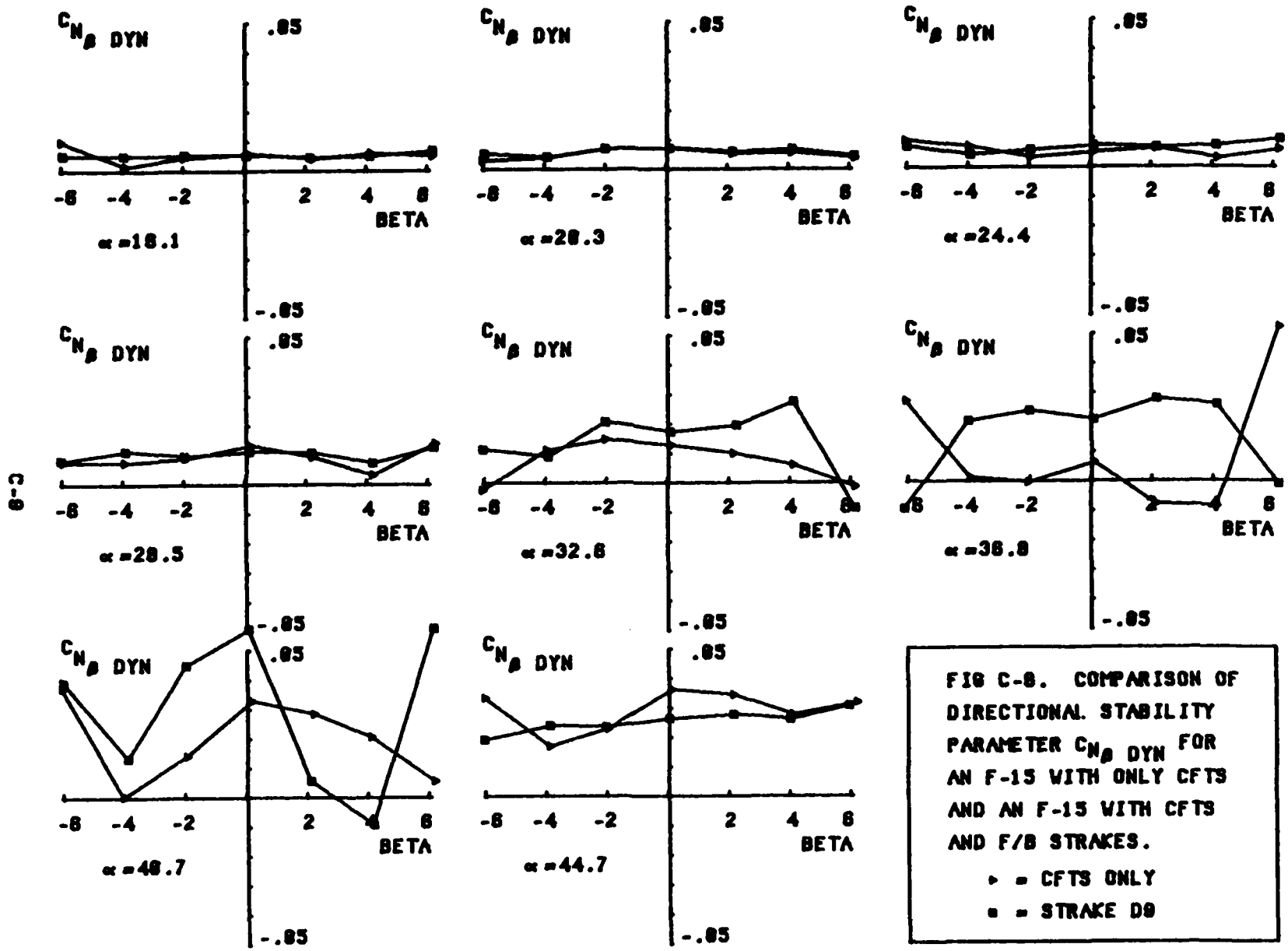

FIG C-8. COMPARISON OF DIRECTIONAL STABILITY PARAMETER $C_{N_\beta\ DYN}$ FOR AN F-15 WITH ONLY CFTS AND AN F-15 WITH CFTS AND F/B STRAKES.

▸ = CFTS ONLY

▪ = STRAKE DB

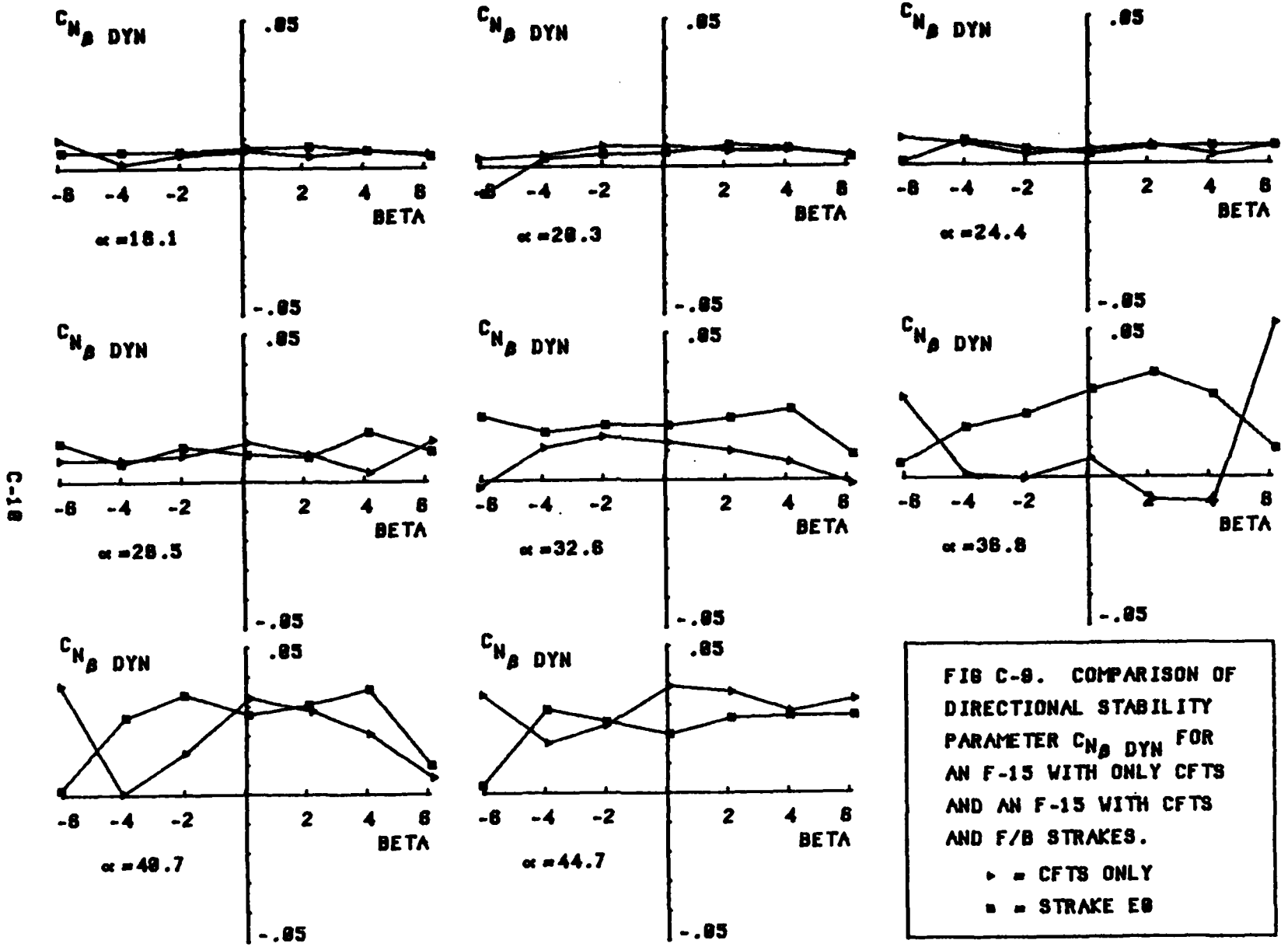

FIG C-8. COMPARISON OF DIRECTIONAL STABILITY PARAMETER $C_{N_\beta\ DYN}$ FOR AN F-15 WITH ONLY CFTS AND AN F-15 WITH CFTS AND F/B STRAKES.

▸ = CFTS ONLY

▪ = STRAKE E8

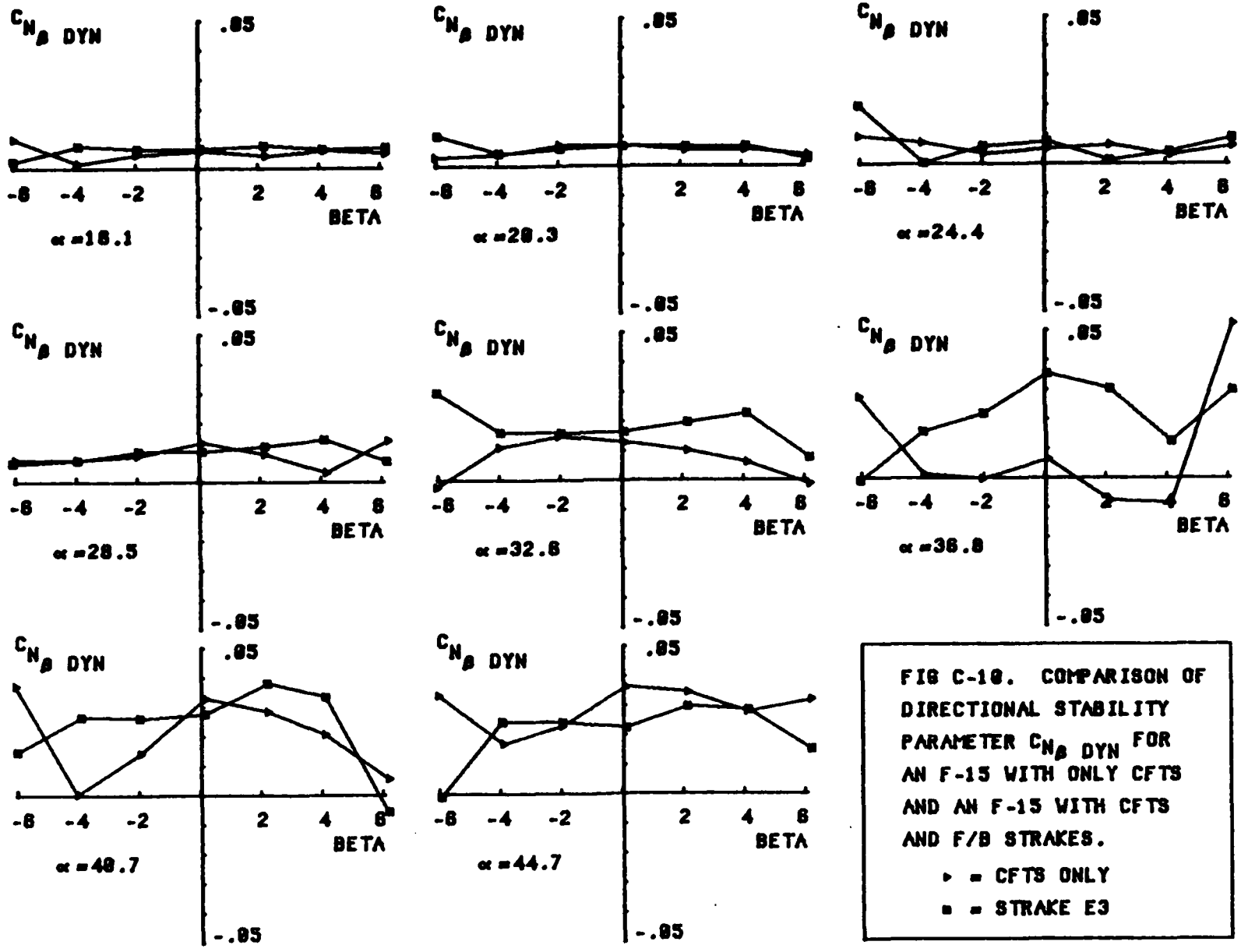

FIG C-10. COMPARISON OF DIRECTIONAL STABILITY PARAMETER C_{N_β} DYN FOR AN F-15 WITH ONLY CFTS AND AN F-15 WITH CFTS AND F/B STRAKES.

▸ = CFTS ONLY

▪ = STRAKE E3

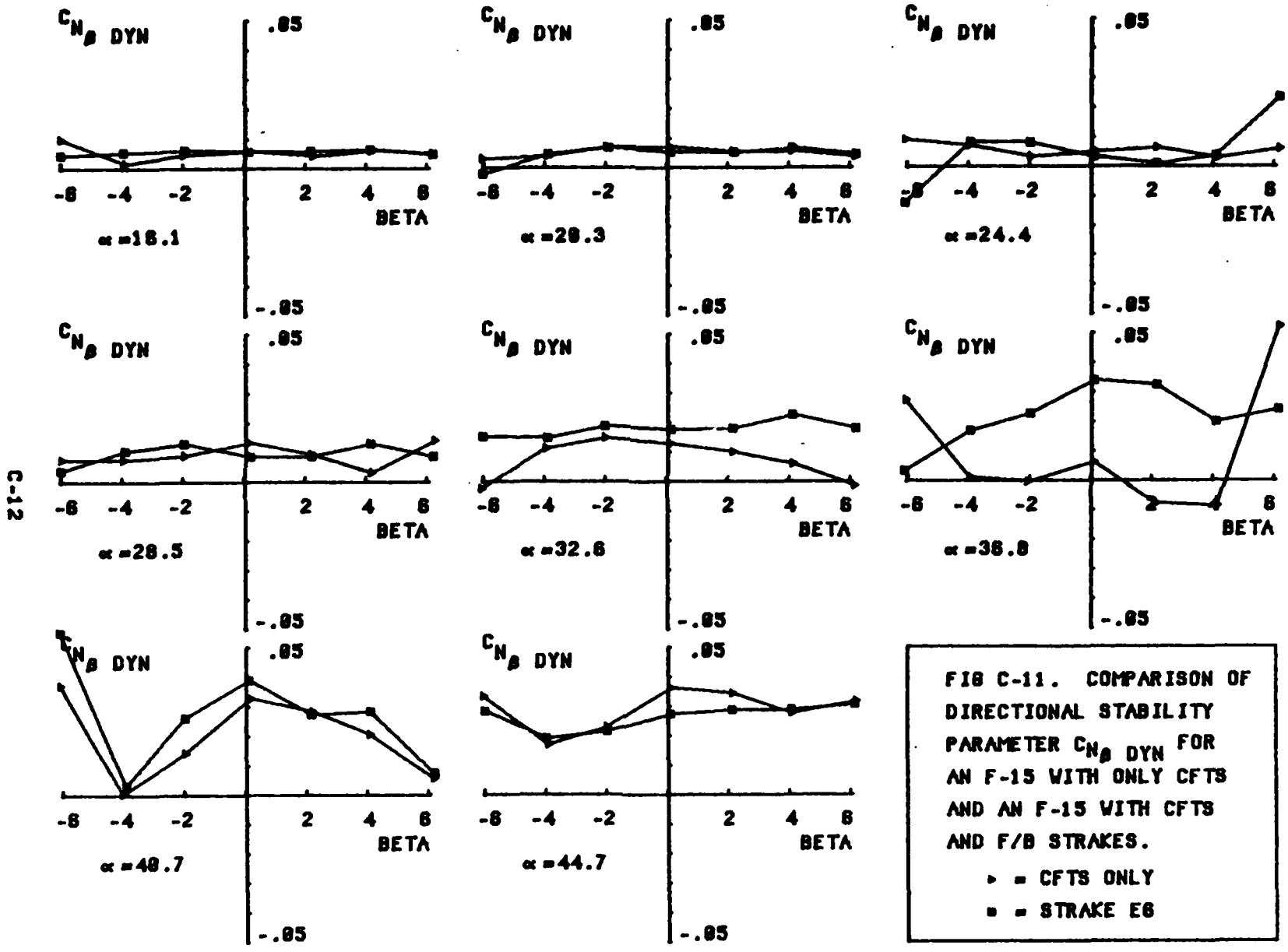

FIG C-11. COMPARISON OF DIRECTIONAL STABILITY PARAMETER C_{N_β} DYN FOR AN F-15 WITH ONLY CFTS AND AN F-15 WITH CFTS AND F/B STRAKES.

▸ = CFTS ONLY

▪ = STRAKE E6

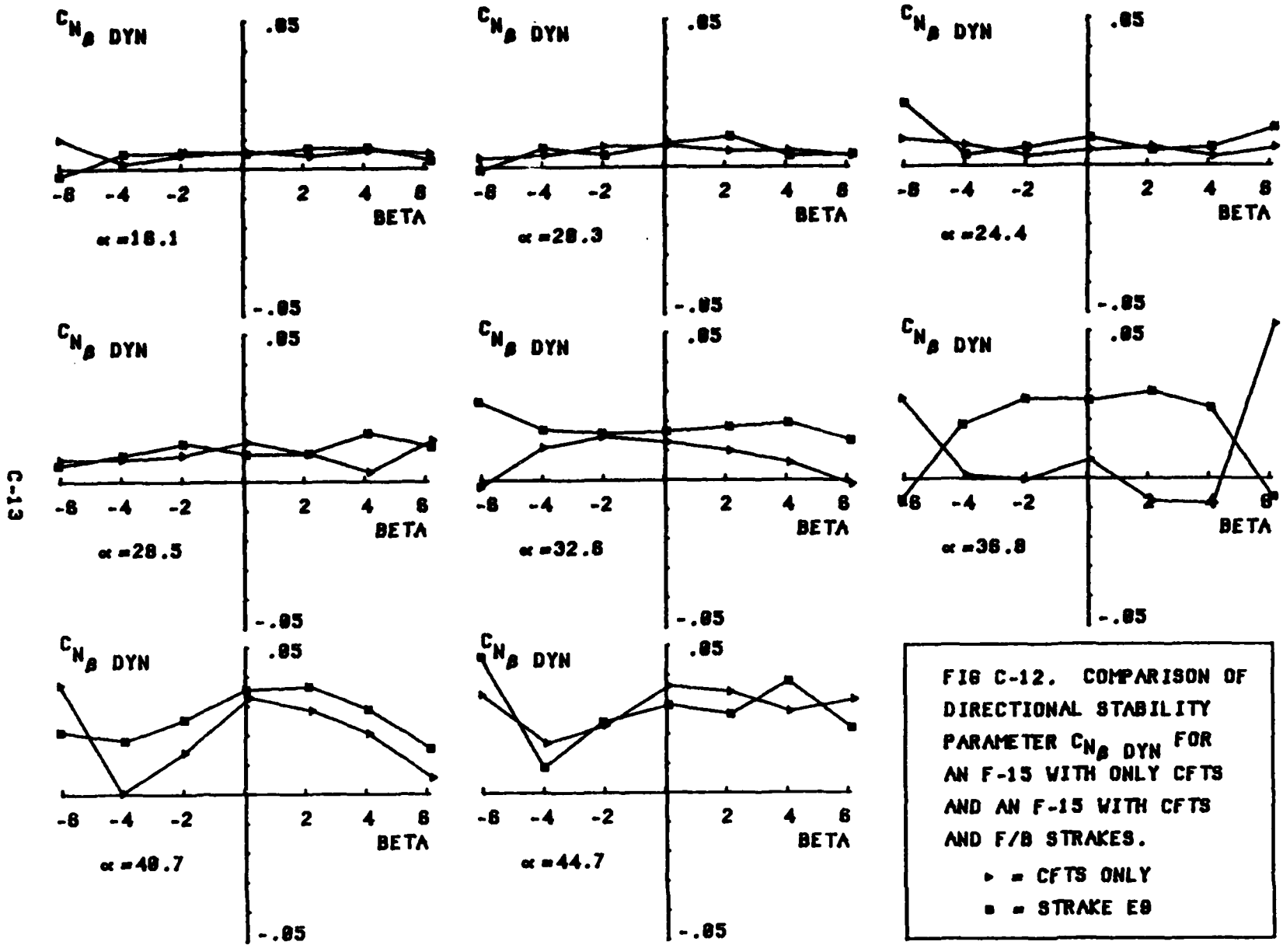

FIG C-12. COMPARISON OF DIRECTIONAL STABILITY PARAMETER C_{N_β} DYN FOR AN F-15 WITH ONLY CFTS AND AN F-15 WITH CFTS AND F/B STRAKES.

▸ = CFTS ONLY

▪ = STRAKE E9

Lateral Stability Data

C_N +vs β

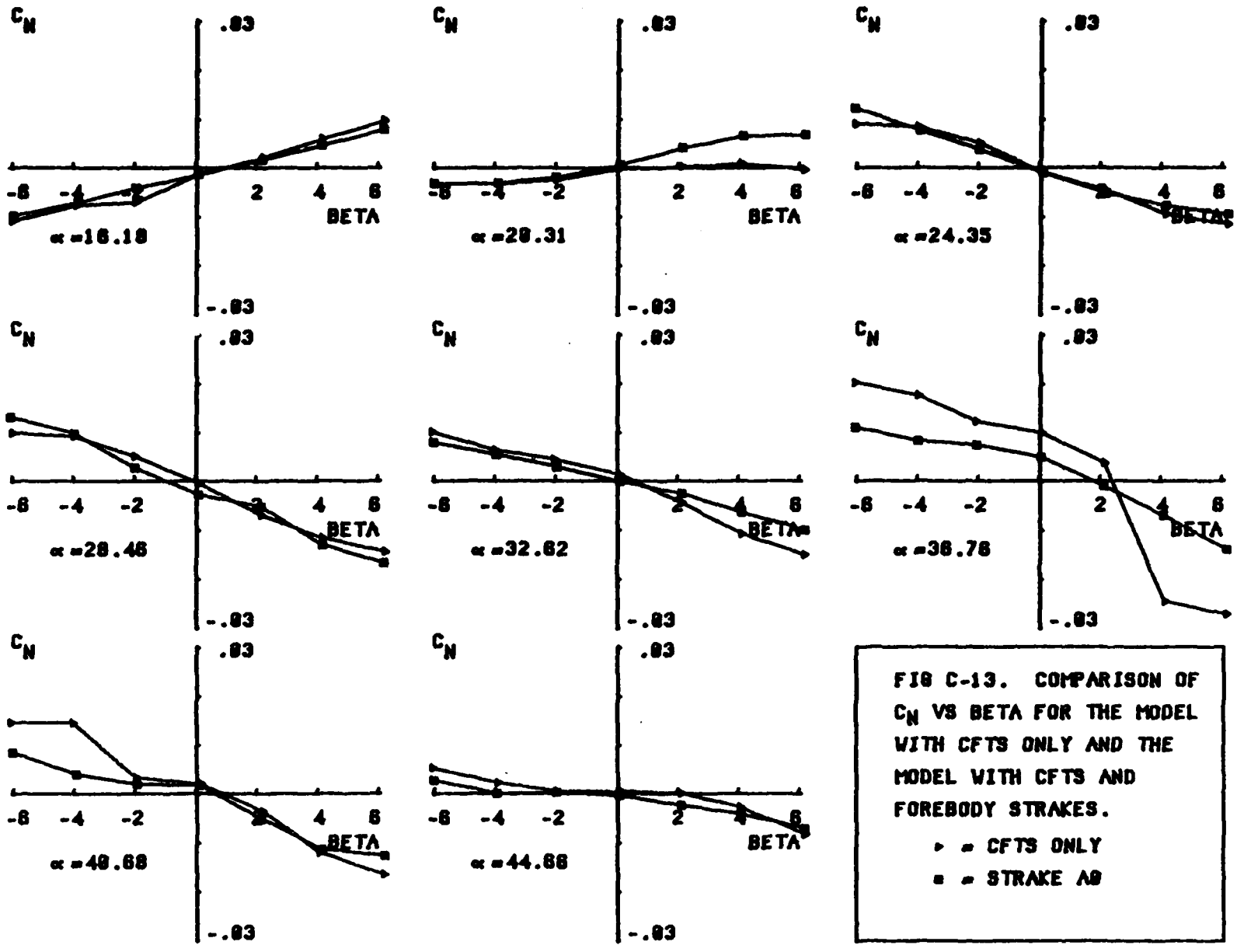

FIG C-13. COMPARISON OF C_N VS BETA FOR THE MODEL WITH CFTS ONLY AND THE MODEL WITH CFTS AND FOREBODY STRAKES.

▸ = CFTS ONLY

▪ = STRAKE A8

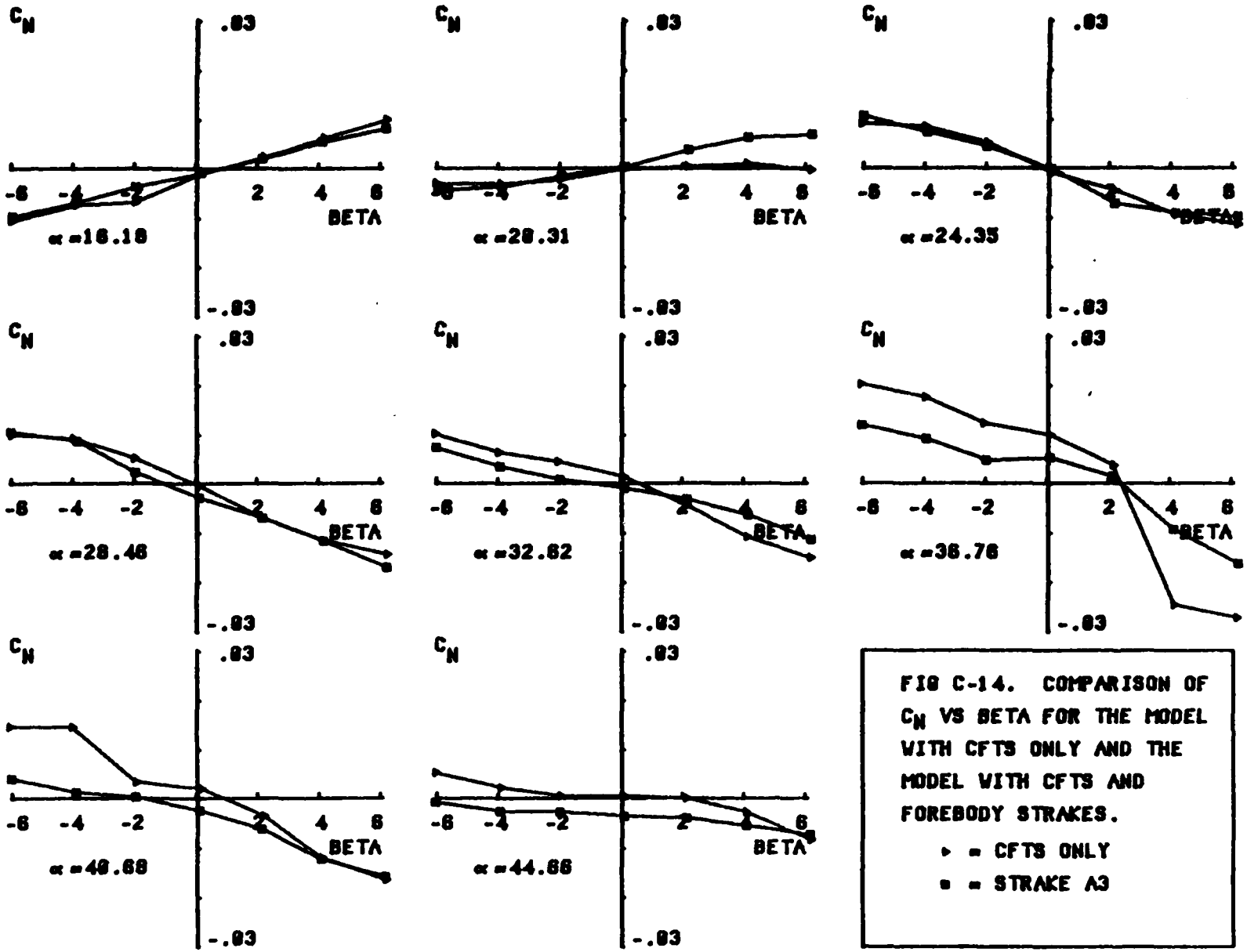

FIG C-14. COMPARISON OF C_N VS BETA FOR THE MODEL WITH CFTS ONLY AND THE MODEL WITH CFTS AND FOREBODY STRAKES.

▸ = CFTS ONLY

▪ = STRAKE A3

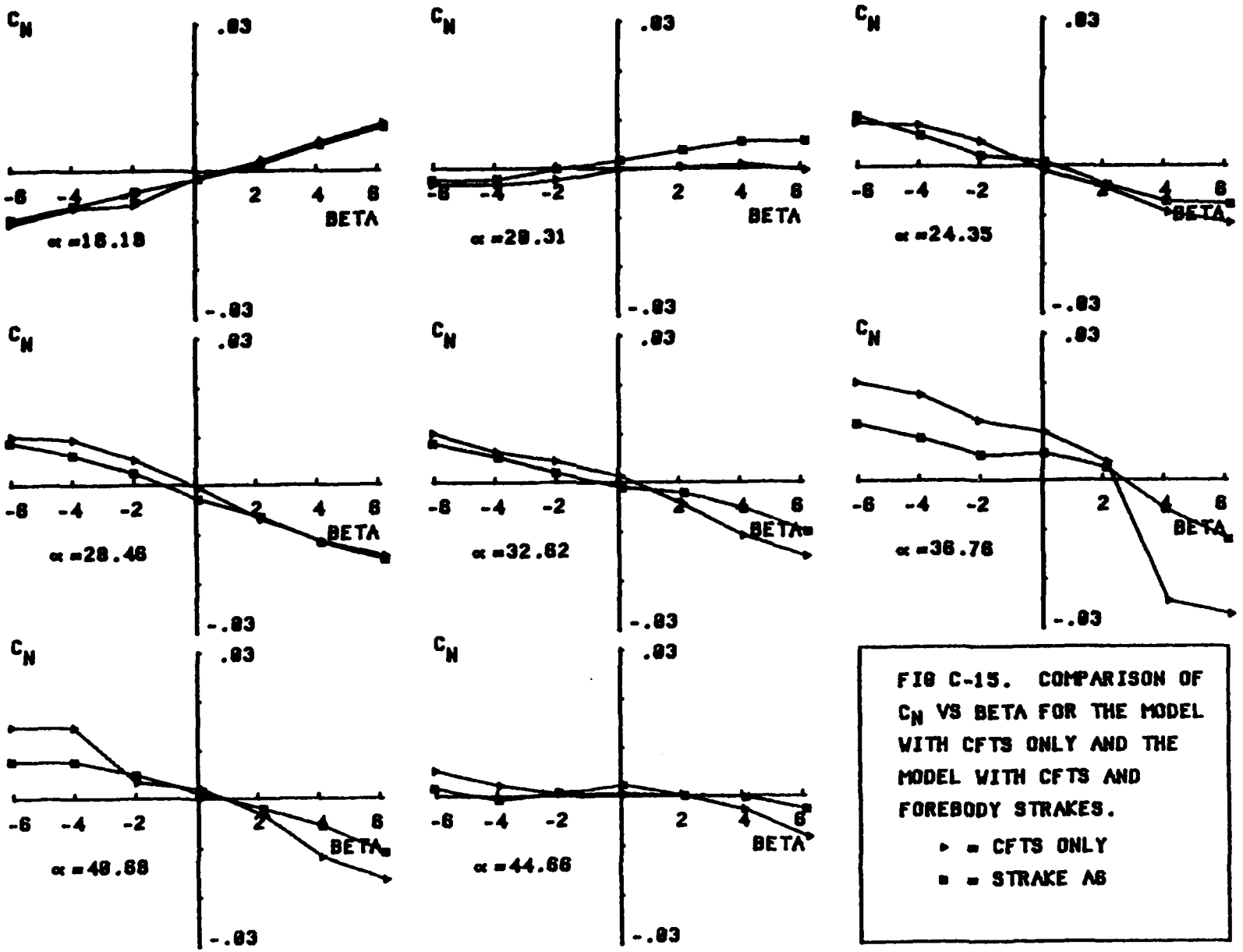

FIG C-15. COMPARISON OF C_N VS BETA FOR THE MODEL WITH CFTS ONLY AND THE MODEL WITH CFTS AND FOREBODY STRAKES.

▸ = CFTS ONLY

▪ = STRAKE A6

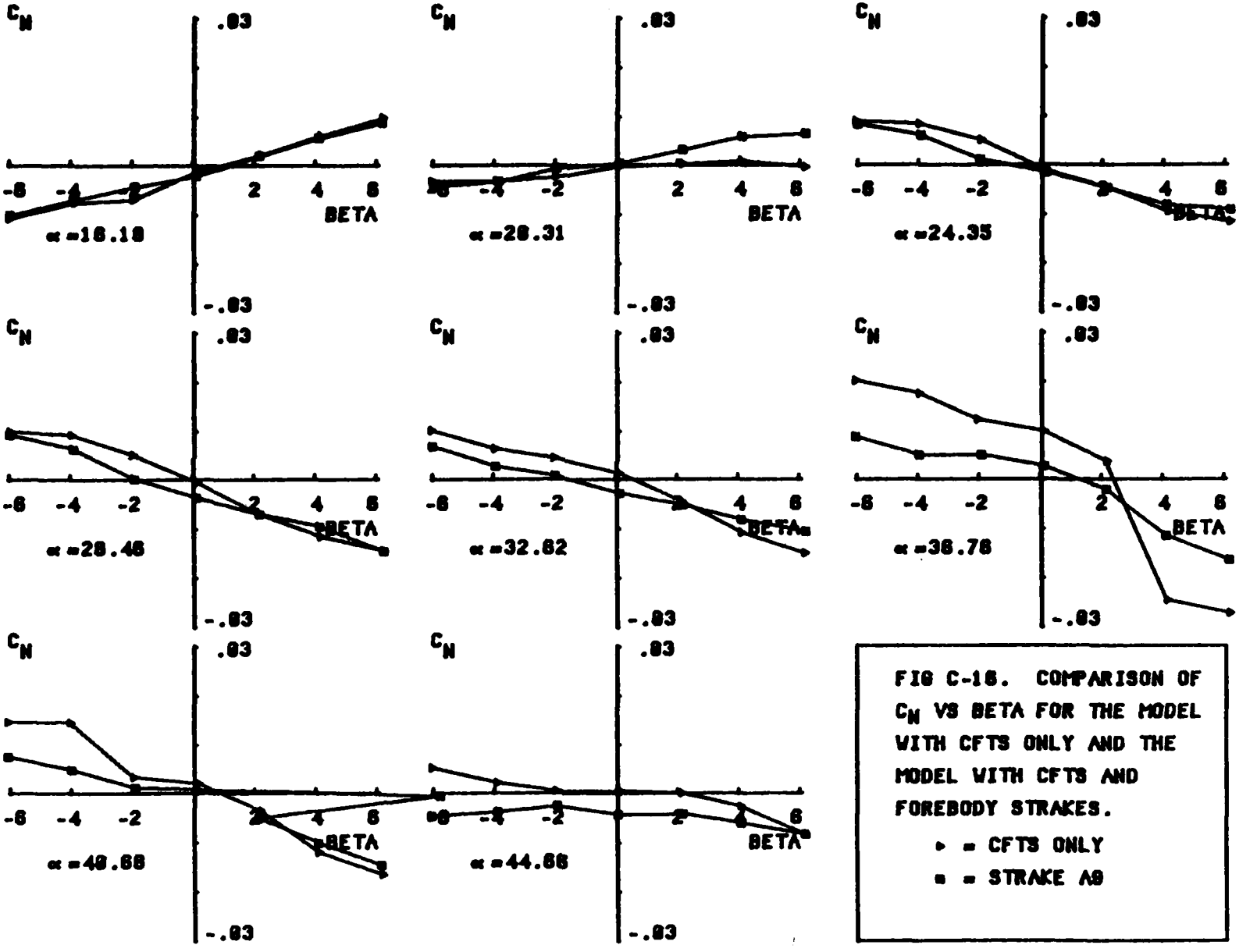

FIG C-16. COMPARISON OF C_N VS BETA FOR THE MODEL WITH CFTS ONLY AND THE MODEL WITH CFTS AND FOREBODY STRAKES.

▸ = CFTS ONLY

▪ = STRAKE A9

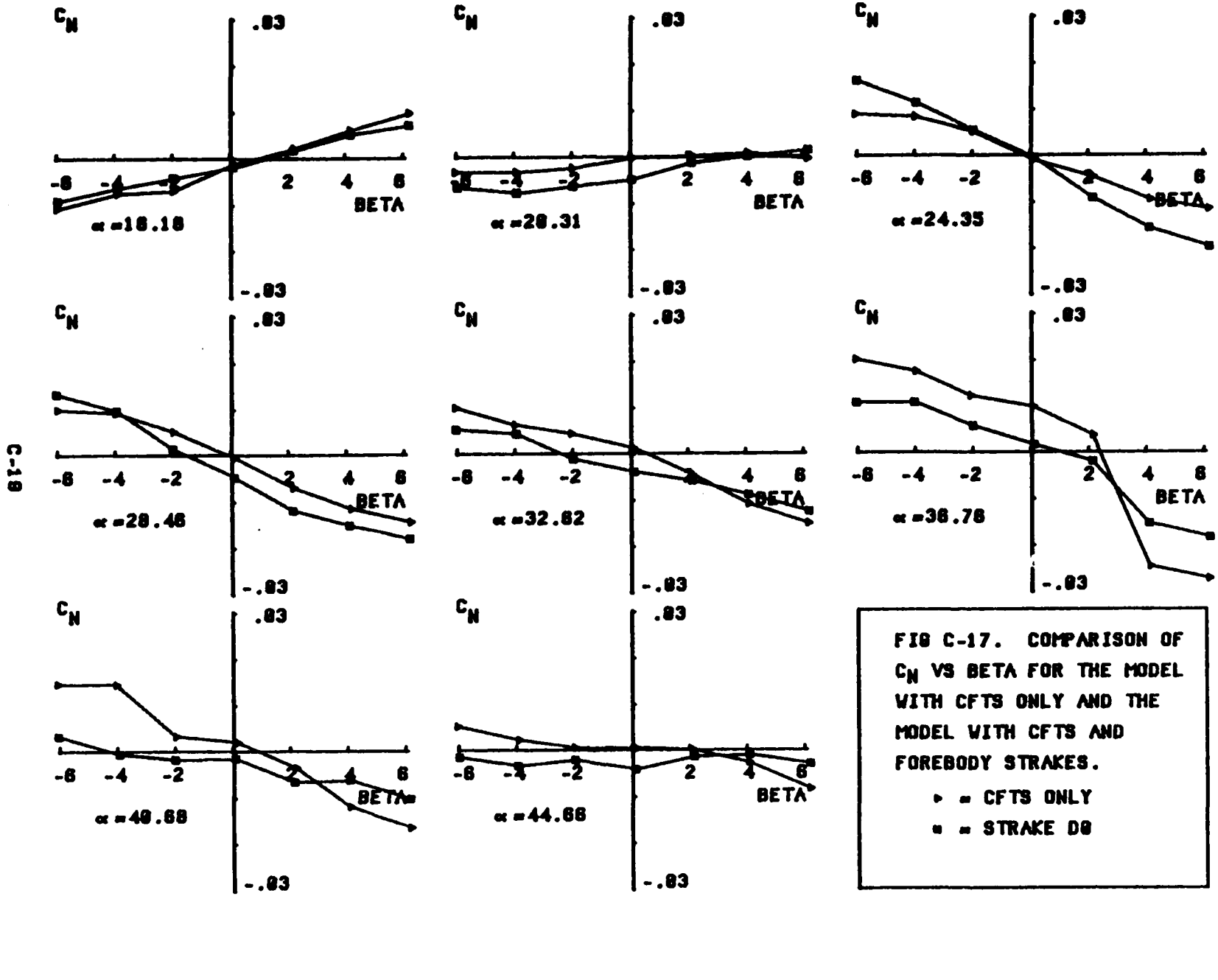

C-19

FIG C-17. COMPARISON OF C_N VS BETA FOR THE MODEL WITH CFTS ONLY AND THE MODEL WITH CFTS AND FOREBODY STRAKES.

▸ = CFTS ONLY

▪ = STRAKE D8

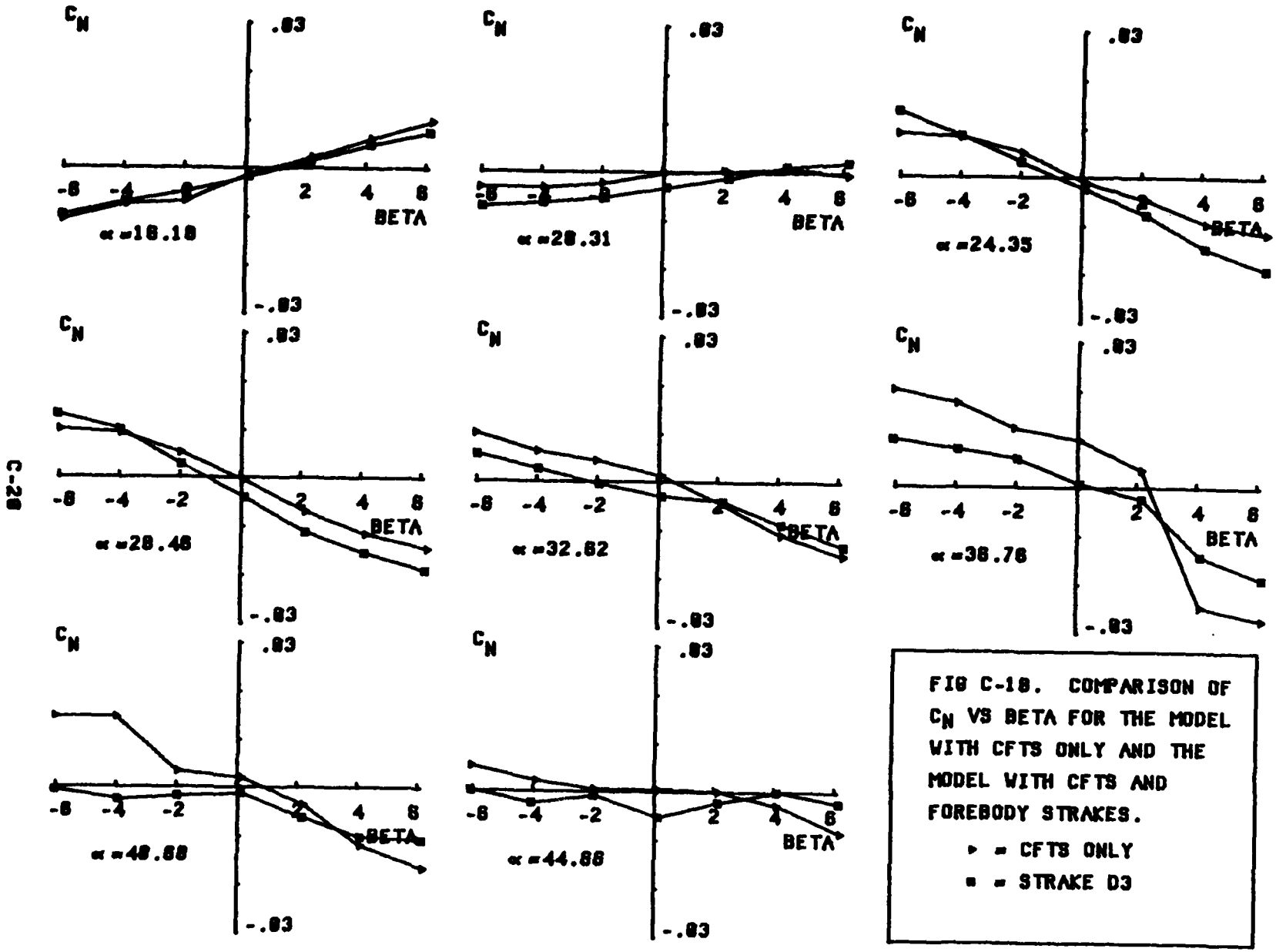

FIG C-18. COMPARISON OF C_N VS BETA FOR THE MODEL WITH CFTS ONLY AND THE MODEL WITH CFTS AND FOREBODY STRAKES.

▸ = CFTS ONLY

▪ = STRAKE D3

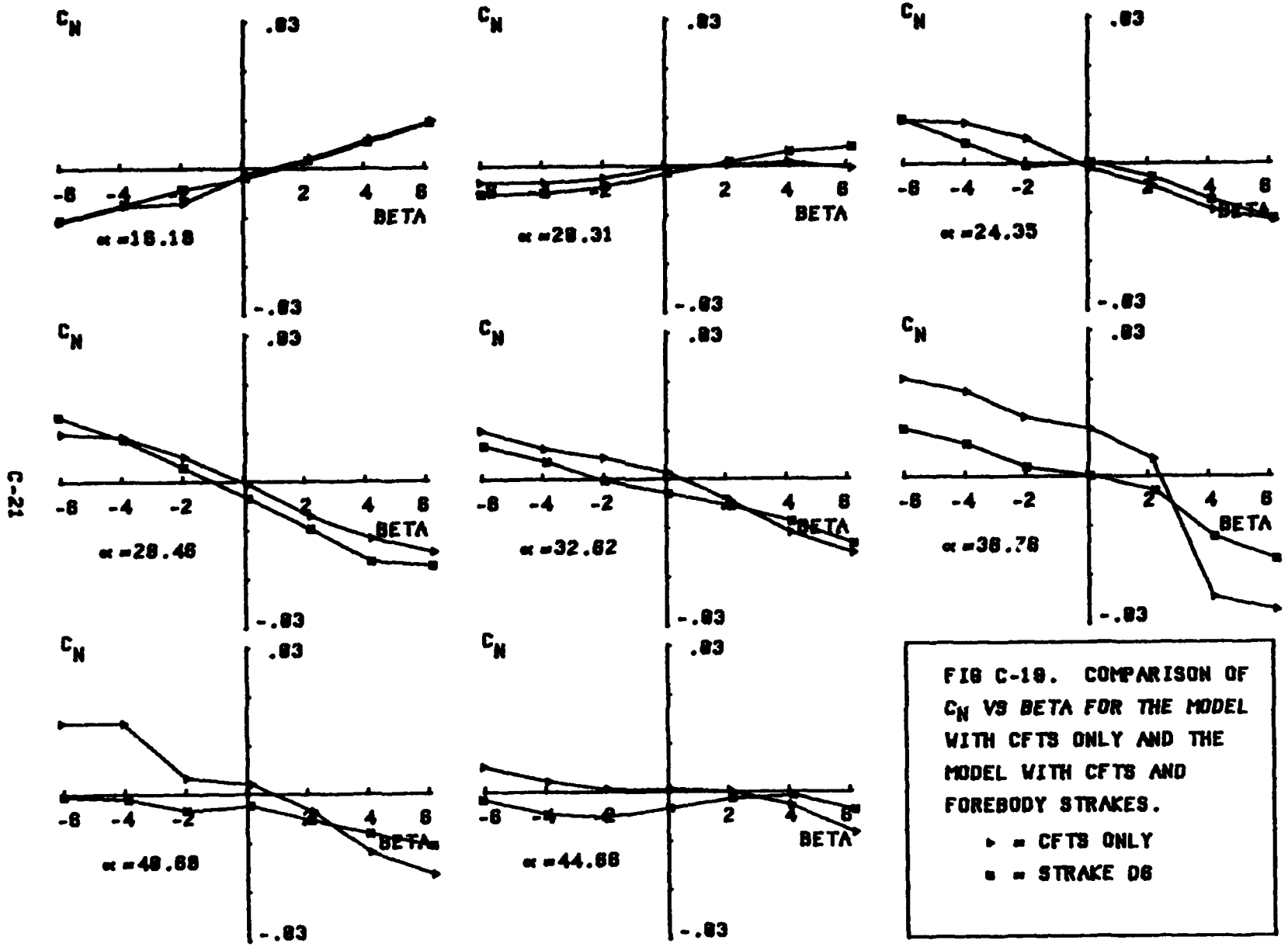

FIG C-19. COMPARISON OF C_N VS BETA FOR THE MODEL WITH CFTS ONLY AND THE MODEL WITH CFTS AND FOREBODY STRAKES.

▸ = CFTS ONLY

▪ = STRAKE 06

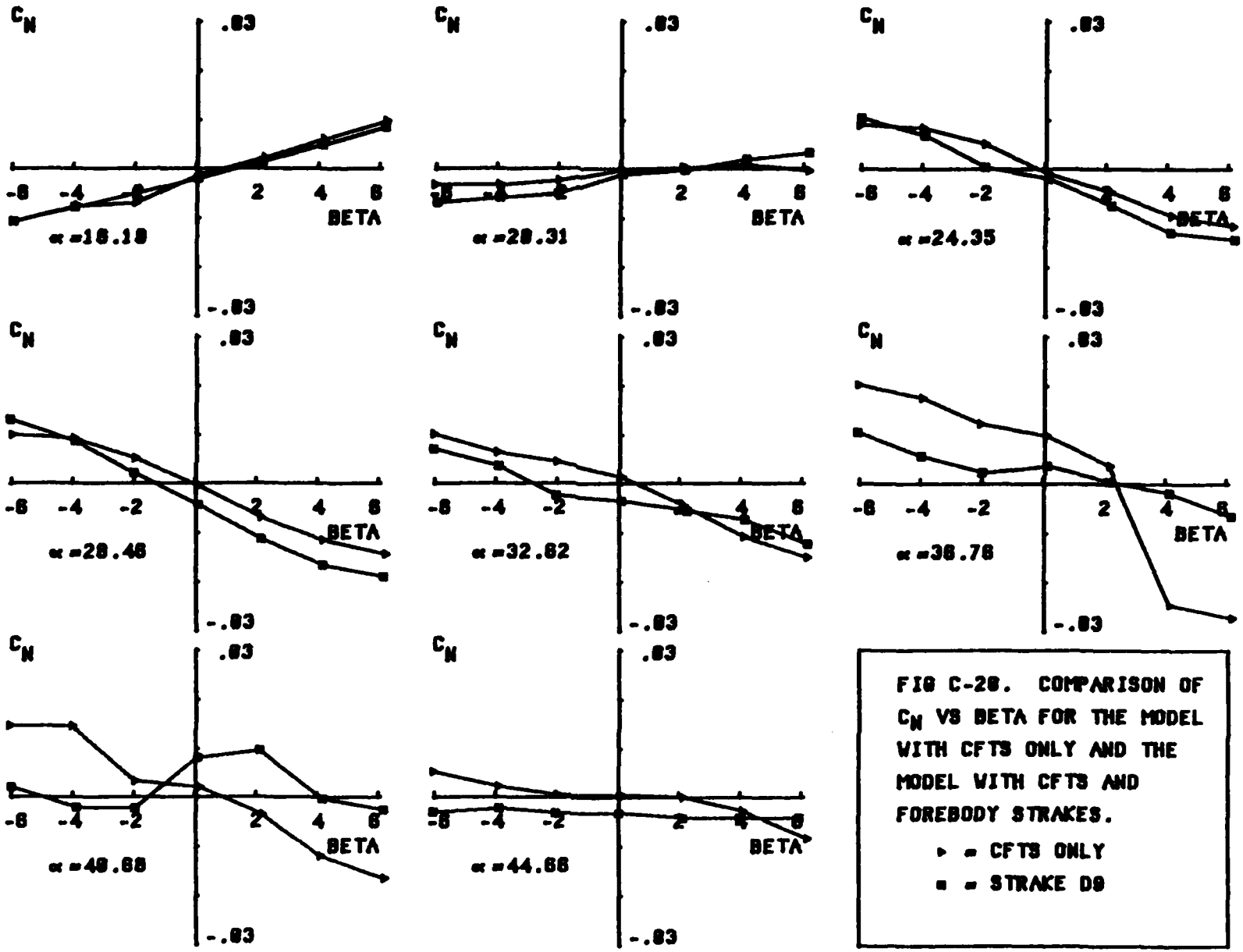

FIG C-28. COMPARISON OF C_N VS BETA FOR THE MODEL WITH CFTS ONLY AND THE MODEL WITH CFTS AND FOREBODY STRAKES.

▸ = CFTS ONLY

▪ = STRAKE D9

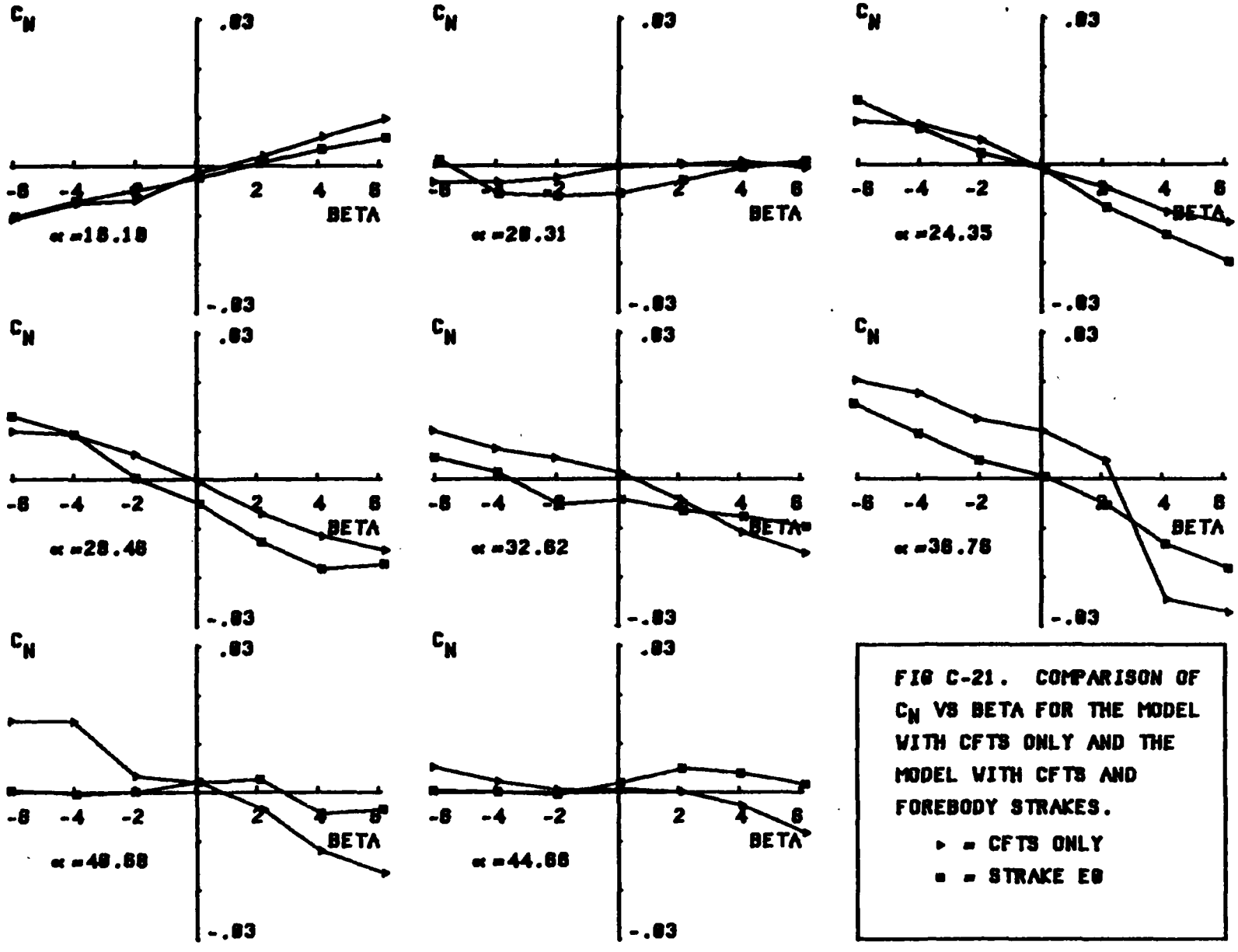

FIG C-21. COMPARISON OF C_N VS BETA FOR THE MODEL WITH CFTS ONLY AND THE MODEL WITH CFTS AND FOREBODY STRAKES.

▸ = CFTS ONLY

▪ = STRAKE E8

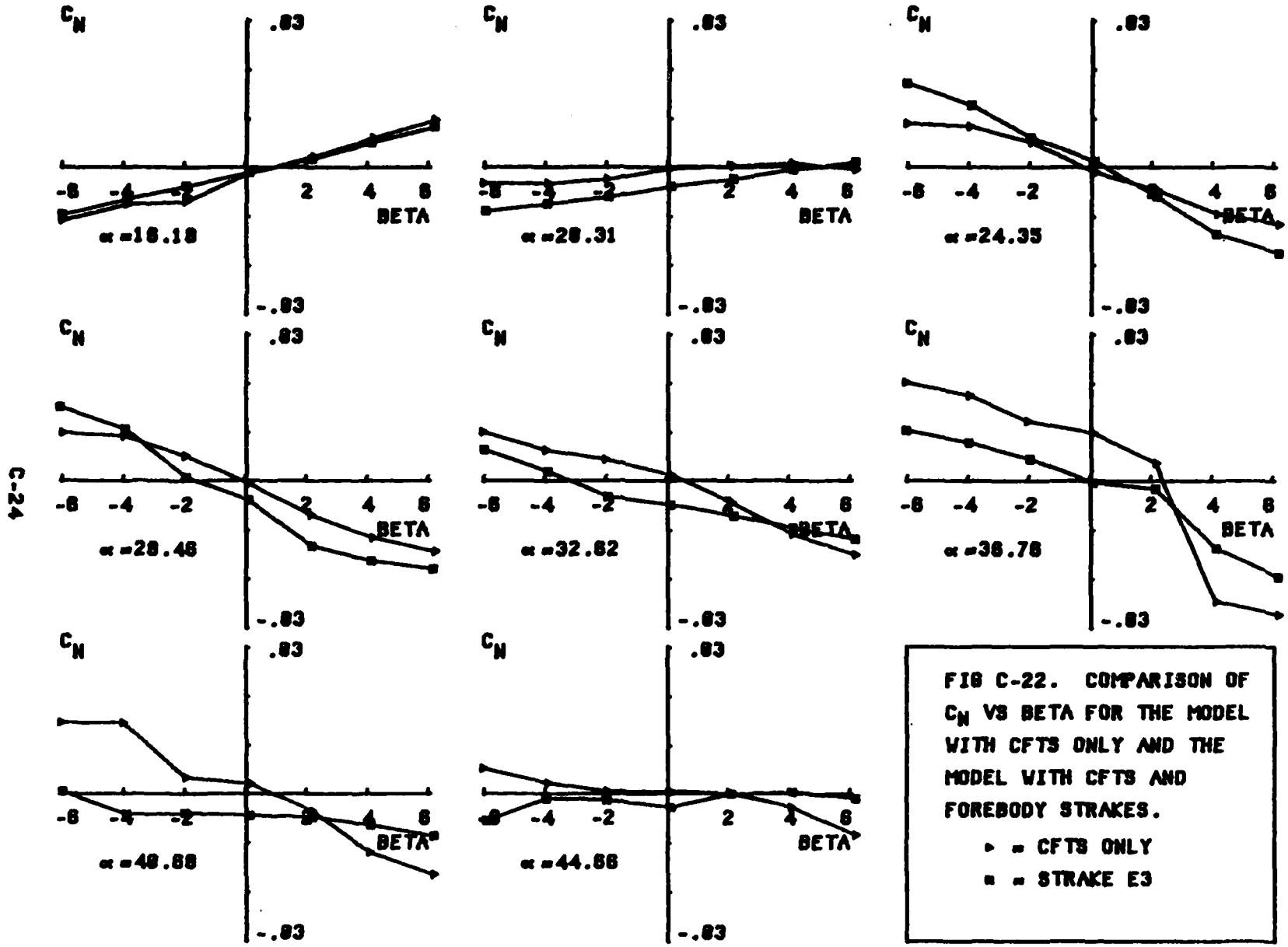

C-24

FIG C-22. COMPARISON OF C_N VS BETA FOR THE MODEL WITH CFTS ONLY AND THE MODEL WITH CFTS AND FOREBODY STRAKES.

▸ = CFTS ONLY

▪ = STRAKE E3

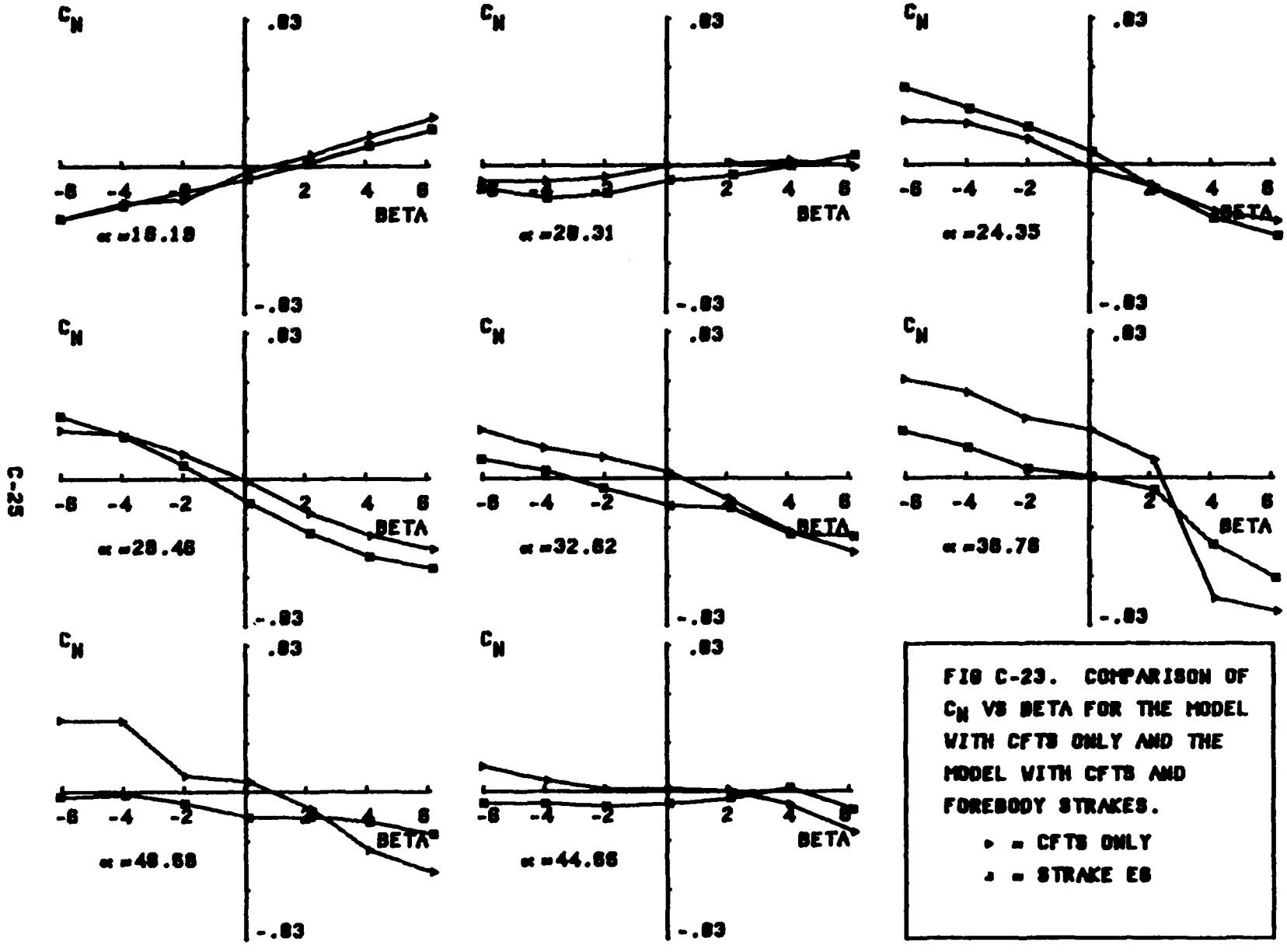

FIG C-23. COMPARISON OF C_N VS BETA FOR THE MODEL WITH CFTS ONLY AND THE MODEL WITH CFTS AND FOREBODY STRAKES.

▸ = CFTS ONLY

▵ = STRAKE ES

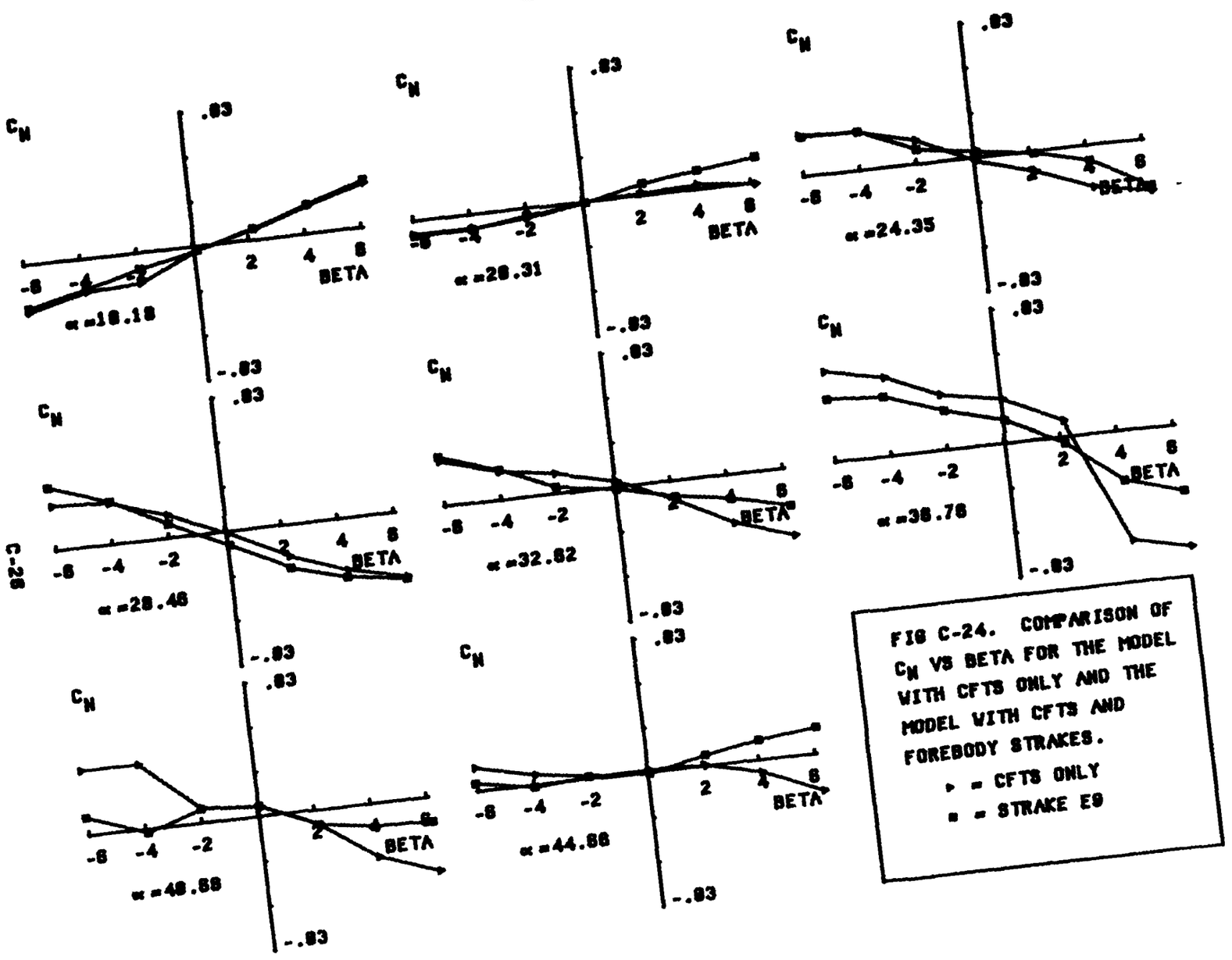

FIG C-24. COMPARISON OF C_N VS BETA FOR THE MODEL WITH CFTS ONLY AND THE MODEL WITH CFTS AND FOREBODY STRAKES.

▸ = CFTS ONLY

▪ = STRAKE E9

Lateral Stability Data

C_ℓ vs β

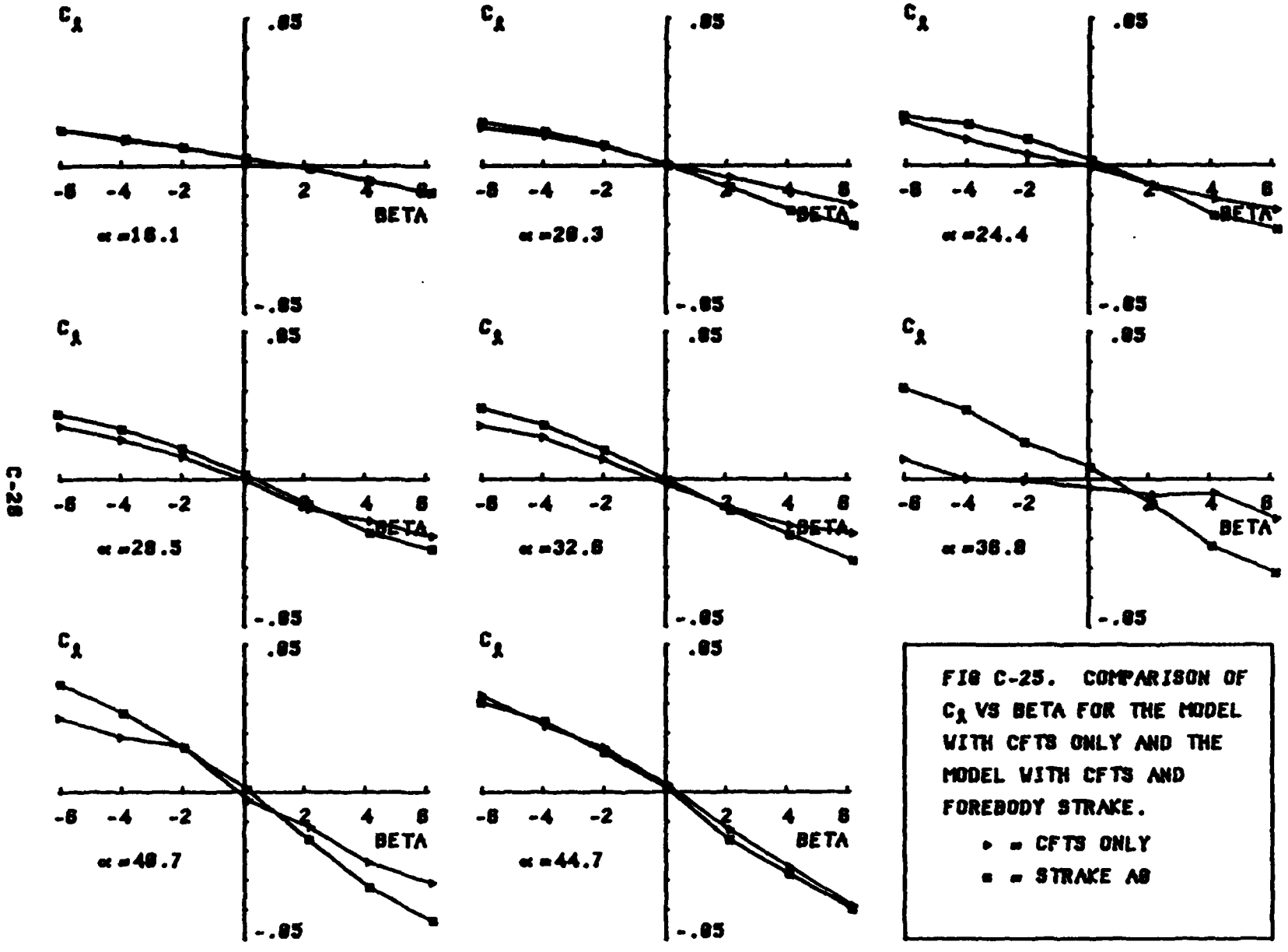

FIG C-25. COMPARISON OF C_ℓ VS BETA FOR THE MODEL WITH CFTS ONLY AND THE MODEL WITH CFTS AND FOREBODY STRAKE.

▸ = CFTS ONLY

▪ = STRAKE AS

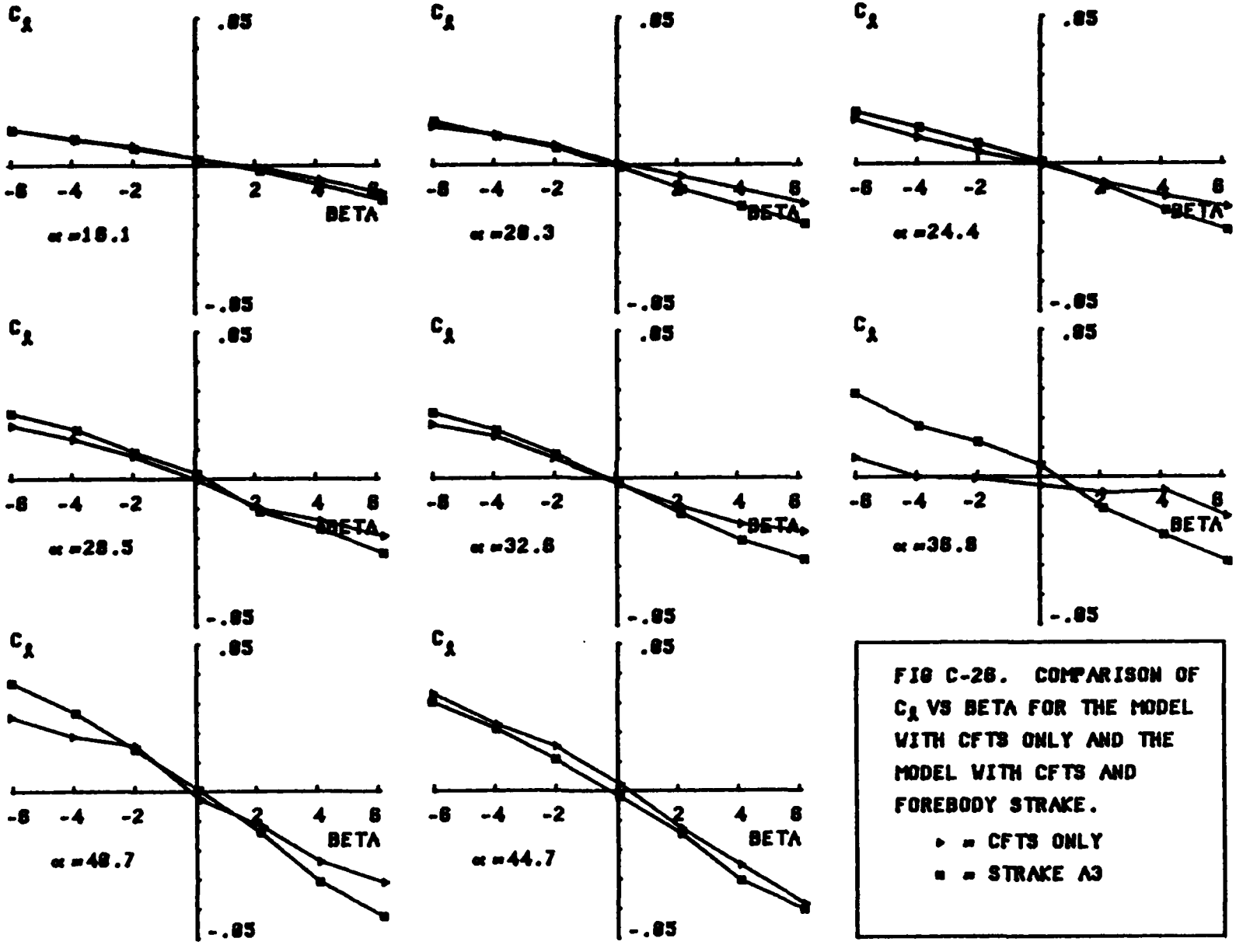

C-28

FIG C-28. COMPARISON OF C_ℓ VS BETA FOR THE MODEL WITH CFTS ONLY AND THE MODEL WITH CFTS AND FOREBODY STRAKE.

▸ = CFTS ONLY

▪ = STRAKE A3

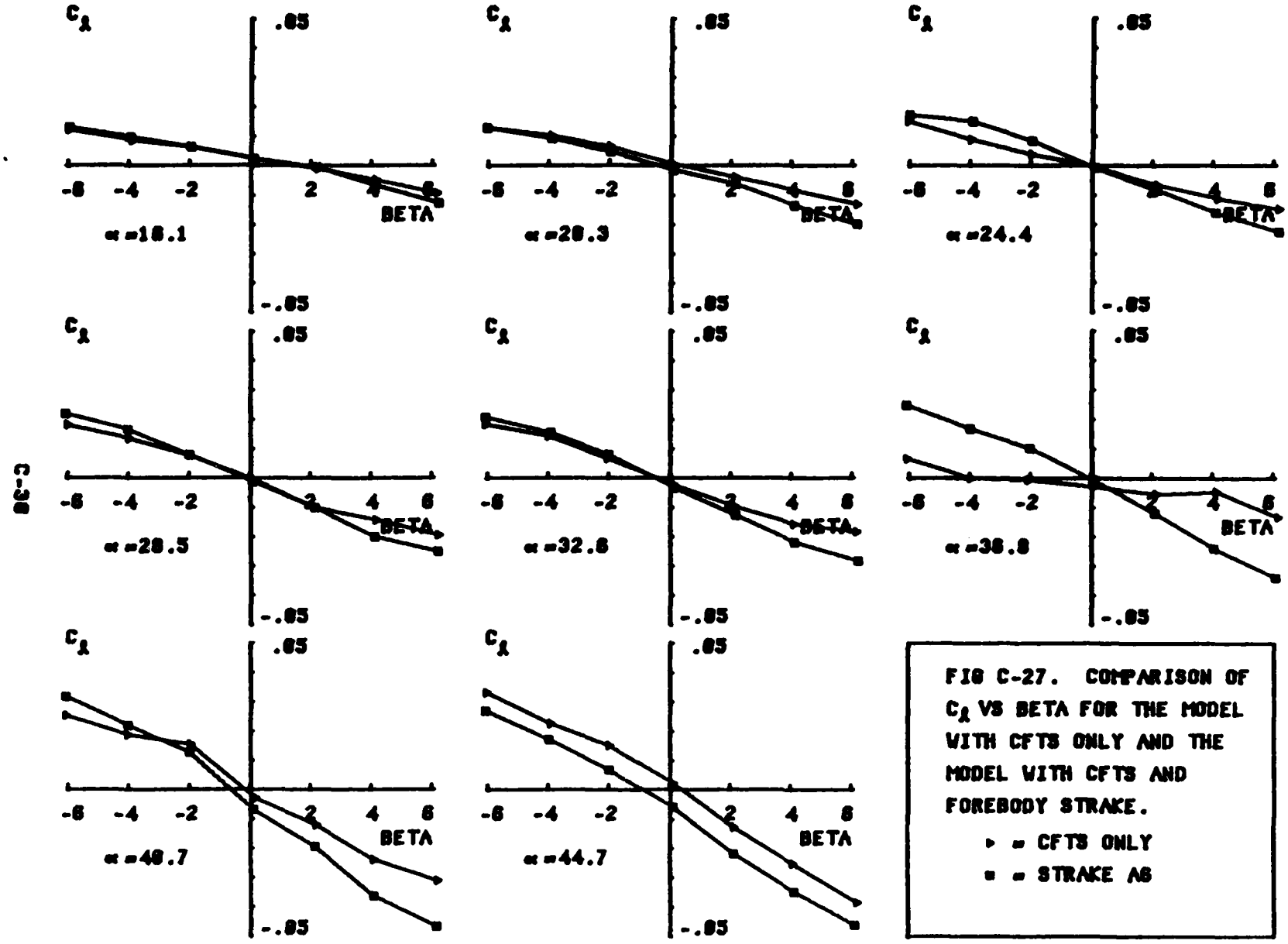

FIG C-27. COMPARISON OF C_ℓ VS BETA FOR THE MODEL WITH CFTS ONLY AND THE MODEL WITH CFTS AND FOREBODY STRAKE.

▸ = CFTS ONLY

▪ = STRAKE AS

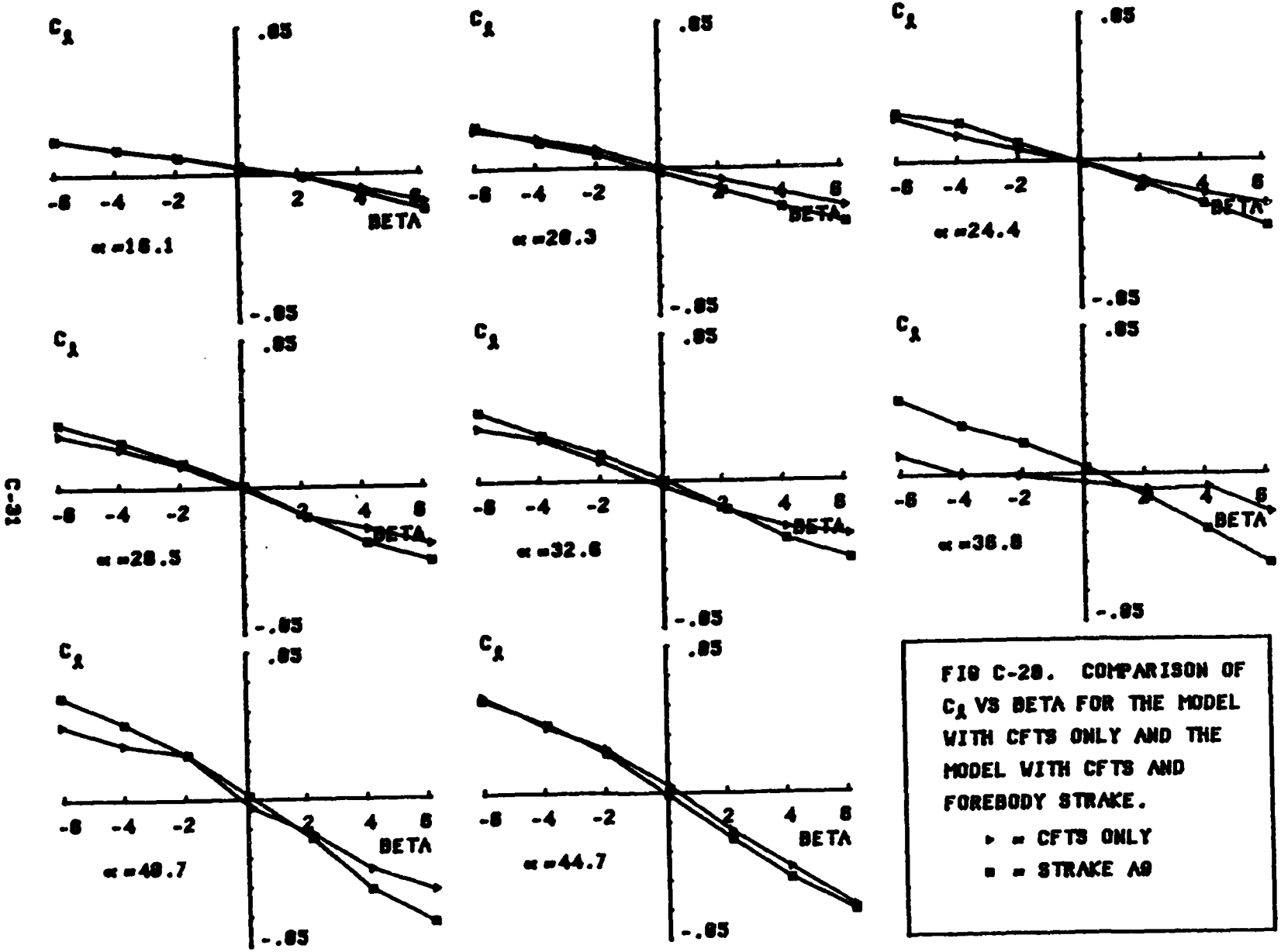

FIG C-28. COMPARISON OF C_ℓ VS BETA FOR THE MODEL WITH CFTS ONLY AND THE MODEL WITH CFTS AND FOREBODY STRAKE.

▸ = CFTS ONLY

▪ = STRAKE A9

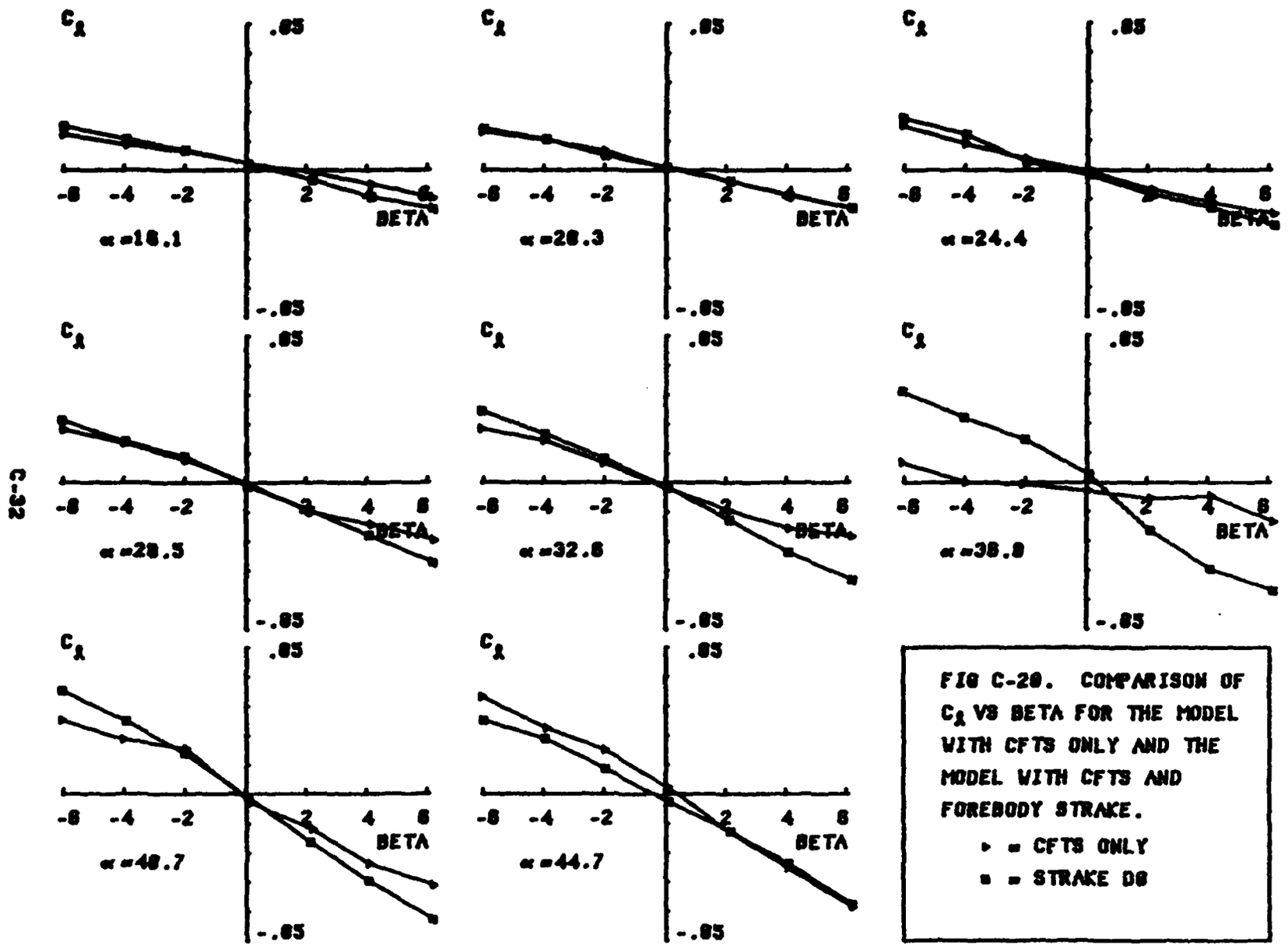

C-32

FIG C-20. COMPARISON OF C_l VS BETA FOR THE MODEL WITH CFTS ONLY AND THE MODEL WITH CFTS AND FOREBODY STRAKE.

▸ = CFTS ONLY

▪ = STRAKE DB

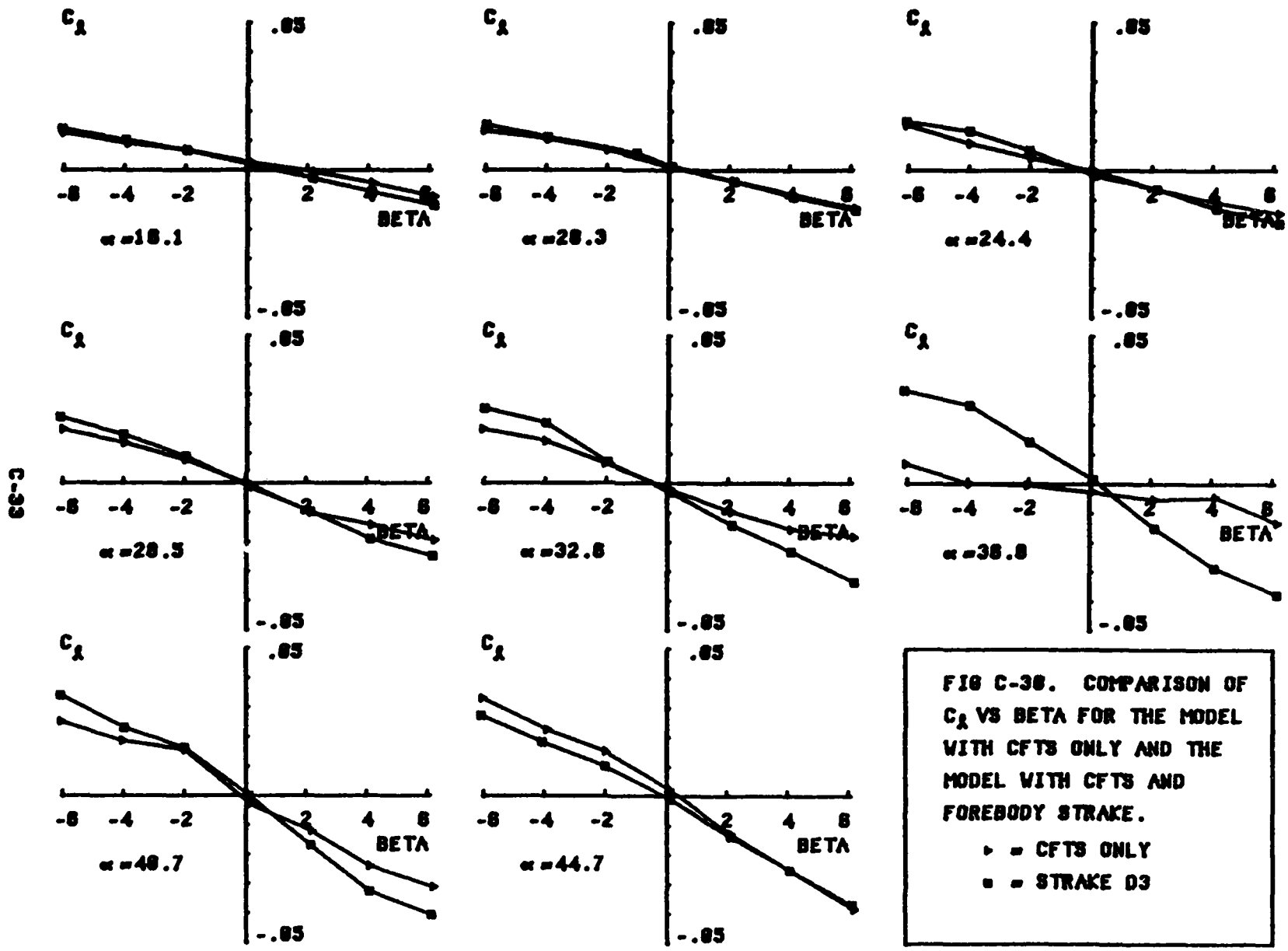

FIG C-38. COMPARISON OF C_ℓ VS BETA FOR THE MODEL WITH CFTS ONLY AND THE MODEL WITH CFTS AND FOREBODY STRAKE.

▸ = CFTS ONLY

▪ = STRAKE 03

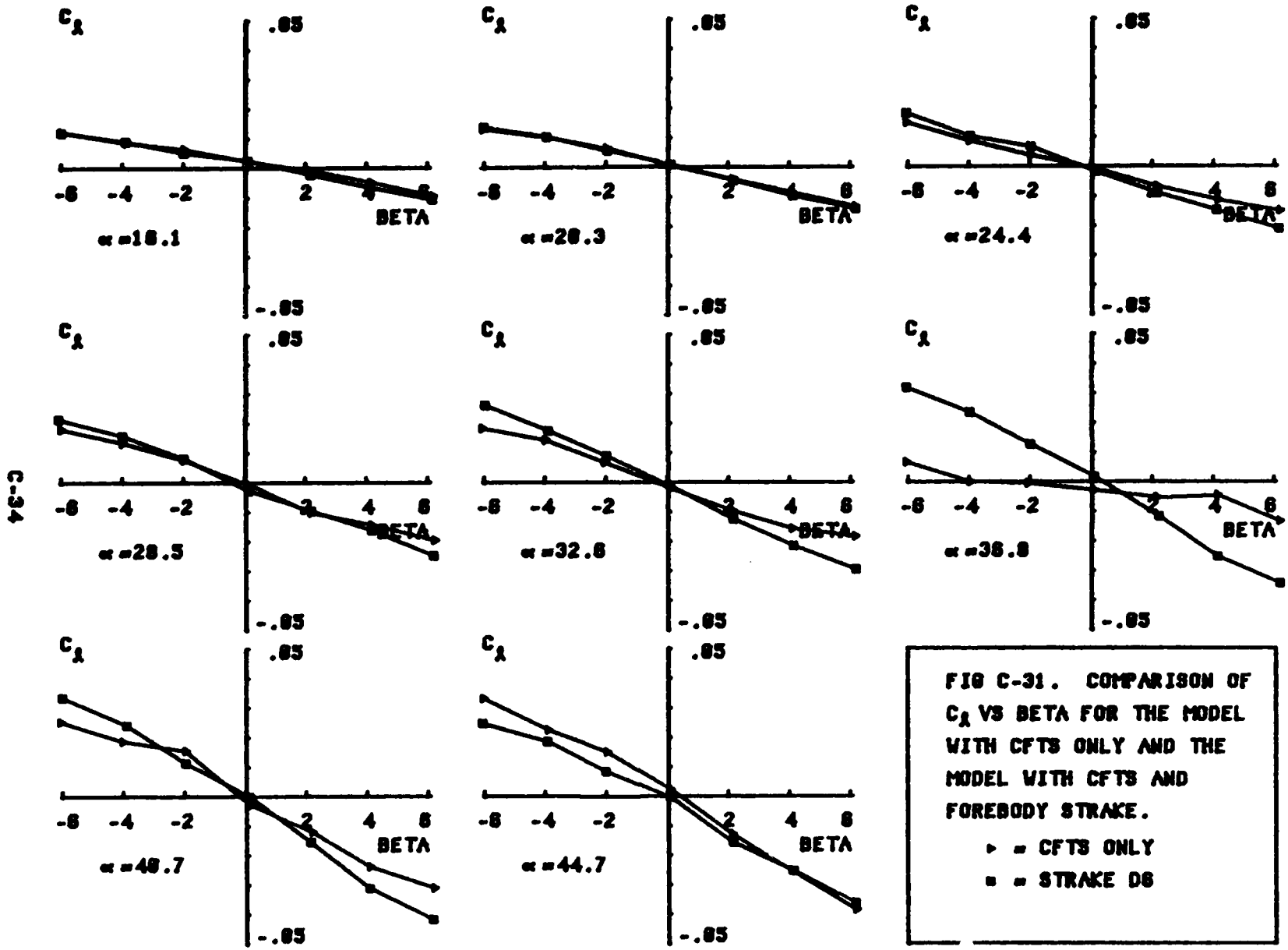

FIG C-31. COMPARISON OF C_ℓ VS BETA FOR THE MODEL WITH CFTS ONLY AND THE MODEL WITH CFTS AND FOREBODY STRAKE.

▸ = CFTS ONLY

▪ = STRAKE D6

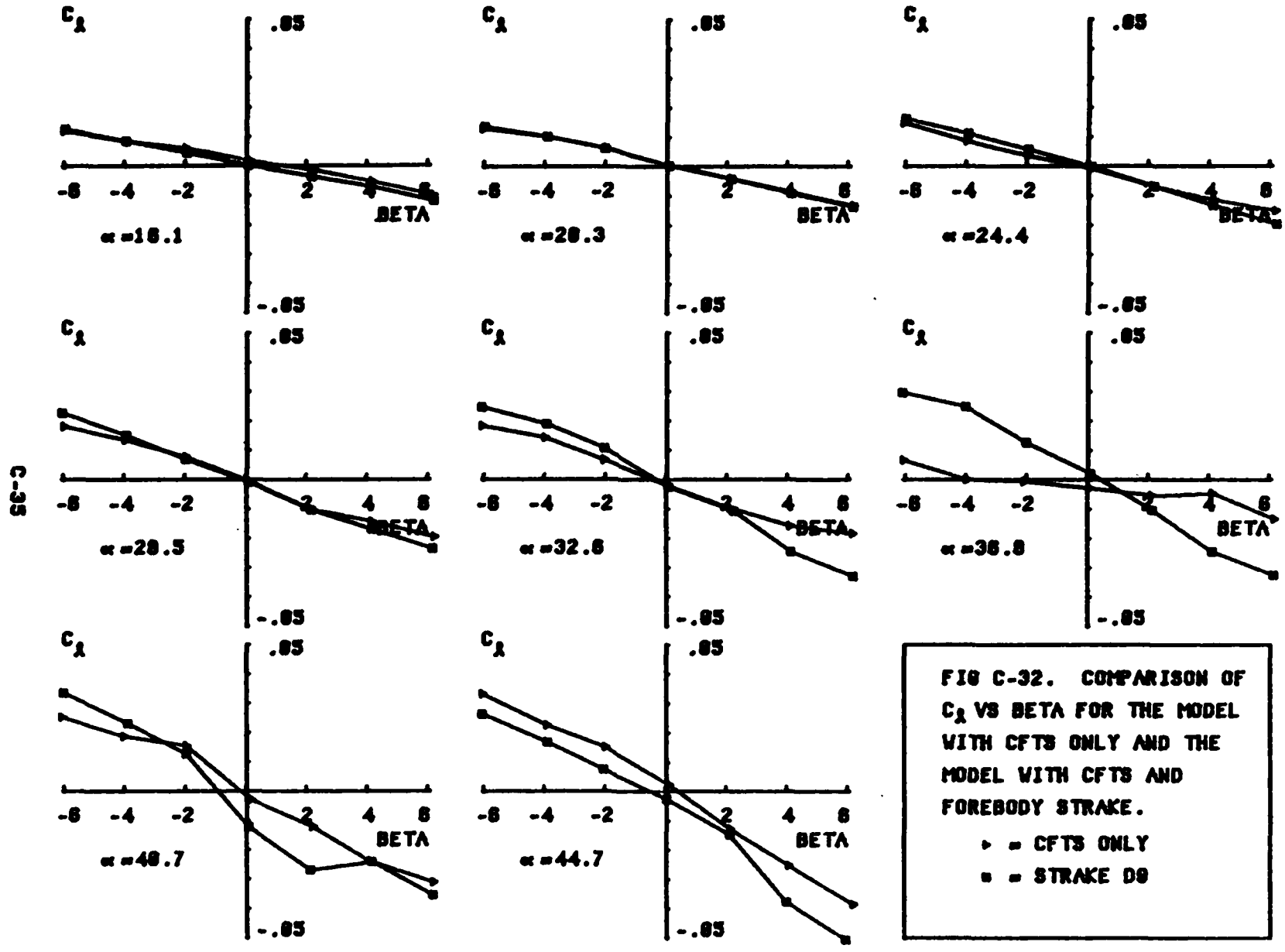

C-35

FIG C-32. COMPARISON OF C_ℓ VS BETA FOR THE MODEL WITH CFTS ONLY AND THE MODEL WITH CFTS AND FOREBODY STRAKE.

▸ = CFTS ONLY

▪ = STRAKE D9

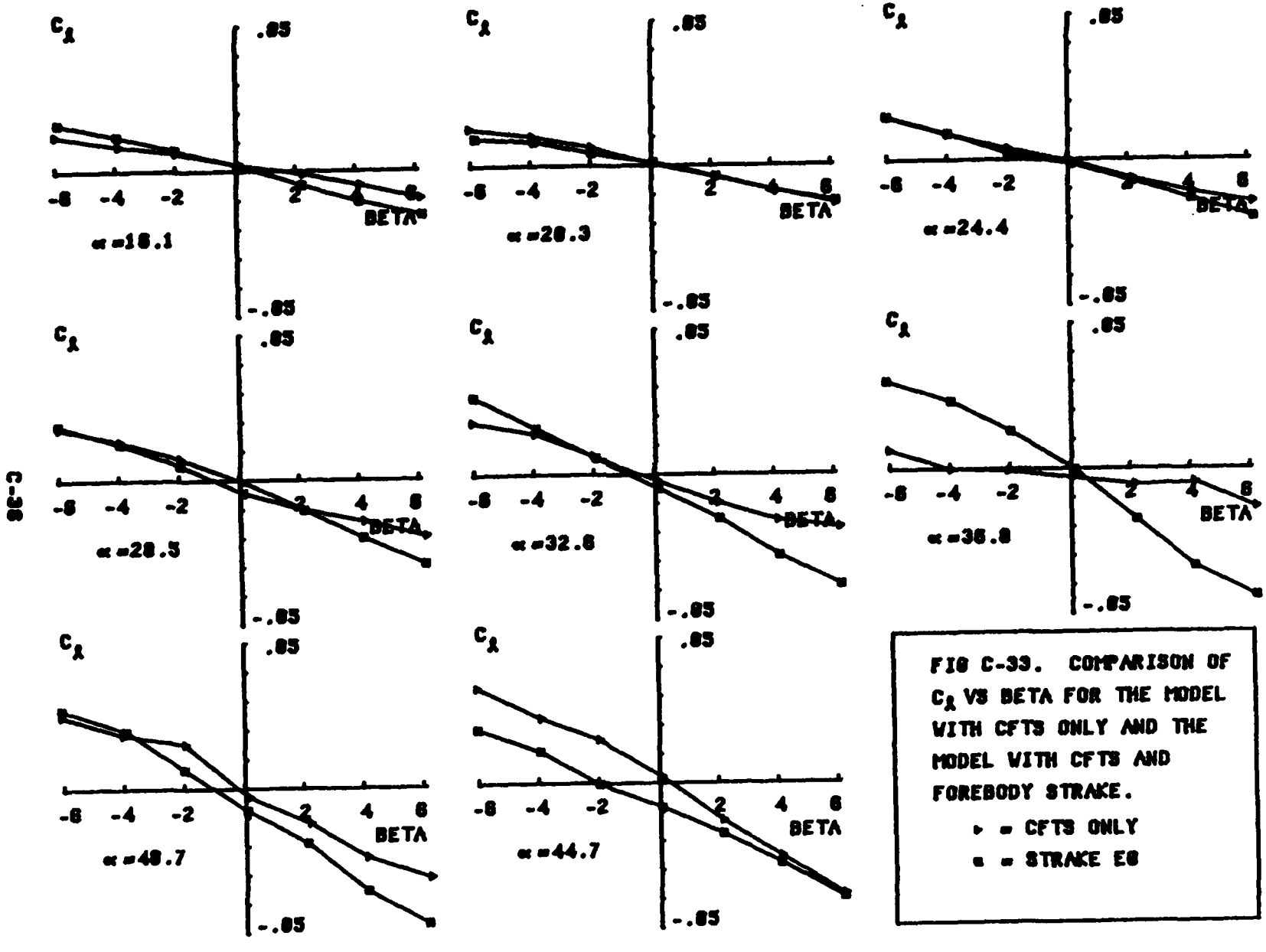

FIG C-33. COMPARISON OF C_ℓ VS BETA FOR THE MODEL WITH CFTS ONLY AND THE MODEL WITH CFTS AND FOREBODY STRAKE.

▸ = CFTS ONLY

▪ = STRAKE E8

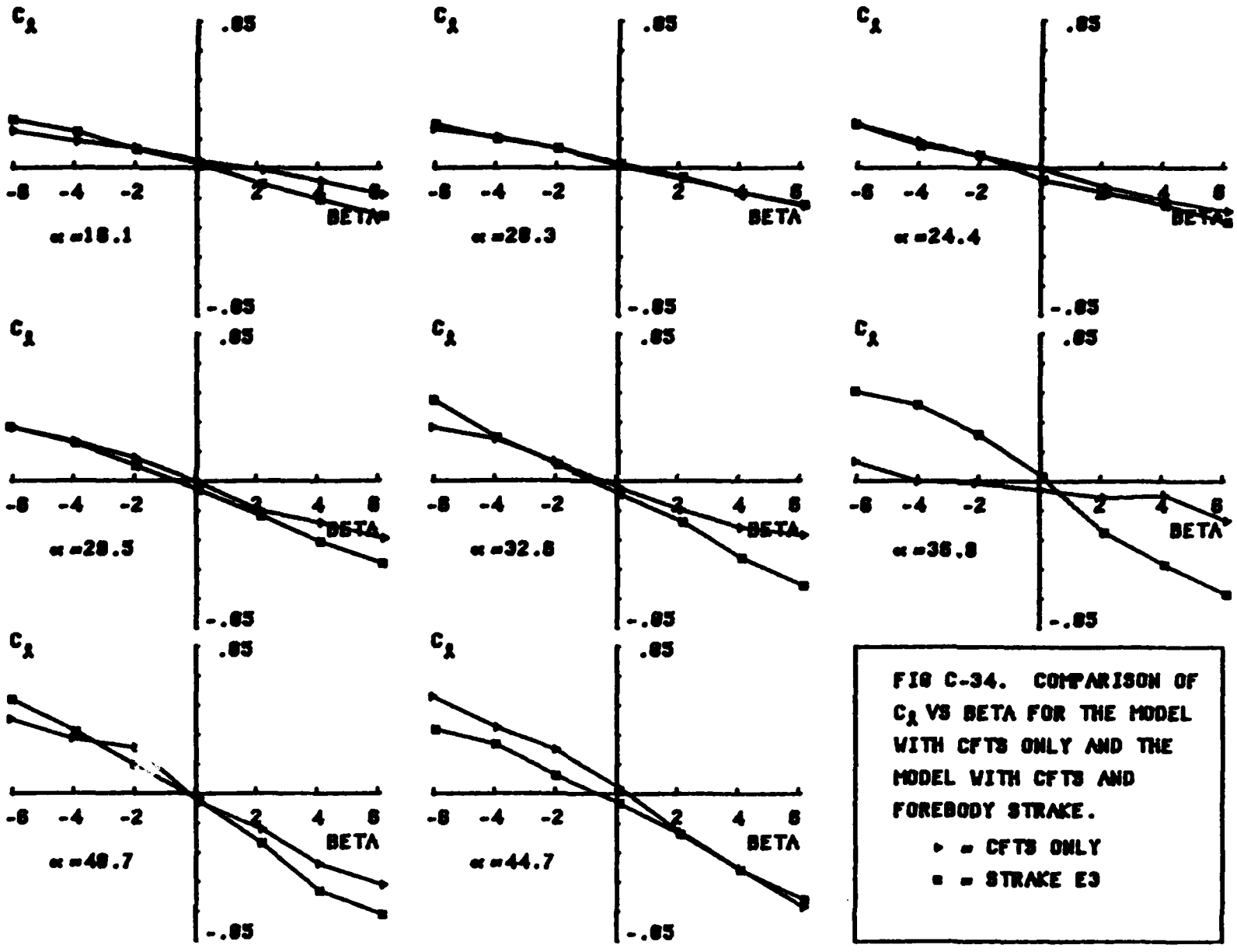

FIG C-34. COMPARISON OF C_ℓ VS BETA FOR THE MODEL WITH CFTS ONLY AND THE MODEL WITH CFTS AND FOREBODY STRAKE.

▸ = CFTS ONLY

▪ = STRAKE E3

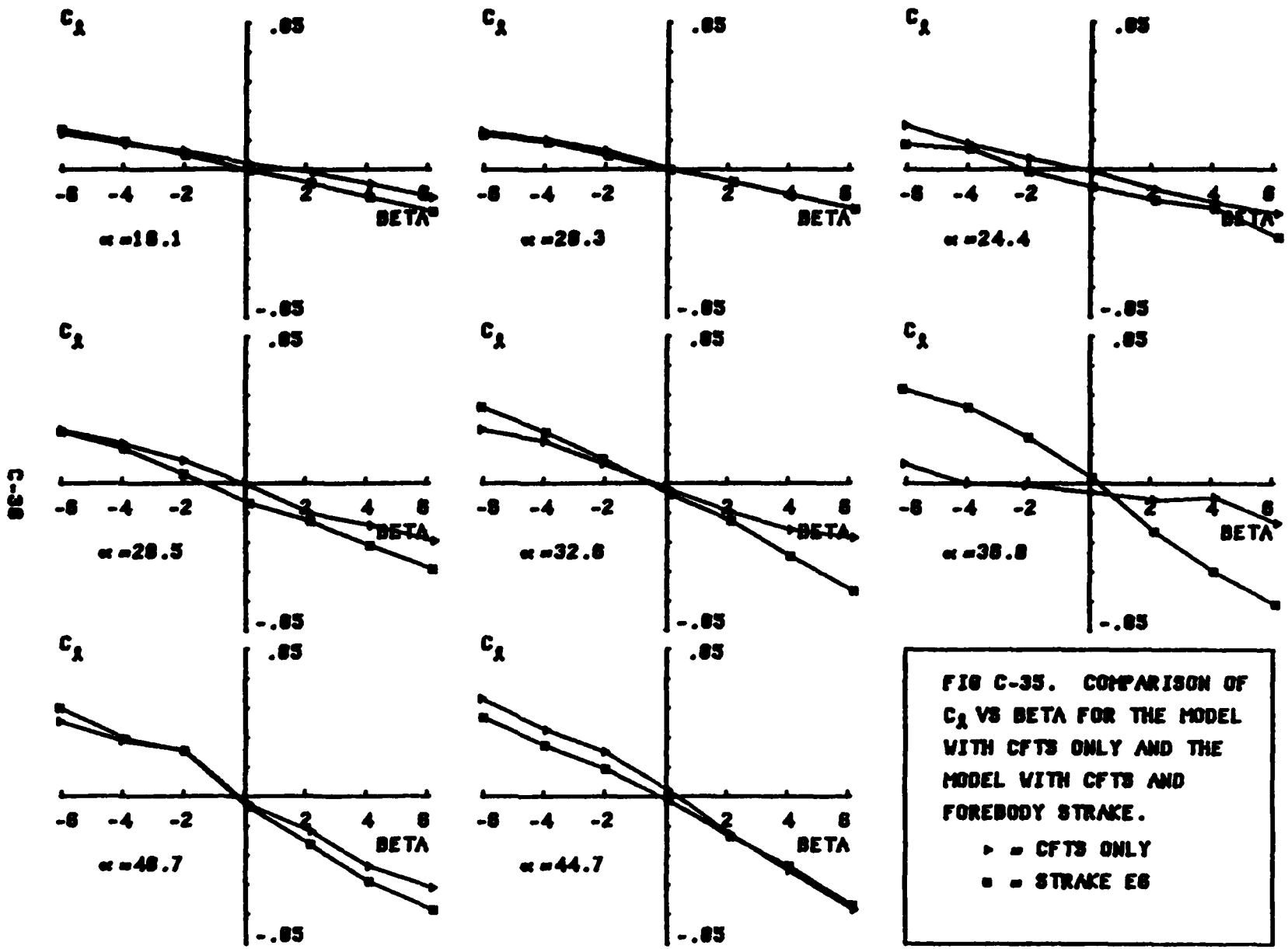

FIG C-35. COMPARISON OF C_λ VS BETA FOR THE MODEL WITH CFTS ONLY AND THE MODEL WITH CFTS AND FOREBODY STRAKE.

▸ = CFTS ONLY

▪ = STRAKE ES

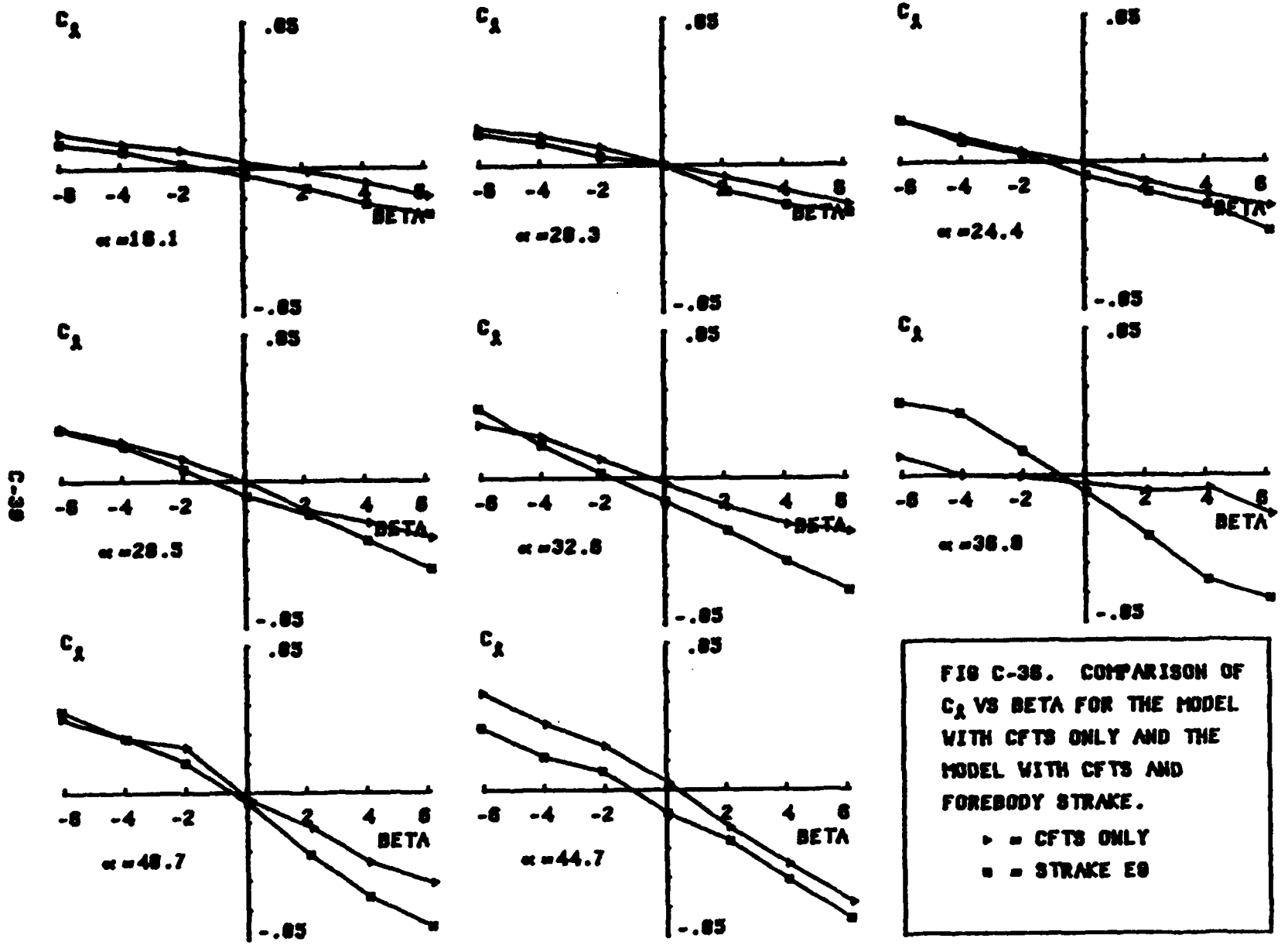

FIG C-38. COMPARISON OF C_ℓ VS BETA FOR THE MODEL WITH CFTS ONLY AND THE MODEL WITH CFTS AND FOREBODY STRAKE.

▸ = CFTS ONLY

▪ = STRAKE E8

REPORT DOCUMENTATION PAGE

1a. REPORT SECURITY CLASSIFICATION	1b. RESTRICTIVE MARKINGS
2a. SECURITY CLASSIFICATION AUTHORITY	3. DISTRIBUTION/AVAILABILITY OF REPORT
2b. DECLASSIFICATION/DOWNGRADING SCHEDULE	Unlimited
4. PERFORMING ORGANIZATION REPORT NUMBER(S) AFIT/GAE/AA/83D-7	5. MONITORING ORGANIZATION REPORT NUMBER(S)
6a. NAME OF PERFORMING ORGANIZATION Air Force Institute of Technology 6b. OFFICE SYMBOL (If applicable) AFIT/ENA	7a. NAME OF MONITORING ORGANIZATION
6c. ADDRESS (City, State and ZIP Code) Wright-Patterson AFB, Ohio 45433	7b. ADDRESS (City, State and ZIP Code)
8a. NAME OF FUNDING/SPONSORING ORGANIZATION 8b. OFFICE SYMBOL (If applicable)	9. PROCUREMENT INSTRUMENT IDENTIFICATION NUMBER
8c. ADDRESS (City, State and ZIP Code)	10. SOURCE OF FUNDING NOS PROGRAM ELEMENT NO. / PROJECT NO. / TASK NO. / WORK UNIT NO.
11. TITLE (Include Security Classification) A Wind Tunnel Investigation to Det-	
12. PERSONAL AUTHOR(S) Duncan, Terry A., Capt, USAF	
13a. TYPE OF REPORT MS Thesis 13b. TIME COVERED FROM 83/01 TO 83/12	14. DATE OF REPORT (Yr., Mo., Day) 83/Dec. 15. PAGE COUNT 138
16. SUPPLEMENTARY NOTATION	Approved for public release: IAW AFR 190-17. 3 JAN 1984 LYNN E. WOLAVER Dean for Research and Professional Development Air Force Institute of Technology (ATC) Wright-Patterson AFB OH 45433

17. COSATI CODES		
FIELD	GROUP	SUB. GR.
1	3	

18. SUBJECT TERMS (Continue on reverse if necessary and identify by block number)
F-15/Conformal fuel tanks/Forebody Strakes/Strake Incidence Angle/ Stability and Control

19. ABSTRACT (Continue on reverse if necessary and identify by block number)

A parametric study of forebody strakes was made on an F-15C model equipped with conformal fuel tanks in the AFIT 5 foot wind tunnel. Parameters of interest were the strake planform area and the strake angle of incidence. Twenty configurations were evaluated for longitudinal and lateral stability at angles of attack from -4 to 46 degrees.

Lift coefficient (C_L), drag coefficient (C_D), and pitching moment (C_M) were plotted versus angle of attack (α). Data indicated that an excessive positive increase in $\partial C_M/\partial \alpha$ can be expected at angles of attack of 20 degrees or less. Above 20 degrees, C_M may be tailored by varying the strake area and incidence angle. For each strake examined, an angle of incidence of either -3 or -6 degrees (depending on planform area) produced a more nearly linear C_M versus α curve than 0 degrees; therefore, incidence angle should be considered in strake design opti-

20. DISTRIBUTION/AVAILABILITY OF ABSTRACT UNCLASSIFIED/UNLIMITED ☒ SAME AS RPT. ☐ DTIC USERS ☐	21. ABSTRACT SECURITY CLASSIFICATION UNCLASSIFIED
22a. NAME OF RESPONSIBLE INDIVIDUAL Capt. Wesley R. Cox, Asst. Prof.	22b. TELEPHONE NUMBER (Include Area Code) 513-255-5533 22c. OFFICE SYMBOL AFIT/ENA

11. ermine Dominant Forebody Strake Design Characteristics for an F-15 Equipped with Conformal Fuel Tanks.

19. mization.

Lateral stability data were taken on 12 configurations from 16 to 44 degrees angle of attack. To determine spin susceptibility, $C_{N_{\beta\ DYN}}$ (see Section III.) was plotted for the most promising configurations. Very little constructive change in lateral stability was noted for the configurations tested.

END

FILMED

2-84

DTIC